

ELECTRON BEAM WELDING OF TUNGSTEN AND MOLYBDENUM

HARRY A. HOKANSON
WILLIAM I. KERN

HAMILTON STANDARD DIVISION
UNITED AIRCRAFT CORPORATION

DECEMBER 1961

DIRECTORATE OF MATERIALS AND PROCESSES
CONTRACT No. AF 33(616)-7439
PROJECT No. 7351
TASK No. 735102

U.S.A.F.
AERONAUTICAL SYSTEMS DIVISION
AIR FORCE SYSTEMS COMMAND
UNITED STATES AIR FORCE
WRIGHT-PATTERSON AIR FORCE BASE, OHIO

FOREWORD

This report was prepared by the Electron Beam Department and the Materials Engineering Department of the Hamilton Standard Division of the United Aircraft Corporation, Windsor Locks, Connecticut. This contract was initiated 1 July 1960 under United States Air Force Contract No. AF33(616)-7439, Task No. 735102. The work was administered under the direction of Directorate of Materials and Processes, Aeronautical Systems Division, Wright Patterson Air Force Base, Ohio, with Mr. R. E. Bowman acting as project engineer.

The work reported herein was performed under the supervision of Mr. J. W. Meier. This work was terminated on 31 August 1961.

Acknowledgement is made of the valuable assistance of Messrs. H. P. Langston, R. D. Burge, J. L. Cutler, W. H. Colman, E. L. Bancroft, and W. F. Kearns.

ABSTRACT

Techniques for the high-voltage electron beam welding of pure tungsten and arc-cast molybdenum-0.5% titanium were developed and evaluated. Welds were produced in sheet thicknesses of 0.005, 0.050, and 0.100 in. for each material. Primary emphasis was placed on producing butt welds of maximum strength and ductility. Limited work was also performed on lap, seam, edge, and spot welding.

The effects of various welding conditions on weld-zone characteristics were evaluated by visual, radiographic, fluorescent penetrant, and metallographic inspection. Welds were inspected for extent of fusion and recrystallization, grain size, cracking, porosity, and other pertinent effects.

Butt welds of each thickness exhibiting optimum weld-zone characteristics were evaluated for mechanical properties. Weld ductilities were determined by transverse bend testing at temperatures to 1200°F. Weld tensile properties were determined at room temperature and at temperatures to 2800°F.

Results of the metallographic and mechanical property investigations of the electron beam welds were compared with base-metal properties and with published data for other joining techniques.

PUBLICATION REVIEW

This report has been reviewed and is approved.

FOR THE COMMANDER



E. M. KENNEDY JR. Lt. Col, USAF
Actg Chief, Physical Metallurgy Branch
Metals and Ceramics Laboratory
Directorate of Materials and Processes

TABLE OF CONTENTS

	Page No.
SUMMARY.....	1
INTRODUCTION.....	3
CONCLUSIONS.....	4
RECOMMENDATIONS.....	5
DESCRIPTION OF TESTS.....	6
Material.....	6
Machining.....	6
Base-metal Evaluation.....	7
Welding Equipment.....	8
Trial Welding.....	10
Trial-weld Evaluation.....	11
Final Welding.....	12
Final-weld Evaluation.....	13
RESULTS OF TESTS.....	15
Base-metal Evaluation Results.....	15
Trial-weld Evaluation Results.....	15
Final-weld Evaluation Results.....	18
DISCUSSION OF RESULTS.....	20
Base-metal Discussion	20
Trial-weld Discussion	21
Final-weld Discussion	26
BIBLIOGRAPHY.....	31
APPENDIX.....	32
Tables.....	32
Figures.....	43

LIST OF FIGURES

Figure No.		Page No.
1	Molybdenum Tensile Specimen Drawing.....	43
2	Molybdenum Tensile Specimen.....	43
3	Tungsten Tensile Specimen Drawing.....	44
4	Tungsten Tensile Specimen.....	44
5	Room-temperature Tensile Testing Fixture.....	45
6	Elevated-temperature Tensile Testing Setup.....	46
7	Elevated-temperature Tensile Pull-rod and Grip Assembly...	47
8	Transverse Bend-test Specimen Drawing.....	48
9	Transverse Bend-test Specimen.....	48
10	Elevated-temperature Bend-test Setup.....	49
11	Electron Beam Welding Machine Schematic.....	50
12	Zeiss Electron Beam Welding Machine.....	51
13	Hamilton-Zeiss Electron Beam Welding Machine.....	52
14	Trial Butt-weld Specimen Drawing.....	53
15	Trial Butt-weld Specimen.....	53
16	Typical Welding Fixture.....	54
17	Seam-weld Specimen Drawing.....	55
18	Lap-weld Specimen Drawing.....	55
19	Spot-weld Specimen Drawing.....	55
20	Edge-weld Specimen Drawing.....	55
21	Final Butt-weld Specimen Drawing.....	56
22	Final Butt-weld Specimen.....	56
23-28	As-received and Recrystallized Molybdenum Base Metal.....	57-58
29-34	As-received and Recrystallized Tungsten Base Metal.....	58-59

LIST OF FIGURES (continued)

Figure No.		Page No.
35	Molybdenum Weld Penetration vs Current and Voltage.....	60
36	Tungsten Weld Penetration vs Current and Voltage.....	61
37	Molybdenum Weld Penetration vs Welding Speed.....	62
38	Tungsten Weld Penetration vs Welding Speed.....	63
39	Molybdenum Weld Penetration vs Transverse Oscillation.....	64
40	Tungsten Weld Penetration vs Transverse Oscillation.....	65
41-52	Trial Weld Microstructures; 0.100-in. Mo-0.5% Ti.....	66-69
53-54	Trial Weld Microstructures; 0.055-in. Mo-0.5% Ti.....	69
55-62	Trial Weld Microstructures; 0.005-in. Mo-0.5% Ti.....	70-71
63-66	Tungsten Weld Beads.....	72
67-78	Trial Weld Microstructures; 0.100-in. Tungsten.....	73-76
79-82	Trial Weld Microstructures; 0.050-in. Tungsten.....	77
83-86	Trial Weld Microstructures; 0.005-in. Tungsten.....	78
87-89	Final Welds; 0.005-in. Mo-0.5% Ti.....	79
90-93	Final Welds; 0.055-in. Mo-0.5% Ti.....	80
94-97	Final Welds; 0.100-in. Mo-0.5% Ti.....	81
98-100	Final Welds; 0.005-in. Tungsten.....	82
101-104	Final Welds; 0.050-in. Tungsten.....	83
105-108	Final Welds; 0.100-in. Tungsten.....	84
109-112	Seam Welds; Tungsten and Mo-0.5% Ti.....	85
113-116	Lap Welds; Tungsten and Mo-0.5% Ti.....	86
117-120	Spot Welds; Tungsten and Mo-0.5% Ti.....	87
121-124	Edge Welds; Tungsten and Mo-0.5% Ti.....	88
125	Strength vs Temperature; 0.055-in. Mo-0.5% Ti Welds.....	89

LIST OF FIGURES (continued)

Figure No.		Page No.
126-128	Tensile Failures; 0.055-in. Mo-0.5% Ti Welds.....	90
129	Strength vs Temperature; 0.050-in. Tungsten Welds.....	91
130-132	Tensile Failures; 0.050-in. Tungsten Welds.....	92
133-134	Bend Angle vs Temperature; Mo-0.5% Ti Welds.....	93-94
135-136	Bend Angle vs Temperature; Tungsten Welds.....	95-96

LIST OF TABLES

Table No.		Page No.
1	Test Material.....	32
2	Trial Welding-condition Ranges.....	33
3	Final Welding Conditions.....	34
4	Base-metal Chemical Analyses.....	35
5	Base-metal Hardness Properties.....	36
6	Base-metal Tensile Properties.....	37
7	Base-metal Ductile-to-brittle Transition Temperatures.....	38
8	Electron Beam Weld Hardness Properties.....	39
9	Electron Beam Weld Tensile Properties.....	40
10	Electron Beam Weld Ductile-to-brittle Transition Temperatures.....	42

SUMMARY

Electron beam welding techniques were developed for producing sound, crack-free welds in commercially available pure tungsten and arc-cast molybdenum-0.5% titanium (Mo-0.5% Ti) in thicknesses of 0.005, 0.050, and 0.100 in. Primary emphasis was concentrated on butt welding; however, lap, seam, edge, and spot welds were also produced.

Preliminary welding was concerned with the development of optimum welding techniques through an evaluation of the effects of various welding conditions on the weld-zone characteristics in each material thickness. Specific welding conditions evaluated included accelerating voltage (to 150,000 volts), beam current (to 20 milliamperes), welding speed (to 120 inches per minute), beam diameter (0.010 to 0.025 in.), beam oscillation (to amplitudes of ± 0.100 in.), and beam pulsing techniques (10 to 3,000 cycles per second with beam on-times of 0.5 to 1.0 milliseconds).

Trial welds produced in preliminary welding were evaluated for surface condition, cracking, porosity, degree of penetration, extent of fusion and recrystallized zone, grain size, and grain solidification pattern. Limited mechanical-property data were also obtained from the trial welds.

Evaluation of the trial welds indicated that weld-zone characteristics are strongly influenced by welding conditions. Welds of maximum strength and ductility were found to be dependent on limited fusion and heat-affected zones of minimum grain size in combination with smooth, continuous, non-undercut, crack-free weld beads. Minimum grain size and limited fusion and heat-affected zones were achieved through the use of maximum possible welding speed and minimal beam diameter. Highest-quality weld beads were produced using 60-cycle beam oscillation in the direction of welding. Grossly defocused beams, slow welding speeds, and beam deflection across the seam developed welds that were inferior with respect to grain size and extent of fusion and heat-affected zones.

Using the optimum techniques determined in trial welding, final welds were produced in each material thickness for comprehensive mechanical testing. Before testing, all final welds were inspected by radiographic and fluorescent penetrant techniques. The tensile properties of the welds were determined at room temperature and 1600°F, 1900°F, and 2200°F for the Mo-0.5% Ti and at room, 2200°F, 2500°F, and 2800°F for the pure tungsten. Weld ductilities were determined by transverse bend testing at temperatures to 1200°F. Ductile-to-brittle transition temperatures were established from the bend-test results.

The tensile-test results revealed that welds in both tungsten and Mo-0.5% Ti retained base-metal strength at temperatures approaching the recrystallization temperatures. Relative tensile strengths decreased with decreasing temperature, reaching at room temperature eighty percent of the base-metal strength for molybdenum-0.5% titanium and fifty percent of the base-metal strength for pure tungsten.

Manuscript released by authors September 1961 for publication as an ASD Technical Report.

SUMMARY (continued)

The room-temperature ductility of electron beam welds in both tungsten and Mo-0.5% Ti was inferior to the corresponding base-metal ductility. The tungsten welds were particularly brittle at room temperature. In the ductile region, weldment ductilities approached base-metal ductilities, becoming equal at approximately 300°F above the weld transition temperature.

Based on the elevated-temperature bend-test results, the ductile-to-brittle transition temperatures, depending on the material and thickness, varied from less than 200°F to greater than 400°F above the associated base-metal transition temperature.

Analysis of the bend testing technique indicated that ductility and associated ductile-to-brittle-transition temperature data cannot be directly compared with comparable data for arc welds. In every case the ductility data generated for electron beam welds was derived from a much more severe testing technique.

INTRODUCTION

The introduction of tungsten and molybdenum to aerospace applications has required the development of welding techniques for the production of reliable joints of adequate strength in these difficult-to-weld materials. Conventional fusion welding techniques for producing welded joints in tungsten and molybdenum have been investigated. In general, such welds demonstrated problems relative to cracking, low ductility, or comparatively low room or elevated-temperature strength.

Recently-developed high-voltage electron beam welding processes offer advantages which show promise of minimizing many of the disadvantages generally associated with other fusion techniques. Among such advantages are the ability to weld in an extremely high vacuum at comparatively high welding speeds with minimal energy input to the workpiece.

The present program was undertaken to investigate the use of high-voltage electron beam welding as a joining technique for molybdenum and tungsten. The primary objective was to develop techniques capable of producing sound welds of optimum strength and ductility in pure tungsten and arc-cast molybdenum-0.5% titanium in a variety of configurations.

CONCLUSIONS

Results of the electron beam welding development program on tungsten and molybdenum lead to the following conclusions.

1. Sound, crack-free welds can be produced in commercially available pure tungsten and arc-cast molybdenum-0.5% titanium by high-voltage, high-power-density electron beam welding techniques. Configurations weldable include butt, seam, edge, lap and spot. With the equipment used in the program, molybdenum-0.5% titanium can be through-welded at reasonable speeds in thicknesses exceeding 0.250 in. and tungsten in thicknesses exceeding 0.200 in.
2. Welds of maximum strength and ductility in both metals are associated with minimum fusion and heat-affected zones in combination with smooth, continuous weld beads. Minimum fusion and heat-affected zones are dependent on minimum energy input to the workpiece; smooth continuous weld beads are produced through the use of beam oscillation. Thus, highest quality welds are produced with maximum possible welding speeds, minimal spot sizes, and moderate beam oscillation in the direction of welding.
3. Electron beam welds in tungsten and molybdenum-0.5% titanium possess tensile strengths equivalent to base-metal strength at temperatures approaching the recrystallization temperature. Relative tensile strengths decrease with decreasing temperature, reaching at room temperature eighty percent of the base-metal strength for molybdenum-0.5% titanium and fifty percent of the base-metal strength for tungsten. For both materials, electron beam welds have tensile strengths superior to arc welds.
4. Electron beam welds in both tungsten and molybdenum-0.5% titanium have ductile-to-brittle transition temperatures less than 450°F above the base-metal transition temperature. Below the transition temperature, extreme weld brittleness is particularly associated with welds of relatively large grain size and extended fusion and heat-affected zones. In the ductile region, the weld ductility approaches the base-metal ductility, becoming equal at approximately 300°F above the weldment transition temperature.

RECOMMENDATIONS

The following recommendations are based on the results of the program.

1. The successful welding methods developed in the present program should be evaluated as production techniques through the welding of prototype parts in tungsten and molybdenum. The prototypes should represent a variety of configurations and should be evaluated by techniques pertinent to the end use of the parts.
2. Further work should be conducted on the high-power-density electron beam welding of both tungsten and molybdenum at extremely high welding speeds. The tungsten used should be of quality superior to the commercially available tungsten used in the present program. The electron beam welding of molybdenum alloys should be concentrated on molybdenum-0.5% titanium-0.08% zirconium. Evaluation of the welds should be concentrated on ductile-to-brittle transition-temperature testing and on tensile testing at temperatures above the brittle-transition temperature.
3. To provide further design flexibility in the use of tungsten and molybdenum, electron beam welding techniques should be developed for the joining of tungsten to molybdenum.

DESCRIPTION OF TESTS

Material

Commercially available pure tungsten and molybdenum-0.5% titanium (Mo-0.5% Ti) in sheet thicknesses of 0.005, 0.050, and 0.100 in. were used for the bulk of the welding program. A small amount of 0.187-in. Mo-0.5% Ti and pure tungsten was also available for miscellaneous use. All of the Mo-0.5% Ti was arc-cast material; the pure tungsten was produced by powder metallurgy techniques. Table 1 lists the material used in the program. A complete description of the materials appears in Results of Tests, Base Metal.

Machining

The inherent brittleness of the metals, particularly tungsten, required the development of specialized and carefully controlled machining procedures. Particular emphasis was placed on developing the lowest-cost techniques consistent with acceptable quality. Techniques were developed for cutting, grinding, milling, drilling, and polishing.

Cutting of both tungsten and Mo-0.5% Ti in thicknesses of 0.050 in. to 0.187 in. was performed with a 0.032-in. by 6-in. alumina cut-off wheel (de Sanno No. Al20-F-R107). The 0.005-in. tungsten and Mo-0.5% Ti were cut with a 0.015-in. by 6-in. wheel (No. Al50-R-R90). The wheels were mounted on a surface grinder and cutting was performed by a multiple-pass technique using excess cooling fluid to eliminate heat-induced checking, lamination, or other machining damage. Approximately 0.015 in. of stock was removed per pass. The surfaces produced were very smooth, free from laminations, and had sharp, 90-degree corners. Mo-0.5% Ti was also cut with all-purpose 0.062-in. by 10-in. cut-off wheels and on Do-All saws. Cutting conditions on both the wheel and the saw were similar to those used for mild steels. The resulting edges were, of course, not as smooth as those produced with the thin cut-off wheels.

Surface grinding of the tungsten and Mo-0.5% Ti was performed with alumina grinding wheels using slow feeds and excess coolant. To eliminate laminations, all surface grinding was performed parallel to the sheet-rolling direction. Similarly, all edge grinding was performed along, rather than across, the edge.

Contoured surfaces were successfully formed in tungsten using jig-grinding techniques. Satisfactory results were obtained using a Moore Special Tool Co. 35-3/8D wheel at 8500 RPM with slow material feed. Spark erosion cutting was also used for forming contours in tungsten; however, jig-grinding was preferred because of lower cost. Contoured surfaces in Mo-0.5% Ti were formed by both slab and end milling with relatively slow feeds and speeds. Whenever possible all slab milling was performed parallel to the sheet-rolling direction.

Spark erosion techniques were used for drilling holes in tungsten. Brass tools were used with very slow feed. End milling was used for drilling holes in the Mo-0.5% Ti.

All machined surfaces on specimens subjected to mechanical testing were polished to minimize all machining defects which could propagate premature

DESCRIPTION OF TESTS (continued)

specimen failure. For Mo-0.5% Ti, the polishing was performed with a fine-grade emery paper. Tungsten machined surfaces were chemically polished by a five-minute immersion in a solution of 67% lactic acid, 22% HNO₃, and 11% HF followed by a water rinse. (All percentages in volume percent.) After machining, all specimens intended for final welding or for mechanical testing were fluorescent penetrant inspected for cracks and laminations.

Base-metal Evaluation

Each individual sheet of material used in the program was visually inspected in the as-received condition for cracks, laminations, and general surface quality.

Chemical analysis was conducted on samples extracted from each sheet thickness of each heat. Oxygen and hydrogen contents were determined by vacuum fusion analysis, the nitrogen content was determined by the Kjeldahl method, and metallic alloying elements and impurities were determined by spectrographic analysis. Lack of facilities prevented carbon determinations; however, carbon analyses were supplied by the material vendors.

All material thicknesses were subjected to thorough metallographic examination in both the as-received and recrystallized condition. The evaluation included hardness testing and metallographic examination for the presence of inclusions (such as carbides, nitrides and oxides), laminations, and other defects that would inhibit weldability.

All specimens for metallographic examination were mounted in bakelite and prepared for examination by standard grinding and polishing techniques. Microstructures were revealed by swab etching for 20 to 30 seconds with Murakami's Reagent (10g K₃Fe(CN)₆ + 100 cc H₂O). Recrystallization was accomplished by heating the specimens one hour in a vacuum at 2450°F for the Mo-0.5% Ti and 2950°F for the tungsten.

Diamond-pyramid hardness values were determined on a Zwick Microhardness Testing Machine. Anisotropic behavior of material hardness was investigated by determining the hardness on three planes of the material. A 3Kg load was used on sheet thicknesses of 0.050 in. and 0.100 in., and a 0.5Kg load was used on the 0.005-in. material.

Room-temperature tensile tests were conducted on the 0.005, 0.050, and 0.100-in. thicknesses of both Mo-0.5% Ti and tungsten. Additionally, tensile tests were performed on the 0.055-in. Mo-0.5% Ti at 1600°F, 1900°F, and 2200°F and on the 0.050-in. tungsten at 2200°F, 2500°F, and 2800°F. The specimens used for both room and elevated-temperature tensile testing, Figures 1 through 4, were manufactured and inspected using the techniques developed in the machining investigations.

The room-temperature tensile tests were performed using the tensile fixture illustrated in Figure 5. The fixture was equipped with a rigid, removable member which isolated all stresses from the tensile specimen during test set-up. This minimized premature brittle failures induced by specimen

DESCRIPTION OF TESTS (continued)

mishandling. The fixture also provided a more positive method of gripping the specimens during application of the tensile-test load.

Elevated-temperature tensile tests were conducted in a Marshall 3000°F tensile-testing furnace at a vacuum of approximately 1×10^{-4} millimeters of mercury. Figure 6 illustrates the furnace and control console in operating position. The specimen pull-rod and gripping assembly for the high-temperature tests is shown in Figure 7. The grips, either Mo-0.5% Ti bar or tungsten bar, depending on the testing temperature, were threaded into Inconel X pull rods, which operated in cooler regions of the furnace. The tensile specimens were held in the grips with tungsten pins. To minimize stresses, and thus eliminate specimen failure during setup, a close-fitting, smooth-walled tube was placed into the furnace prior to specimen-pull rod insertion. This tube guided the assembled pull-rod and gripping unit into position and also protected the furnace heating element from damage during setup. Temperature measurements were made at the specimen surface with a platinum/platinum-10% rhodium thermocouple. All specimens were stabilized at temperature for five minutes prior to testing. The short time at temperature was justified because of the long heat-up times (approximately one hour) and the relatively thin specimen thickness.

Transverse bend tests were conducted at room temperature on all thicknesses of both the tungsten and the Mo-0.5% Ti. Figures 8 and 9 illustrate the bend-test specimen configuration. All specimens were bent about an axis parallel to the material surface but perpendicular to the sheet rolling direction. As the 0.055-in. Mo-0.5% Ti and 0.050-in. and 0.100-in. tungsten were brittle at room temperature, their ductile-to-brittle transition temperatures were determined by bend testing at temperatures to 1000°F.

Both the elevated-temperature and room-temperature bend tests were conducted using the setup illustrated in Figure 10. The figure shows the ambient box and heating coils used for obtaining the elevated temperatures. During test, a span of 1.25 inches was maintained between specimen-supporting shoulders. Bend radii employed for the various thicknesses were 1.25 T (T = material thickness) for the 0.050-in. and 0.100-in. material and 3.00 T for the 0.005-in. thickness. The rate of deflection used for all bend testing was 0.5 in. per minute. At elevated temperatures the specimen temperature was continuously monitored with a thermocouple placed in direct contact with the specimen. All specimens were bent until failure occurred or the limit of the fixture was reached.

Subsequent to bend testing, the specimens were visually examined to determine the degree of ductility exhibited in the failure. Angle of bend at failure was defined as the angle through which the specimen was bent, from the horizontal plane, at the onset of failure. To serve as a standard for the comparison of weld and base-metal properties, the ductile-to-brittle transition temperature was arbitrarily defined as the temperature at which a bend angle of 30 degrees was achieved before initiation of failure.

Welding Equipment

All welding was performed on Zeiss and Hamilton-Zeiss high-voltage, high-power-density electron beam welding machines. A schematic representing the

DESCRIPTION OF TESTS (continued)

electron gun and work chamber of the machines is shown in Figure 11. The electron optical column contains, in the upper part, the electron beam source or gun consisting of a cathode emitter, a grid, and an anode. The electron emitter is a small-diameter, heated tungsten wire in the shape of a hairpin or a coil. Surrounding the emitter is a long focal-length, cup-shaped grid. The grid provides the initial beam shaping by means of an electrostatic field which forces the fog of electrons emitted by the cathode into a cylindrical column with a focal point downstream of the anode. A second purpose of the grid is to provide regulation of beam intensity. This is accomplished by varying the negative voltage imposed on the grid so that it, in effect, acts as a valve controlling the flow of electrons to the workpiece. As more negative voltage is applied to the grid, the stream of electrons to the target decreases. Voltage can be imposed on the grid in a cyclic manner to provide cyclic, or pulsed, operation of the beam. Directly below the cathode and grid is the anode. The potential between the anode, at ground, and the cathode, at up to 150,000 volts negative, provides the accelerating potential for the electrons.

Below the anode are beam adjusting coils. These coils are electro-magnetic lenses which can be adjusted to align the beam with the optical axis of the main electro-magnetic focusing lens. A water-cooled diaphragm below the adjustment system blanks off electrons whose paths are not in the high-power-density center portion of the beam. After passing through the diaphragm, the beam reaches the main electro-magnetic focusing lens. The focal length of the lens is adjustable by the machine operator so that the beam can be precisely focused on the surface of the workpiece. The beam can also be reproducibly defocused to any desired diameter.

Below the main focusing lens is a deflection coil of the same general design as the adjusting coils. By imposing on this coil any shape 60-cycle A.C. signal with adjustable amplitude, the beam can be oscillated in either the "X" (along the weld seam) or "Y" (across the weld seam) direction. Using a D.C. signal the beam can be permanently deflected to any desired location within a range of approximately 1/2 inch. If desired, A.C. and D.C. signals may be used simultaneously.

A viewing system shown in the approximate center of the column makes possible observation of the workpiece and weld spot along an axis coincidental with the beam. Beneath the column is the main welding chamber containing the work table. A weld is accomplished by passing the seam requiring welding under the beam. The equipment contains its own vacuum system required to create and maintain the necessary vacuum of 10^{-4} to 10^{-5} millimeters of mercury.

The Zeiss equipment is illustrated in Figure 12 and the Hamilton-Zeiss in Figure 13. At the same operating conditions, the welding characteristics of the two machines are equivalent. However, the Hamilton-Zeiss equipment has greater operating flexibility with regard to beam power and welding speeds. Specific welding condition ranges available are summarized, as follows, for each machine.

DESCRIPTION OF TESTS (continued)

	<u>Zeiss</u>	<u>Hamilton-Zeiss</u>
Accelerating Voltage	0 to 150,000 volts	0 to 150,000 volts
Beam Current	0 to 20 milliamperes	0 to 20 milliamperes
Maximum Beam Power	2 kilowatts	3 kilowatts
Welding Speed	0 to 27 inches per minute	0 to 120 inches per minute
Beam Oscillation Amplitude	0 to 0.500 in.	0 to 0.250 in.
Beam Pulsing Rate	1 to 3000 cps	0.1 to 3000 cps
Beam Pulse On Times	0.05 to 10 milli-seconds	0.05 to 10 milli-seconds

Trial Welding

The best welding techniques for each material thickness were established through a comprehensive, trial-welding program. The primary purpose of trial welding was to establish welding parameters for each material thickness that gave welds of optimum strength and ductility. The work was concentrated on butt welding; however, spot, seam, edge, and lap welds were also studied.

Trial butt welding was performed using the specimens illustrated in Figures 14 and 15. Seam, lap, spot, and edge welds were produced in accordance with Figures 17 through 20. To provide good fit-up, the mating edges of specimen pairs were finish ground to approximately 32 RMS with sharp, non-broken edges. Before welding, all specimens were degreased in hot trichloroethylene and then chemically cleaned. The Mo-0.5% Ti specimens were cleaned by a 10-minute immersion in a 180°F solution of 10% NaOH + 5% KMnO₄ + 85% H₂O, followed by a 10-minute immersion in a room-temperature solution of 15% HCl + 15% H₂SO₄ + 10% CrO₃ + 60% H₂O, followed by a cold-water rinse. (All percentages refer to weight percent.) Tungsten weld specimens were cleaned by a 10-second immersion in a solution of 50% HF + 50% HNO₃ followed by a water rinse. To ensure clean surfaces during welding, particular emphasis was placed on limiting the time delay between cleaning and welding. At no time was the time lapse allowed to exceed eight hours.

A typical butt-welding fixture is illustrated in Figure 16. The pieces for welding were butted together and held in place by clamps. When desired, end pressure was applied to the pieces by a spring-loading mechanism. Spot, seam, edge, and lap welds were made in similar fixtures with modified clamping arrangements.

Approximate welding conditions required for each metal thickness were established by making weld passes at a variety of settings in solid blocks of 0.187-in. Mo-0.5% Ti and pure tungsten. Parameters studied included accelerating voltage, beam current, welding speed, beam oscillating conditions, and

DESCRIPTION OF TESTS (continued)

beam pulsing conditions. Experience has shown that under identical welding conditions weld-zone characteristics developed in solid material closely approximate those developed in actual butt welds. Therefore, a cross-section of the weld passes provided a quick approximation of the range of setting required for a given penetration.

Butt welds were produced in all thicknesses of the Mo-0.5% Ti and pure tungsten at a variety of machine settings. Table 2 lists ranges of settings used for each material thickness. Welding speeds to 100 inches were not used on all material thicknesses because the Hamilton-Zeiss equipment, which has the 100-inch-per-minute capability, was not available until relatively late in the program. In addition to the settings listed, variations in fixturing technique and pre- and post-heating were also studied. As the trial-welding program progressed, selection of trial-weld settings for each material thickness was closely coordinated with feedback from trial-weld evaluation.

Early in trial welding it was established that the 0.050-in. and 0.100-in. material reacted similarly to similar welding conditions. That is, with suitable adjustment to take care of the thickness differences, welding conditions which induced specific weld-zone characteristics in the 0.100-in. material were found to have the same effect on the 0.050-in. material. Thus, the trial welding program was generally divided into (1) welding of 0.055-in. and 0.100-in. Mo-0.5% Ti, (2) welding of 0.005-in. Mo-0.5% Ti, (3) welding of 0.050-in. and 0.100-in. tungsten, and (4) welding of 0.005-in. tungsten. Overall, 75 to 100 trial-weld specimens were produced in each of the four butt-welding phases.

Trial welding of edge, spot, seam, and lap configurations was conducted on the 0.055-in. Mo-0.5% Ti and the 0.050-in. tungsten. Five to ten trial welds were produced for each configuration in each material.

Trial-weld Evaluation

The main purpose of trial-weld evaluation was to determine, by various weld evaluation procedures, which combination of welding machine settings produced the weld-zone characteristics that would promote optimum weld strength and ductility. The best settings established in trial welding would then be used for producing welds for final testing. Initially, the assumption was made that optimum weld characteristics would include minimum fusion and heat-affected zones, minimum grain growth in both the base metal and fused zones, and a complete lack of undercutting, cracking, and porosity. As trial-weld evaluation progressed the validity of each of the assumed points was verified.

The evaluation procedure was conducted in three general phases: (1) visual inspection, (2) metallographic evaluation, and (3) fluorescent penetrant and radiographic inspection. Welds which were unacceptable with regard to visual inspection were either rejected immediately or were metallographically evaluated for microstructure characteristics. Naturally, all welds that were visually acceptable were also subjected to metallographic evaluation. Radiographic and fluorescent penetrant inspection was applied only to trial welds associated with welding conditions being considered for final welding.

DESCRIPTION OF TESTS (continued)

Visual inspection of the welds was performed on all specimens. In fact, in many cases, the workpiece itself was observed during and immediately after welding through the welding-machine optical viewing system. All welds were visually inspected for undercutting, cracking, extreme bead roughness, and similar surface effects. As mentioned above, all visually-acceptable welds were subjected to metallographic evaluation; unacceptable welds were either rejected or subjected to metallographic evaluation of other characteristics.

Metallographic examination of the welds was performed on specimens mounted and suitably prepared for metallographic evaluation following the same procedures used for the base material. For the solid blocks containing simulated welds and the butt welds in 0.100-in. and 0.050-in. thicknesses, cross-sections of the welds taken normal to the welding direction were examined. Trial weldments in 0.005-in. material were evaluated by microexamination of the weld beads, which in the thin material, gave a clearer indication of weld-zone characteristics than did a cross-section.

The welds in the solid blocks were measured for depth of penetration. Depth of penetration is defined as the distance, in a weld cross-section, from the original surface of the sheet to the bottom of the fusion zone. The penetration values obtained from the simulated welds were plotted graphically as a function of the pertinent welding settings.

Weld microstructures were evaluated for overall weld quality and soundness. Particular emphasis was placed on determining the degree of penetration, extent of fusion and heat-affected zones, grain size, and grain solidification pattern. The weld zones were also examined for microcracking and microporosity. Examination was conducted both before and after etching. Murakami's etch was used on all welds excepting the 0.005-in. tungsten welds which were etched by a 10-second immersion in 50% HF plus 50% HNO₃. Results of metallographic evaluation were correlated with the pertinent welding conditions, and the information was used in a feedback manner to guide in the selection of further trial-welding settings.

Fluorescent penetrant and radiographic inspection techniques were used on welds produced by potential final-weld settings. The extreme narrowness of electron beam weld beads required careful radiographic inspection to reveal all defects. Thus, welds in 0.050-in. and 0.100-in. material were radiographed both normal to the weld bead and at a 45-degree angle across the seam.

The accumulative results of all of the trial-weld evaluation procedures guided the selection of the final-welding settings. To ensure expected results, all settings selected for final welding were thoroughly evaluated, by the trial-weld evaluation procedures discussed above, immediately before the initiation of final welding.

Final Welding

The best welding techniques established in trial welding were used to produce weldments in each thickness for mechanical testing. The final-weld specimen configuration is illustrated in Figures 21 and 22. The specimens were

DESCRIPTION OF TESTS (continued)

manufactured so that the edges for welding were perpendicular to the rolling direction. All specimens were cleaned and fixtured by the same techniques used in trial welding. Butt, lap, seam, and edge welding was performed perpendicular to the sheet rolling direction. The final-weld settings used for each material, thickness, and configuration are listed in Table 3.

Final-weld Evaluation

All final weld specimens were visually inspected for undercutting, weld cracking, and degree of penetration. Fluorescent penetrant and radiographic inspection techniques were used on all specimens for the detection of cracks and porosity. Representative final weld specimens from each material thickness were inspected by metallographic techniques for extent of fusion and heat-affected zones, grain size, and grain solidification pattern. Microhardness values were determined in weld zone cross-sections by testing techniques identical to those used on the base metal.

The tensile properties of electron beam welded Mo-0.5% Ti and tungsten were evaluated at room and elevated temperatures. Specimens and testing procedures were similar to those used for the base-metal tensile property evaluation. All tests were conducted on weldments in the as-welded condition. That is, the original weld-bead surface was intact with no machining cleanup, and no specimens were stress relieved.

Specimens of welds in all material thicknesses were tested at room temperature. Elevated-temperature testing of electron beam welds was performed on specimens of 0.055-in. Mo-0.5% Ti at 1600°F, 1900°F, and 2200°F and on specimens of 0.050-in. tungsten at 2200°F, 2500°F, and 2800°F. Particular care was used in handling the specimens during setup through the use of the fixtures discussed under base-metal testing. After fracture, all specimens were examined for origin (weld or base metal) and type (transgranular or intergranular) of failure.

Elevated-temperature tensile testing was limited to the 0.050-in. Mo-0.5% Ti and the 0.055-in. tungsten because of limitations imposed by the present testing technique and equipment. Testing of the 0.005-in. material with the present test-specimen configuration at elevated temperature would have resulted in tear-type failures at the pinning holes in the specimen tangs. Thus, special shouldered and/or pressure-gripping assemblies would have been required. Testing of the 0.100-in. material at elevated temperatures imposed excessively high stresses on the gripping assemblies, particularly the pins. Modification of both the specimen and pull-rod assembly would be required to overcome the stress problem.

The transverse bend-ductility of electron beam welds in tungsten and Mo-0.5% Ti was determined on all material thicknesses in the as-welded condition. In addition, to investigate the effects of stress relieving, tests were conducted on 0.055-in. Mo-0.5% Ti and 0.005-in. tungsten specimens that were stress relieved one hour at 1850°F and 1900°F respectively. The specimens and testing procedure were similar to those used on the base material.

DESCRIPTION OF TESTS (continued)

During all testing, the face of the weld (beam impingement side) was placed in tension. Primary emphasis was placed on elevated-temperature bend testing for the determination of the ductile-to-brittle transition temperature. The transition temperature for the 0.050-in. and 0.100-in. tungsten weldments was above the temperature capabilities of the ambient box used for obtaining elevated temperatures. Therefore, propane torch heating was used to perform bend tests in the range of 1000°F to 1200°F. As with the base metal, the specimens were visually inspected after test to determine the angle at failure. The location of the failure, relative to the weld centerline, was also noted.

RESULTS OF TESTS

Base-metal Evaluation Results

Visual inspection of the as-received base metal for cracks, laminations, and other effects revealed no defects in any of the material except the 0.055-in. Mo-0.5% Ti. One side of the 0.055-in. Mo-0.5% Ti was completely satisfactory; however, the other side exhibited small striations oriented perpendicular to the sheet rolling direction.

The results of the chemical analyses of all sheet thicknesses from each heat appear in Table 4.

Representative sections of all three base-metal thicknesses in both the as-received and the recrystallized condition are illustrated in Figures 23 through 34. Metallographic examination of the as-received materials showed no detectable inclusions at magnifications to 1000X. Hardness test results on three planes of each material thickness are listed in Table 5.

Base-metal tensile test results at both room and elevated temperatures are presented in Table 6. For reference, the variation of base-metal strength with temperature is shown in Figures 125 and 129 for the 0.055-in. Mo-0.5% Ti and the 0.050-in. tungsten, respectively. Due to the extreme brittleness of the tungsten material in all three thicknesses, values for the yield strength at 0.2% offset were not realized.

Before the tungsten brittleness problem was fully appreciated, tensile specimens were manufactured in accordance with the Mo-0.5% Ti configuration. However, the small-diameter hole and relatively small gripping tang apparently concentrated too much stress in the gripping area, and many gripping failures resulted. Much better success was realized using the larger-tanged specimens. Even so, the problem of brittleness in the tungsten material accounted for four premature failures. Two specimen failures occurred during setup, and two specimens failed during testing with all failures occurring outside of the gauge section.

The ductile-to-brittle transition temperatures determined for the several material thicknesses are listed in Table 7. For reference, the variation of base-metal ductility with temperature is shown in Figure 133 for the 0.055-in. molybdenum-0.5% titanium alloy sheet, and in Figure 136 for the 0.050-in. tungsten, respectively. In all cases, the ductile-to-brittle transition temperature was arbitrarily chosen to be that temperature at which a bend angle of 30 degrees was achieved before the onset of cracking.

Trial-weld Evaluation Results

Penetration Test Results: Results of the simulated weld tests for the determination of approximate welding settings are illustrated in Figures 35 through 40. Depth of weld penetration as a function of beam current and accelerating voltage is plotted in Figure 35 for Mo-0.5% Ti and in Figure 36 for tungsten. Figures 37 and 38 present plots of weld penetration versus welding speed for Mo-0.5% Ti and tungsten, respectively. The effect of transverse beam oscillation ("Y" oscillation) on penetration in Mo-0.5% Ti is shown in

RESULTS OF TESTS (continued)

Figure 39 and in tungsten in Figure 40. Because of varying welding speeds and limited penetration, the pulsing test results were not suitable for graphical presentation.

Mo-0.5% Ti Trial-weld Results: In general, all three thicknesses of the Mo-0.5% Ti were easily weldable by electron beam techniques. No problems were encountered in producing sound, crack-free welds. As expected, weld quality was strongly dependent on welding conditions. Best quality welds were associated with minimum fusion and heat-affected zones in combination with smooth, continuous, crack-free, non-undercut weld beads. Minimum fusion and heat-affected zones were dependent on minimum energy input to the workpiece through welding at high speeds with minimum beam diameter. High-quality weld beads were promoted by moderate beam oscillation along the weld ("X" oscillation).

Micrographs of weld cross-sections and microstructures for the 0.100-in. and 0.055-in. Mo-0.5% Ti butt welds are presented in Figures 41 through 54. In brief, Figures 41 and 42 show the effects of welding at slow welding speeds, Figures 43 and 44 represent welds produced at relatively fast welding speeds, Figures 45 and 46 are associated with welding with a pulsed beam, Figures 47 and 48 illustrate the effects of a defocused beam, and Figures 49 and 50 demonstrate the effects of "Y" oscillation. Figures 51 through 54 illustrate the weld cross-sections and microstructures associated with the final weld settings for the 0.100-in. and 0.055-in. Mo-0.5% Ti. Both thicknesses were welded at relatively high welding speeds with focused beams oscillated along the weld seam.

It is of interest that the Mo-0.5% Ti trial welds with extended fusion and heat-affected zones were difficult to cut for bakelite mounting without fracture. On the other hand, the welds of limited fusion and heat-affected zones were not notably prone to fracture during metallographic preparation.

Etched weld beads from trial welds in 0.005-in. Mo-0.5% Ti appear in Figures 55 through 62. Figure 55 shows the grain structure resulting from slow welding speeds while Figure 56 represents a weld made at a relatively fast welding speed. Figures 57 and 58 illustrate the effects of small and large "Y" beam oscillation at relatively fast welding speeds. The weld of Figure 59 was made at similar conditions to the weld of Figure 58 except at a slower welding speed. The effects of "X" beam oscillation are shown in Figure 60 and the effects of pulsed beam operation in Figure 61. The weld of Figure 62 was made at settings similar to the weld of Figure 60 except the weld was chilled by backing the seam with copper during welding.

Tungsten Trial-weld Results: All three thicknesses of the pure tungsten were successfully welded by electron beam techniques. As with the Mo-0.5% Ti, best quality welds were associated with minimum fusion and heat-affected zones in combination with smooth, continuous, crack-free, non-undercut weld beads. Again, minimum fusion and heat-affected zones were dependent on minimum energy input to the workpiece through welding at maximum speeds with minimal beam diameters. Acceptable weld beads were induced by moderate "X" beam oscillation. Further, the elimination of weld bead cracking was dependent on correct fixturing techniques.

RESULTS OF TESTS (continued)

Early in the trial welding of tungsten an effect resembling fine shrinkage cracking was consistently observed on weld-bead surfaces in all three thicknesses. Figures 63 and 65 illustrate this effect on unetched weld beads in 0.005-in. tungsten. Attempts to eliminate this apparent weld cracking were based on preheating, on fixturing modifications, and on many changes in welding machine settings. Preheating was the only technique that appeared to reduce the effect.

Comprehensive study of the "cracks" revealed that many of the tungsten welds that were thought to be cracked were simply showing grain-boundary relief on the weld-bead surface. Comparison of the unetched weld-bead surfaces of Figures 63 and 65 with their etched counterparts of Figures 64 and 66 illustrates this effect. Note that the fine surface traces, which appear to be cracks, are replaced, upon etching, by grain boundaries.

Other evidence also indicated that the surface effect was not cracking. Fluorescent penetrant inspection of the specimens revealed no crack indications. Careful metallographic inspection of weld cross-sections indicated that the effect did not extend into the interior of the weld bead.

Resolution of the weld-bead grain-boundary effect did not mean that all weld-cracking problems in tungsten were immediately eliminated. A number of welds in all three thicknesses did show true weld cracking. For example, Figures 67 and 68 exhibit a weld containing both intergranular and transgranular cracking. In general, the cracking was associated with extended fusion and heat-affected zones. However, to eliminate cracking in welds of even narrow weld zones, spring-loading of the butted pieces was required.

Micrographs of weld cross-sections and microstructures in 0.100-in. and 0.050-in. tungsten are illustrated in Figures 67 through 82. The weld of Figures 67 and 68 was welded at a slow speed, while the weld of Figures 69 and 70 was welded at a relatively fast welding speed. Figures 71 and 72 illustrate a weld produced with "Y" oscillation at slow welding speed. The weld of Figures 73 and 74 was also produced with "Y" oscillation but at a faster welding speed. Beam oscillation in the "X" direction was employed in producing the weld of Figures 75 and 76. Figures 77 and 78 illustrate the cross-section and microstructure associated with the final weld settings for 0.100-in. tungsten. Figures 79 and 80 illustrate a weld produced with settings that were intended for final welding of the 0.050-in. tungsten. Initial final-weld evaluation indicated that the weld was of inferior quality. Therefore, new settings were developed employing the faster welding speeds available on a recently acquired Hamilton-Zeiss machine. Figures 81 and 82 illustrate the cross-section and microstructure developed by the new final-welding technique.

As with the Mo-0.5% Ti, the trial welds associated with extended fusion and heat-affected zones were extremely prone to fracture during metallographic preparation. This again demonstrated the desirability of producing limited fusion and heat-affected zones.

Etched weld beads from trial welds in the 0.005-in. tungsten are illustrated in Figures 83 through 86. The weld of Figure 83 was welded at a relatively

RESULTS OF TESTS (continued)

fast speed. Figure 84 illustrates a weld made with "y" oscillation while the weld of Figure 85 was produced with "x" oscillation. Using the higher welding speeds available with the Hamilton-Zeiss equipment, the weld of Figure 86 was produced at extremely high welding speeds. In general, the effects of the various welding conditions on weld-zone characteristics duplicated the effects on the 0.005-in. Mo-0.5% Ti.

Miscellaneous Trial-weld Results: The welding effects noted in trial butt welding also held for the lap, seam, edge, and spot welding. However, in view of the varying configurations, many of the successful butt-welding settings had to be altered to suit the particular configuration desired. In lap, seam, and edge welding, emphasis was placed on welding at high speeds. However, significant "y" oscillation was also employed to create a wide interface between the welded surfaces. In spot welding emphasis was placed on minimum energy input consistent with adequate weld interface formation.

Final-weld Evaluation Results

Visual inspection of the final welds indicated that the weld beads were smooth, continuous, and crack-free. In the 0.100-in. tungsten, a slight amount of smooth, shallow undercutting was noted. Radiographic and fluorescent penetrant inspection revealed no cracking or porosity in the final welds.

Representative examples of the final butt welds in all three thicknesses of each material are illustrated in Figures 87 through 108. Figures 87, 88, and 89 illustrate, in order, an overall view of the 0.005-in. Mo-0.5% Ti weldment, a 20X magnification of the etched weld bead, and a 200X magnification of the weld-zone microstructure. Figures 90, 91, 92, and 93 illustrate, respectively, an overall view of the 0.055-in. Mo-0.5% Ti weldment, a 20X magnification of the weld bead, a 20X magnification of the weld-zone cross-section, and a 100X magnification of the microstructure. Figures 94, 95, 96, and 97 illustrate, in the same order as in the 0.055-in. Mo-0.5% Ti, the weldment, weld bead, weld cross-section, and weld microstructure for the final welds in 0.100-in. Mo-0.5% Ti. Figures 98 through 108 present identical illustrations for the final butt welds in 0.005, 0.050, and 0.100-in. tungsten.

Microhardness values taken from fusion zones of the final electron beam welds in all material thicknesses are presented in Table 8. For comparative purposes, the hardnesses of the base metal in both the as-received and recrystallized condition are also listed.

Figures 109 through 124 illustrate final welds produced in the miscellaneous welding configurations. Figures 109 and 110 show an overall view and a 20X cross-section of a seam weld in Mo-0.5% Ti. The seam weld in 0.050 tungsten is shown in Figures 111 and 112. Lap welds in the Mo-0.5% Ti material are shown in Figures 113 and 114, and tungsten lap welds in Figures 115 and 116. Figures 117 and 118 illustrate spot welding results in the 0.055-in. Mo-0.5% Ti, and Figures 119 and 120 show the final spot welds in 0.050-in. tungsten. Final edge welds are shown in Figures 121 and 122 for the Mo-0.5% Ti and in Figures 123 and 124 for the tungsten.

RESULTS OF TESTS (continued)

Results obtained from tensile testing the final electron beam weldments at both room and elevated-temperatures are presented in Table 9. The table includes room-temperature tensile results from seam welds in the 0.055-in. Mo-0.5% Ti. Test results from the tungsten weldments are incomplete due to the high incidence of premature failures, both in the weld and in the base metal, during specimen manufacture and test setup. Test results are also missing for most of the miscellaneous configurations because such configurations did not lend themselves to a standard test technique. In every case, strengths for seam, lap, spot, and edge welds could be varied at will up to at least the strength of the recrystallized base metal by varying the weld interface area.

Figure 125 illustrates the effect of increasing temperature upon the tensile strength of electron beam welded 0.055-in. Mo-0.5% Ti. Base metal results are also included on the plot.

Photomicrographs representative of tensile failures in the 0.055-in. Mo-0.5% Ti weldments are presented in Figures 126 through 128. Figure 126 shows a relatively brittle weld-zone failure representative of room-temperature fractures. Figure 127 illustrates the ductile weld-zone failures that occurred at 1600°F. A representative base-metal failure in a Mo-0.5% Ti weld tested at 2200°F is shown in Figure 128.

Tensile strength versus temperature for electron beam welded 0.050-in. tungsten is shown in Figure 129 along with similar data for the base metal. Because of the lack of room-temperature data, the curve for the electron beam welded material is a rough extrapolation, probably on the conservative side.

A typical room-temperature brittle weld-zone failure in tungsten is shown in Figure 130. Figure 131 illustrates a ductile failure representative of testing at 2500 F. A 2800°F base-metal failure, with the weld-zone completely out of the image area, is shown in Figure 132.

The ductile-to-brittle transition temperatures for electron beam weldments in all three thicknesses of Mo-0.5% Ti and tungsten are summarized in Table 10. The changes in transverse bend ductility with temperature for weldments in 0.055-in. and 0.100-in. Mo-0.5% Ti and 0.005-in. and 0.050-in. tungsten are shown in Figures 133 through 136. For reference the base-metal results are included on the same plots (except the 0.100-in. Mo-0.5% Ti, which was ductile at room temperature). Bend ductility of 0.005-in. Mo-0.5% Ti electron beam welds are not plotted as a function of temperature as they were ductile at room temperature.

Bend tests on the 0.100-in. tungsten welds showed that the welds were brittle to at least 900°F. Further testing was temporarily discontinued for lack of specimens. When more specimens became available it was discovered that superior results were being obtained in the 0.050-in. tungsten by welding at extremely high speeds. Lack of time prevented the welding of both 0.050-in. and 0.100-in. tungsten at high speeds. Therefore, instead of pursuing bend testing of welds known to be of less than optimum quality, work was concentrated on the evaluation of high-speed welding of 0.050-in. tungsten.

DISCUSSION OF RESULTS

Base-metal Discussion

Visual inspection of the as-received Mo-0.5% Ti and pure tungsten indicated that, except for the 0.055-in. Mo-0.5% Ti, all sheets were of acceptable quality. Sheets that were supplied as-rolled exhibited some lamination near the edges, but these were removed by trimming. The small striations on the one surface of the 0.055-in. Mo-0.5% Ti were probably introduced during rolling. To minimize detrimental effects on ductility, all bend testing was performed with the striated surface in compression.

The chemical analysis of the base materials (Table 4) were within normally expected limits.

Metallographic examination of the base-metal microstructures (Figures 23 through 34) revealed some unexpected grain size differences. As anticipated, the 0.005-in. material (Figures 23, 24, 29, and 30) exhibited relatively fine grain size. However, the grain size of the 0.050-in. tungsten (Figures 31 and 32) and particularly the 0.055-in. Mo-0.5% Ti (Figures 25 and 26) was larger than the grain sizes of the corresponding 0.100-in. material, in both the as-received and recrystallized condition. This indicates that after the last recrystallization, the percentage reduction in sheet thickness in rolling to the 0.100-in. thickness was greater than in rolling to the 0.055-in. thickness.

The effects of the fabrication-induced microstructural differences were manifested in the hardness, tensile, and bend properties of the base metal. As listed in Table 5, the diamond-pyramid hardness values for the 0.055-in. Mo-0.5% Ti were significantly lower than the 0.100-in. properties in two of the three planes of testing. These differences are not apparent in the 0.050-in. and 0.100-in. tungsten data, probably because of the smaller difference in comparative grain size.

The tensile properties of the 0.005-in. and 0.100-in. Mo-0.5% Ti (Table 6) were within the range of expected values. In the 0.055-in. Mo-0.5% Ti, the effects of the relatively large grain size held the room-temperature tensile properties below normally reported values. However, with increasing test temperature the difference between actual and expected values decreased and at temperatures above 1900°F was non-existent.

Review of the fabricating history of the 0.055-in. sheet with the supplier¹ confirmed that this particular sheet of Mo-0.5% Ti was not of representative quality. The inferior mechanical properties were related to the sheet rolling schedule and surface condition. The rolling schedule consisted of a series of reductions and recrystallizations to a 0.125-in. thickness before final reduction. Therefore, the final roll pass, after a recrystallization at 2450°F, represented less than a 60% reduction in sheet thickness, (thus, the relatively coarse grain size of Figures 25 and 26.) Recent experience has indicated that a reduction of greater than 60% is required to promote the desired strength and ductility. The small surface striations (0.020 in. to 0.050 in. in length) on the Mo-0.5% Ti may have also contributed to the low room-temperature tensile properties by acting as stress-concentrating sites.

DISCUSSION OF RESULTS (continued)

The room-temperature tensile properties of all thicknesses of the tungsten base-metal were obscured by the extreme brittleness of the material. The brittleness resulted, in part, from the surface imperfections present in the commercially available tungsten that act as stress-concentration sites and promote brittle fracture ². Every reasonable precaution was taken to eliminate notches, laminations, and other defects that could initiate brittle failures. This included careful machining, comprehensive visual and fluorescent penetrant inspection, and chemical polishing. Still, as the widely-variant test results indicate, defects were present that propagated failure at relatively low stresses. In fact, in both base-metal and weld testing, premature fractures occurred in all phases of specimen manufacture and test. Further, even after successful manufacture and tensile-test initiation, a number of specimens failed outside the reduced test section. Therefore, the room-temperature data reflect only limited information relative to the actual tensile strength and are included solely for rough comparison to weld data.

The tungsten specimens tested at temperatures in the range of 2200°F to 2800°F all failed in a ductile manner at reasonably uniform values. Therefore, these data are considered valid.

The bend-test results (Table 7) again demonstrate the difference in quality between the 0.005-in. and 0.100-in. Mo-0.5% Ti, ductile at room temperature, and the 0.055-in. material, which was completely ductile only at temperatures exceeding 200°F. All testing of the 0.055-in. material was performed with the striations in compression.

In bend testing tungsten, as in tensile testing, the notch sensitivity induced extreme brittleness at room temperature in both the 0.050-in. and 0.100-in. material. However, the ductile-to-brittle transition temperatures of the two thicknesses (Fig. 136 and Table 7) were within the range of expected results. The 0.005-in. material demonstrated good room-temperature ductility. This was undoubtedly associated with the smoother surface finish and finer grain size.

Trial Weld Discussion

Penetration Tests: The effect of current and voltage on weld penetration in Mo-0.5% Ti (Figure 35) and tungsten (Figure 36) indicated, as expected, an increase in penetration with increasing current and voltage. A simple calculation from the data demonstrates that at a given beam power greater penetration is achieved with higher accelerating voltages. In Figure 35, for example, weld penetration of 0.100 in. is achieved in Mo-0.5% Ti at 1300 watts using an accelerating voltage of 130 KV and a beam current of 10 ma. With an accelerating voltage of 150 KV (and a current of 8.7 ma) the penetration increases to approximately 0.115 in.

Figures 37 and 38 indicate the effect of increased penetration with decreased welding speed. It appears that with a beam of maximum power (150 KV, 20 ma) Mo-0.5% Ti could be welded at five inches per minute in thicknesses exceeding 0.250 in. and tungsten in thicknesses exceeding 0.200 in. Data are not included for welding speeds in the area of 100 inches per minute because this capability became available only very late in the program. However,

DISCUSSION OF RESULTS (continued)

experience has shown that 0.050-in. tungsten can be welded at 100 inches per minute with welding conditions in the range of 150 KV and 14 ma.

Figures 39 and 40 indicate that weld penetration at first falls off rapidly and then levels out with increased transverse ("Y") beam oscillation amplitude. The results are reasonable, because welding with an oscillating beam should create the same effect on weld penetration as welding at higher speed. In fact, it is interesting to note the similarity of the beam oscillation plots to the welding speed plots.

No curves are included for the effect of pulsing on weld penetration. The requirement for the simultaneous variation of welding speed, pulsing frequency, and beam on-time made the data unacceptable for graphical presentation. It should be noted, however, that the introduction of pulsing drastically reduced penetration in tungsten and Mo-0.5% Ti.

Mo-0.5% Ti Trial Welds: The wide range of settings used in the production of electron beam welds in Mo-0.5% Ti indicates a high degree of weldability for the alloy. The welds illustrated in Figures 41 through 62 are representative of the many welds produced by a variety of settings. Almost all of the welds illustrated were sound and crack-free. There are, however, definite differences in weld characteristics.

The weld of Figure 41, produced at a relatively slow welding speed (7ipm) exhibits the classical wedge-shaped fusion zone. However, the heat-affected zone is relatively wide and the fusion-zone grain size (Figure 42) is comparatively large (ASTM Ferrous Grain Size Standard 3 to 4 at 100X).

By increasing the welding speed to 27 ipm, a weld (Figure 43) of drastically reduced heat-affected zone was produced. Moreover, the grain size (Figure 44) has dropped to ASTM 5 to 6. However, the weld bead is characterized by a notch-like undercut. Even narrower welds were produced using higher voltages; however, the undercutting became increasing pronounced.

The weld of Figure 45, produced with a pulsed beam, represents an attempt to eliminate the undercut of Figure 43 while retaining the limited heat-affected zone. It is obvious that pulsing the beam has decreased the power to such an extent that penetration is inadequate. Further, even with so little penetration the heat-affected zone represents no improvement, and the grain size (Figure 46) has actually increased to ASTM 3 to 4.

Results of welding with a defocused beam are illustrated in Figure 47. The undercut has been effectively eliminated. However, the greatly increased energy input to the workpiece has promoted extended fusion and recrystallization. Although not completely shown in Figure 48, grain size varied across the weld from ASTM 2 to 4.

The effects of welding with a beam oscillated in the "Y" direction are illustrated in Figure 49. Both the fusion and recrystallized zones are extremely large as is the grain size (Figure 50) at ASTM 2.

DISCUSSION OF RESULTS (continued)

The weld-zone characteristics induced by welding with an oscillated beam as well as with a defocused beam (Figure 47) will, of course, vary with the severity of the deflection or defocus. The tendency of the weldments of both Figure 47 and 49 to fracture during metallographic preparation demonstrates the desirability of limiting the fusion and recrystallized zones. Thus, if required, "Y" oscillation or beam defocusing should be kept to a minimum consistent with the retention of other desirable weldment characteristics.

In an attempt to eliminate the requirement for defocusing, welds were produced using "X" beam oscillation. An example is shown in Figure 51. The fusion and heat-affected zones are slightly wider than with a non-oscillated beam (Figure 43); however, the undercutting has been eliminated. (The apparent defect at the bottom of the weld occurred during metallographic preparation). The microstructure of the weld is illustrated in Figure 52. The relatively fine grain size (5 to 6) at the center of the illustration represents the last area to solidify. Grain size increased at the edge of the weld to 3. The settings used to produce this weld were chosen as the final settings for the welding of 0.100-in. Mo-0.5% Ti.

As discussed under Description of Tests, the 0.055-in. Mo-0.5% Ti reacted to like welding conditions in a manner similar to the 0.100-in. material. Therefore, to prevent undercutting, an "X" oscillated beam was again required on the 0.055-in. material. Figure 53 illustrates a trial weld in 0.055-in. Mo-0.5% Ti produced with settings that were chosen for final welding. Because of the thinner sheet thickness the depth-to-width ratio of the weld is decreased relative to the 0.100-in. weld. The grain size (Figure 54) and the slightly increased fusion and heat-affected zone width result from the fact that with decreased thickness comparatively less mass is available to chill the weld.

Weld beads, rather than weld cross-sections, were used in evaluating the trial welds in the 0.005-in. Mo-0.5% Ti. Weld-cross sections in such thin material are of insufficient thickness to assume characteristic weld-zone patterns. However, a view of the weld solidification pattern along the bead gave meaningful results.

The weld in Figure 55, produced at a relatively slow speed, shows a wide recrystallized zone and slightly elongated grain growth. (The direction of welding in Figures 55 through 62 is right to left). By increasing the speed (Figure 56), the width of the heat-affected zone was decreased. The tendency for grain elongation was also inhibited.

Oscillation of the beam in the "Y" direction aggravated the grain-growth problem. In succession, Figures 56, 57, and 58 illustrate welds of zero, 0.020-in., and 0.040-in. "Y" oscillation. As expected the fusion-zone width increases with increased oscillation. However, the extent of recrystallization in the thin material is apparently not dependent on oscillation amplitude.

Comparison of Figures 58 and 59 demonstrates, as expected, that decreasing the speed while maintaining beam oscillation simply induces a wider heat-affected zone.

DISCUSSION OF RESULTS (continued)

The use of "X" beam oscillation (Figure 60) gives results almost identical to those obtained when welding with a non-oscillated beam (Figure 56). The only apparent difference is a slightly varied grain pattern and a slightly increased heat-affected zone. These "X" oscillation results are consistent with those noted in the 0.100-in. Mo-0.5% Ti (Figure 51).

Welding with a pulsed beam (Figure 61) tended to reduce the heat-affected zone, but with the particular settings used, a very straight, continuous grain boundary was formed down the center of the weld.

The use of chills was very effective in reducing the extent of recrystallization. In fact, the weld of Figure 62 has almost no heat-affected zone. Further, the weld-zone grain size is extremely small and shows no oriented grain growth. The welding conditions associated with Figure 62 were chosen for the final welding of the 0.005-in. Mo-0.5% Ti. Chilling was practical only for the 0.005-in. Mo-0.5% Ti. The 0.100-in. and 0.055-in. material were so massive relative to the extremely small fusion-zone size, that chilling was of little value.

As with the 0.055-in. and 0.100-in. material, the welds in the 0.005-in. Mo-0.5% Ti again demonstrated the desirability of limited fusion and heat-affected zones. Many of the welds of wide fusion zone (e.g. those of Figures 55, 57, 58, and 59) failed during handling; whereas those of more limited weld-zone size were considerably more rugged.

Summarizing the trial welding of Mo-0.5% Ti, best welds were produced by welding at relatively high welding speeds with minimum spot size. Slight beam oscillation along the weld was required to produce weld beads of acceptable quality. Extremely high-speed welding was not investigated on Mo-0.5% Ti because, as mentioned, the high-speed capability was not available until late in the program. However, in view of the superior results achieved with the tungsten, discussed below, it appears that high-speed welding of Mo-0.5% Ti may offer advantages not exploited in the Mo-0.5% Ti trial welding of the present program.

Tungsten Trial Welds: In general, all thicknesses of tungsten revealed weld characteristics similar to the Mo-0.5% Ti. However, due to the extreme brittleness of the material, less latitude was available in choosing welding techniques. Figures 63 through 86 illustrate welds representative of those produced during the trial welding of tungsten.

The fine, grain-boundary effect, illustrated in Figures 63 through 66, was noted on all electron beam welds in tungsten. The apparent decrease of the effect with preheating resulted from the formation of larger grains. Because of the larger grain size, there were fewer grain boundaries and thus less evidence of grain-boundary relief on the weld-bead surface. Conversely, when welds of fine grain size were produced, the effects of grain-boundary relief were increased.

True weld cracking was also noted in tungsten. For example, the weld of Figures 67 and 68 illustrates a transgranular crack at the surface and an

DISCUSSION OF RESULTS (continued)

intergranular crack on the interior. The extremely slow welding speed promoted very large grains at the weld surface (ASTM 0), and extended heat-affected zone (out of the photo image area). This coarse grain size undoubtedly contributed to the cracking. However, by using spring-loaded fixtures, welds made at identical welding conditions were crack free. Apparently, although extremely limited shrinkage occurs across the weld (generally less than 0.100 in. in tungsten), cracking will occur if the weld is restrained from shrinking.

The weld of Figures 69 and 70 demonstrates that grain size (ASTM 3 to 4) and extent of fusion and recrystallization were reduced by welding at faster speeds. However, as with the Mo-0.5% Ti, the weld bead was undercut.

Use of extreme "Y" beam oscillation at slow welding speeds eliminated the undercutting, but in the process recrystallized the total weldment (Fig. 71) and promoted large grain size (ASTM 1). Metallographic mounting of welds of such extended heat-affected zone and large grain size resulted in many weld fractures.

Increased welding speed and decreased beam-oscillation amplitude (Figures 73 and 74) reduced both the grain size (ASTM 3) and extent of fusion and recrystallization. However, undercutting again occurred.

Use of "X" beam oscillation (Figures 75 and 76) eliminated undercutting and simultaneously reduced the grain size (ASTM 3) and fusion and heat-affected zones. However, there was a tendency for non-uniform depth of penetration along the bottom of the weld.

Non-uniform penetration was eliminated through the use of a slightly defocused beam in combination with "X" beam oscillation (Figures 77 and 78). Both the grain size (ASTM 3) and fusion and heat-affected zones have been slightly increased. However, the weld-bead condition was improved to acceptable quality. The welding conditions of the weld of Figures 77 and 78 were used in producing the final welds in the 0.100-in. tungsten.

Similar final weld settings were used in producing the initial "final" welds in the 0.050-in. tungsten (Figures 79 and 80). The settings were chosen because the weld exhibited relatively small grains (ASTM 3 to 4) and limited fusion and recrystallized zones. However, initial testing indicated that the welds were extremely notch sensitive and subject to premature fracture.

Improvement in mechanical properties was obtained in the 0.050-in. weld of Figures 81 and 82. This weld, produced at extremely high welding speeds (100ipm), had almost no heat-affected zone. Further, the fusion-zone size was reduced relative to the weld of Figure 79. Grain size was ASTM 4. Because of the improved weld-zone characteristics, the settings used in producing the weld in Figures 81 and 82 were used in final welding the 0.050-in. tungsten.

As with the 0.005-in. Mo-0.5% Ti, trial welds in 0.005-in. tungsten were primarily evaluated by examination of the weld bead. The 0.005-in. material reacted to similar welding conditions in a manner identical to Mo-0.5% Ti, as

DISCUSSION OF RESULTS (continued)

confirmed by Figures 83 through 86.

Welding 0.005-in. tungsten at a relatively fast speed (27ipm) (Figure 83) produced a comparatively narrow fusion and heat-affected zone with some tendency for elongated grain growth. The introduction of "Y" beam oscillation (Figure 84) extended both the fusion and heat-affected zones and developed larger grain size. Use of "X" beam oscillation (Figure 85) produced a finer grain size but larger recrystallized zone than when welding with a non-oscillated beam (Figure 83). Increasing the welding speed to 100 inches per minute (Figure 86) inhibited the recrystallization apparent in the weld of Figure 83. Grain size was also reduced.

Welding with chills reduced the grain size but appeared to promote cracking, perhaps due to extremely fast cooling. Therefore, the weld settings associated with Figure 86 were chosen for final welding of the 0.005-in. tungsten.

In summary, trial welding of the tungsten indicated that best welds were produced with high welding speeds and minimal spot size. A very small amount of defocusing of the beam was required to develop beads of acceptable quality on the 0.100-in. thickness. Premature fractures during metallographic preparation indicated that minimum fusion and recrystallized zones are required for maximum strength and ductility.

Miscellaneous Trial-welds: Effects that were similar to those developed in butt welding were noted in producing the spot, seam, edge and lap configurations. To a great degree, mechanical properties of such configurations are dependent on the width of the weld interface. Thus, the use of "Y" beam oscillation was required, and larger fusion and heat-affected zones resulted. Spot welds were particularly prone to large-grain formation.

Smaller fusion zones with adequate interface area could have been produced in seam welding by making successive high-speed weld passes with a non-oscillated beam. Similarly, a number of small-diameter spot welds could be used in place of a single large-diameter weld. However, an investigation of all of the possible welding techniques for the miscellaneous weld configurations was not within the scope of the program.

Final Weld Discussion

The consistent production of sound crack-free final welds in a variety of configurations indicates that both tungsten and Mo-0.5% Ti are reproducibly weldable by electron beam techniques.

The final butt welds, illustrated in Figures 87 through 108 are, in general, self-explanatory. In every case the size of the fusion zones, the recrystallized zones, and the grain size were less than those generally published for arc welds in the same material thicknesses. Further reduction in grain size and size of fusion and recrystallized zones in all of the Mo-0.5% Ti thicknesses and on the 0.100-in. tungsten would be accomplished by welding at the higher welding speeds now available.

DISCUSSION OF RESULTS (continued)

As noted in trial welding, the grain sizes and fusion and heat-affected zone sizes in the lap, seam, spot, and edge welds (Figures 109 through 124) were larger than in the butt welds. The cross-sections illustrate varying interface contact areas, which are dependent solely on the choice of machine settings. The extremely large grain size associated with the tungsten spot weld (Figure 120) resulted from the comparatively long welding time (16 seconds). In fact, the total final weldment reached red heat during welding.

The room-temperature tensile strength exhibited by electron beam welds in all three material thicknesses of the Mo-0.5% Ti alloy was slightly lower than the tensile strength of recrystallized base metal. The three material thicknesses (0.005, 0.050, and 0.100 in.) all possessed strengths in the same range (70,000 to 90,000 psi), an indication of the uniformity of electron beam welds in various material thicknesses. The elongation obtained in weldments tested at room temperature was, however, lower than that obtained for base metal. This can be explained on the basis of reduced ductility in the weld-zone recrystallized grains.

Figure 125 shows the continuous approach of the tensile strength of the weld to that of the base metal with increasing temperature. At 2200°F, electron beam weldments demonstrated tensile strengths essentially equivalent to base-metal strength at the same temperature—two failures occurring in the base material of welded tensile specimens. Based on the data shown in Figure 125, the tensile strength of electron beam weldments at temperatures approaching the recrystallization temperature (approximately 2450°F) is equivalent to the base-metal strength.

Figures 126 through 128 show tensile failures representative of those occurring at various testing temperatures. Figure 126 is a photomicrograph of a welded tensile specimen, after failure at room temperature. Failure has occurred at the interface of the fused and recrystallized zone, and is both intergranular and transgranular in nature. No apparent elongation of grains has occurred. A weld-zone failure that occurred in a specimen tested at 1600°F is shown in Figure 127. The increased ductility of the weld can be clearly seen in this photo. Considerable elongation has occurred in the fused grains. Failure occurred by transgranular shear. Figure 128 illustrates a base-metal failure in a welded specimen tested at 2200°F. Failure took place in the base material completely out of the heat-affected zone. Weld ductility can be seen in the heat-affected zone.

The results indicate that electron beam welded butt joints in Mo-0.5% Ti possess strength properties in excess of similar joints produced by inert-atmosphere fusion welding techniques³. At service temperatures above 2000°F, electron beam welded joints possess load-carrying capacities 50% greater than conventionally produced weldments.

In addition to butt joints, several seam-welded joints in 0.055-in. material were tested at room temperature. The joint failures were tensile in nature and occurred in the heat-affected zone. Smaller interface areas between the lapped pieces would have promoted shear-type failures within the weld.

DISCUSSION OF RESULTS (continued)

As with the base-metal, tensile testing of tungsten weldments at room temperature failed to generate any meaningful results. The compound problem of brittleness due to surface condition and low weld ductility created many problems in room-temperature testing of the tungsten welds.

From the results of the elevated-temperature tensile testing it can be concluded that good joint integrity can be achieved in butt joints of tungsten sheet. Figure 129 shows that the tensile strength of the electron beam welded tungsten joints approaches that of the base metal as the temperature of testing is increased. As was also the case for Mo-0.5% Ti welds, the tensile strength of the tungsten welds appears to be equivalent to that of the base metal at temperatures approaching the recrystallization temperature.

Room-temperature tensile failures in the weld zone (Figure 130) are brittle in nature, and occur primarily intergranularly. The weld-zone failure at 2500°F (Figure 131) shows relatively good ductility and considerable amount of necking prior to failure. Fused grains were greatly elongated during reduction in area immediately before failure. A failure that occurred in the base metal of a welded specimen tensile tested at 2800°F is shown in Figure 132. The weld zone is completely out of the image area.

In the interpretation of the bend test data, a number of factors must be considered. First, to duplicate expected service application, all bend testing was performed on weldments whose weld beads were in the as-welded condition. That is, they were not finish ground. The weld beads of the 0.005-in. Mo-0.5% Ti and tungsten were comparatively smoother. However, as is apparent from Figures 91, 95, 102, and 106 the beads on the 0.050 and 0.100-in. material, although relatively smooth to the naked eye, exhibited considerable roughness under magnification. Molybdenum and also tungsten¹ are sensitive to surface condition. Semchyshen and Barr⁴ report a significant change in transition temperature between, for example, electropolished and caustic dipped molybdenum. Thus, the ductility for the as-welded electron beam specimens is probably lower than it would have been with finish-ground specimens.

A second factor to be considered is the effect of strain rate on transition temperatures. Weare and Monroe⁵ report that "relatively small changes in strain rate can shift the fracture behavior from ductile to brittle at room temperature". The deflection rates used in bend testing the electron beam welds were on the high side of those reported for other techniques.

The third, and perhaps most important fact to be considered in studying the bend ductility results is the extreme concentration of stress that occurred in the narrow electron beam weld zone during plastic deformation by bending. In bending either arc or electron beam welds, the stronger cold-worked material on either side of the weld does not plastically deform. Thus, the strain must be absorbed by the cast and recrystallized grains until fracture occurs. With normal arc welds, the weld zone is generally wide enough to include the total section of the specimen that is receiving bending stresses. Therefore, plastic deformation can occur over perhaps 0.250 in. (as were the size of Platte's⁶ weld beads), or the portion thereof subjected to plastic strain. However, with electron beam welds, the fusion-zone is much smaller, being

DISCUSSION OF RESULTS (continued)

approximately 0.040-in. wide in welds of Figures 92 and 96. Therefore, no matter how wide the span subjected to bending stresses, all of the strain generated was absorbed by a 0.040-in. wide zone of cast material. Thus in bend testing, the outermost fiber stresses in the weld zone reached extremely high values with very little deflection of the specimen. Failure, therefore, occurred at what appears to be a low ductility value even though the actual local deformation within the strained region was probably quite high.

As apparent in Figures 92 and 96, weld-zone width does not increase appreciably with increasing thickness. (Exception must be made for very thin material which can have somewhat narrower weld zones). The effect of concentrating bending stresses in the weld zone became more severe with increasing thickness due to the type of bend test that was performed. At initial stages of specimen deflection, with the comparatively small bend radii employed, little more than point contact was made with the specimen surface. Thus, with a given amount of deflection ($\frac{Mc}{I}$) the outermost fiber stresses on the thicker material were greater, and these increased stresses had to be absorbed by the same weld width as the lower stressed thinner materials.

The apparent decrease in bend ductility with increasing thickness is demonstrated in Table 10. Note that the 0.055-in. welds achieved greater apparent ductility than the 0.100-in. welds, although the reverse is true for the base metal. Since the grain size and extent of fusion and recrystallization, of the two thicknesses are very similar, the decrease in apparent ductility was probably due to thickness differences. Similar effects are noted for the tungsten, although the extreme inherent brittleness and the widely variant welding conditions undoubtedly had independent effects on ductility.

From the preceding discussion of bend ductility it can be seen that the type of bend test employed does not accurately reflect the true ductility of the welds when such ductility data is compared with base-metal or arc-weld data obtained from similar test conditions. In fact, it would appear that for the sole purpose of generating "good" ductility data, the fusion zones should be of sufficient size to completely comprise the total strained area of the specimen. Test results indicate that this assumption is not true. The advantages of narrow fusion and heat-affected zones were effectively demonstrated in trial welds where low service ductility was associated with the welds of extended fusion and recrystallization.

Correlation of electron beam weld ductility data with comparable data for arc welding is difficult due to differences imposed by the aforementioned considerations and also differences in testing technique. Platte⁶ reports room-temperature bend angles of 80 to 120 degrees for several molybdenum alloys welded by the tungsten-arc method. However, the welds were ground smooth, the strain was lower (0.1 in. per min. as opposed to 0.5 in. per min. in the present program), bend radius was not reported, total deflection was measured instead of permanent bend angle, and base-metal properties were different. Further, as mentioned above, the differences in weld-zone width effect the apparent ductility.

Kulju and Kearns³ report bend angles at room temperature ranging from 20 to 97 degrees. Again comparison of the data is difficult because of considerations

DISCUSSION OF RESULTS (continued)

regarding differences in bend radii, specimen preparation, deflection rates, and weld-zone width.

No comparative data for tungsten welds was available. However, the relatively small grain sizes and limited fusion and recrystallization zones obtained in the electron beam welds should contribute to comparatively superior ductility.

BIBLIOGRAPHY

1. Freeman, R. R., Private Communication, 24 August 1961, Climax Molybdenum Company, New York.
2. Stephens, J. R., An Exploratory Investigation of Some Factors Influencing the Room-temperature Ductility of Tungsten. NASA TN D-304, (1960).
3. Kulju, K. M. and W. H. Kearns, Welding of Molybdenum Alloy Sheet, Welding Journal, Research Supplement, 37 (10), 440s-444s, (1958).
4. Semchyshen, M. and R. Q. Barr, Mechanical Properties of Molybdenum and Molybdenum-base Alloy Sheet, ASTM Special Technical Publication No. 272, (Symposium on New Metals), 1959.
5. Weare, N. E. and R. E. Monroe, Welding and Brazing of Molybdenum, DMIC Report 108, March 1, 1959.
6. Platte, W. N., Joining of Molybdenum, WADC Technical Report 57-309, August 1957.

TABLE 1
Test Material

<u>Material</u>	<u>Sheet Size</u> <u>(inches)</u>	<u>No. of Sheets</u>	<u>Heat No.</u>
Mo-0.5% Ti	0.005 x 6 x 12 (trimmed)	16	T-5042-A2-2
"	0.055 x 26 x 36 (trimmed)	1	XT-5024-B2-2
"	0.100 x 7 x 12 (as-rolled)	7	T-5036B-1-1
"	0.100 x 7 x 12 (as-rolled)	7	T-5077-A2
"	0.187 x 8 x 12 (as-rolled)	2	T-5036B-1-2
Tungsten	0.005 x 3 x 12 (trimmed)	32	U4.5-2974
"	0.050 x 6 x 12 (trimmed)	12	U4.5-2974
"	0.100 x 7 x 12 (as-rolled)	12	U4.5-2974
"	0.187 x 4½ x 12 (as-rolled)	4	U4.8-2974

TABLE 2

Trial Welding-condition Ranges

Material Thickness (in.)	Acceleration Voltage (KV)	Beam Current (ma)	Welding Speed (ipm)	Oscillation Amplitude (in.)	Pulsing Conditions	Beam Diameter (in.)
0.005 Mo-0.5% Ti	65-110	0.5 to 3	4 to 27	X: 0 to 0.200 Y: 0 to 0.055	10 to 3000cps 0.5 to 10ms	0.010 to .025
0.055 "	100-150	5 to 12	4 to 27	X: 0 to 0.100 Y: 0 to 0.050	10 to 300cps 1 to 10ms	0.010 to .025
0.100 "	120-150	7 to 12	4 to 27	X: 0 to 0.050 Y: 0 to 0.050	10 to 300cps 1 to 10ms	0.010 to .025
0.005 Tungsten	85-110	0.5 to 4	4 to 100	X: 0 to 0.200 Y: 0 to 0.050	10 to 3000cps 0.1 to 10ms	0.010 to .025
0.050 "	120-150	6 to 18	4 to 100	X: 0 to 0.100 Y: 0 to 0.050	none	0.010 to .025
0.100 "	135-150	12 to 20	4 to 27	X: 0 to 0.050 Y: 0 to 0.050	none	0.010 to .025

NOTE: X = Oscillation Along Weld Seam

Y = Oscillation Across Weld Seam

TABLE 3

Final Welding Conditions

Material Thickness (in.)	Weldment Configuration	Accelerating Voltage (KV)	Beam Current (ma)	Welding Speed (ipm)	Welding Oscillation Amplitude (in.)	Other
0.005 Mo-0.5% Ti	Butt	85	1.2	27	0.020 X	
0.055 "	"	120	7	27	0.050 X	
0.100 "	"	135	12	27	0.020 X	
0.005 Tungsten	Butt	90	2.9	100	none	Spring-loaded Fixture
0.050 "	"	145	16	100	0.065 X	Defocused Beam (0.015 in. dia.)
0.100 "	"	150	16	20	0.050 X	Spring-loaded Fixture
0.055 Mo-0.5% Ti	Seam	140	12	27	0.055 Y	
0.050 Tungsten	"	145	12	14	0.050 Y	
0.055 Mo-0.5% Ti	Lap	130	10	14	0.035 Y	Focused 0.005 in. on Lap Side
0.050 Tungsten	"	145	12	14	0.020 Y	Focused 0.006 in. on Lap Side
0.055 Mo-0.5% Ti	Edge	130	8	20	0.060 Y	
0.050 Tungsten	"	140	15	10	0.025 Y	
0.055 Mo-0.5% Ti	Spot	145	12	-	0.045 circular	4 Sec On-time
0.050 Tungsten	"	145	12	-	0.045 circular	16 Sec On-time

NOTE: X = Oscillation Along Weld Seam

Y = Oscillation Across Weld Seam

TABLE 4
Base-metal Chemical Analyses

Material Thickness (in.)	Heat	O (ppm)	N (ppm)	H (ppm)	C (%)	Ti (%)
0.005 Mo-0.5% Ti	T-5042A2-2	7	100	50	0.029	0.44
0.055 "	XT-5024-B2-2	6	46	80	0.029	0.44
0.100 "	T-5077-A2	9	55	100	0.026	0.46
0.100 "	T-5036-B1-1	7	55	63	0.040	0.48
0.005 Tungsten	U4.5-2974	200	70	10	-	-
0.050 "	U4.5-2974	200	70	10	-	-
0.100 "	U4.5-2974	200	70	10	-	-

TABLE 5

Room-temperature Base-metal Hardness Properties

Material Thickness (in.)	Orientation*	Vickers Hardness Number (Average of Seven Readings)	
		As-received	Recrystallized
0.005 Mo-0.5% Ti	Top	359	183
0.005 "	End	263	174
0.005 "	Side	325	193
0.055 Mo-0.5% Ti	Top	296	270
0.055 "	End	242	190
0.055 "	Side	244	189
0.100 Mo-0.5% Ti	Top	242	198
0.100 "	End	312	186
0.100 "	Side	324	186
0.005 Tungsten	Top	782	390
0.005 "	End	548	370
0.005 "	Side	467	379
0.050 Tungsten	Top	471	369
0.050 "	End	445	358
0.050 "	Side	451	375
0.100 Tungsten	Top	450	370
0.100 "	End	447	354
0.100 "	Side	457	351

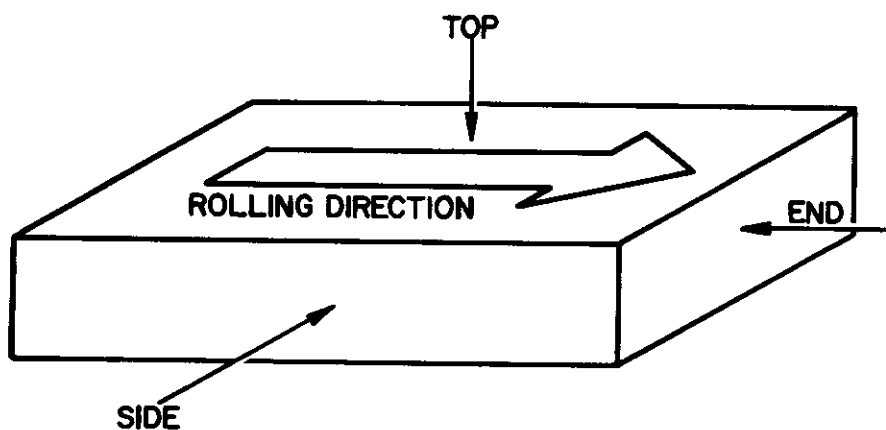


TABLE 6

Base-metal Tensile Properties

Material	Thickness (in.)	Test Temp (°F)	Tensile Strength (psi)	Yield Strength (0.2% offset, psi)	Elong. (%)	Remarks
Mo-0.5% Ti	0.100	RT	144,000	139,600	3	
"	0.100	RT	142,560	138,000	5	
"	0.100	RT	143,700	140,500	6	
"	0.055	RT	93,000	76,600	3	
"	0.055	RT	90,140	73,200	2	
"	0.055	RT	95,750	78,100	2.5	
"	0.055	1600	59,750	54,600	6	
"	0.055	1600	69,200	61,800	10	
"	0.055	1600	66,100	61,700	8	
"	0.055	1900	56,700	42,800	-	Distorted After Test
"	0.055	1900	54,000	49,600	10	
"	0.055	1900	57,100	52,400	10	
"	0.055	2200	34,900	30,600	18	
"	0.055	2200	33,000	30,000	27	
"	0.055	2200	41,280	36,400	14	
"	0.005	RT	121,500	103,500	2	
"	0.005	RT	119,300	107,000	2	
"	0.005	RT	152,500	129,500	6	
Tungsten	0.100	RT	39,300	none	nil	
"	0.100	RT	40,700	none	nil	
"	0.100	RT	-	-	-	Failed During Setup
"	0.050	RT	62,600	none	nil	
"	0.050	RT	85,400	none	nil	
"	0.050	RT	100,050	none	nil	
"	0.050	2200	60,220	56,430	8	
"	0.050	2200	57,300	51,780	8	
"	0.050	2200	58,220	52,890	8	
"	0.050	2500	41,000	37,940	14	
"	0.050	2500	38,500	37,400	24	
"	0.050	2500	-	-	-	Failed During Setup
"	0.050	2800	11,250	7,060	68	

TABLE 6 (continued)

Material	Thickness (in.)	Test Temp (°F)	Tensile Strength (psi)	Yield Strength (0.2% offset, psi)	Elong. (%)	Remarks
Tungsten	0.050	2800	11,520	7,480	51	Data From Base-metal Failures In Weld Specimens
"	0.050	2800	11,800	7,590	46	
"	0.005	RT	344,000	328,000	2	Failed In Grips Failed In Grips
"	0.005	RT	-	-	-	
"	0.005	RT	-	-	-	

TABLE 7

Base-metal Ductile-to-brittle Transition Temperatures

Material	Thickness (in.)	Ductile-to-brittle Transition Temperature
Mo-0.5% Ti	0.100	< RT
"	0.055	170°F
"	0.005	< RT
Tungsten	0.100	820°F
"	0.050	600°F
"	0.005	< RT

TABLE 8

Electron Beam Weld Hardness Properties

Material	Thickness (in.)	Weld-Zone Hardness (VHN)	Comparative Base-metal Hardness	
			As-received (VHN)	Recrystallized (VHN)
Mo-0.5% Ti	0.100	226	312	186
"	0.055	212	242	190
"	0.005	199	263	174
Tungsten	0.100	333	447	354
"	0.050	444	445	358
"	0.005	399	548	370

NOTE: All Hardness Values Are Average Values From Five Or More Determinations.

TABLE 9

Electron Beam Weld Tensile Properties

Material	Thickness (in.)	Test Temp (°F)	Tensile Strength (psi)	Yield Strength (0.2% offset, psi)	Elong (%)	Failure Location
Mo-0.5% Ti	0.100	RT	79,500	74,100	nil	Weld
"	0.100	RT	92,600	78,700	nil	Weld
"	0.100	RT	74,000	69,000	1	Weld
"	0.100	RT	81,500	75,200	2	Weld
"	0.055	RT	78,700	none	nil	Weld
"	0.055	RT	75,000	none	nil	Base Metal
"	0.055	RT	88,100	79,400	nil	Weld
"	0.055	1600	53,200	47,390	7	Weld
"	0.055	1600	54,400	50,750	8	Weld
"	0.055	1600	56,900	51,000	6	Weld
"	0.055	1900	47,850	44,700	6	Base Metal
"	0.055	1900	31,700	28,200	6	Base Metal
"	0.055	1900	50,600	44,400	7	Base Metal
"	0.055	2200	33,100	32,000	6	Weld
"	0.055	2200	37,970	34,220	6	Base Metal
"	0.055	2200	36,360	28,270	6	Base Metal
"	0.005	RT	77,500	none	nil	Weld
"	0.005	RT	72,700	none	nil	Weld
"	0.005	RT	77,700	none	nil	Weld
"	0.005	RT	74,250	none	nil	Weld
Tungsten	0.100	RT	8,900	none	nil	Base Metal
"	0.100	RT	Specimen Failed In Weld During Setup.			
"	0.100	RT	Specimen Failed In Weld During Setup.			
"	0.050	RT	Failure Occurred In Grips At 45,750 psi.			
"	0.050	RT	Failure Occurred In Grips At 34,180 psi.			
"	0.050	RT	Specimen Failed In Weld During Setup.			
"	0.050	2200	30,850	28,500	4	Weld
"	0.050	2200	31,360	27,470	4	Weld
"	0.050	2200	31,970	30,140	4	Weld

Table 9 (continued)

Material	Thickness (in.)	Test Temp (°F)	Tensile Strength (psi)	Yield Strength (0.2% offset, psi)	Elong (%)	Failure Location
Tungsten	0.050	2500	26,360	24,600	4	Weld
"	0.050	2500	28,470	23,580	4	Weld
"	0.050	2500	30,120	26,250	4	Weld
"	0.050	2800	11,520	7,480	51	Base Metal
"	0.050	2800	11,800	7,590	46	Base Metal
"	0.050	2800	12,840	9,260	57	Weld
"	0.005	RT	Specimens Were Not Available For Testing. Welds Failed During			
"	0.005	RT	Specimen Manufacture.			
"	0.005	RT	Specimen Manufacture.			
<u>Seam Welds</u>						
Mo-0.5% Ti	0.055	RT	24,170	-	-	Heat-affected Zone
"	0.055	RT	30,240	-	-	Heat-affected Zone
"	0.055	RT	17,590	-	-	Base Metal

TABLE 10

Electron Beam Weld Ductile-to-brittle Transition Temperatures

Material	Thickness (in.)	Ductile-to-brittle Transition Temperature	Stress Relief	Comparative Base-metal Transition Temperature
Mo-0.5% Ti	0.100	530°F	none	< RT
"	0.055	350°F	none	170°F
"	0.055	350°F	1 hr, 1850°F	170°F
"	0.005	RT		< RT
Tungsten	0.100	>> 900°F	none	820°F
"	0.050	1025°F	none	600°F
"	0.005	435°F	none	< RT
"	0.005	460°F	1 hr, 1900°F	< RT

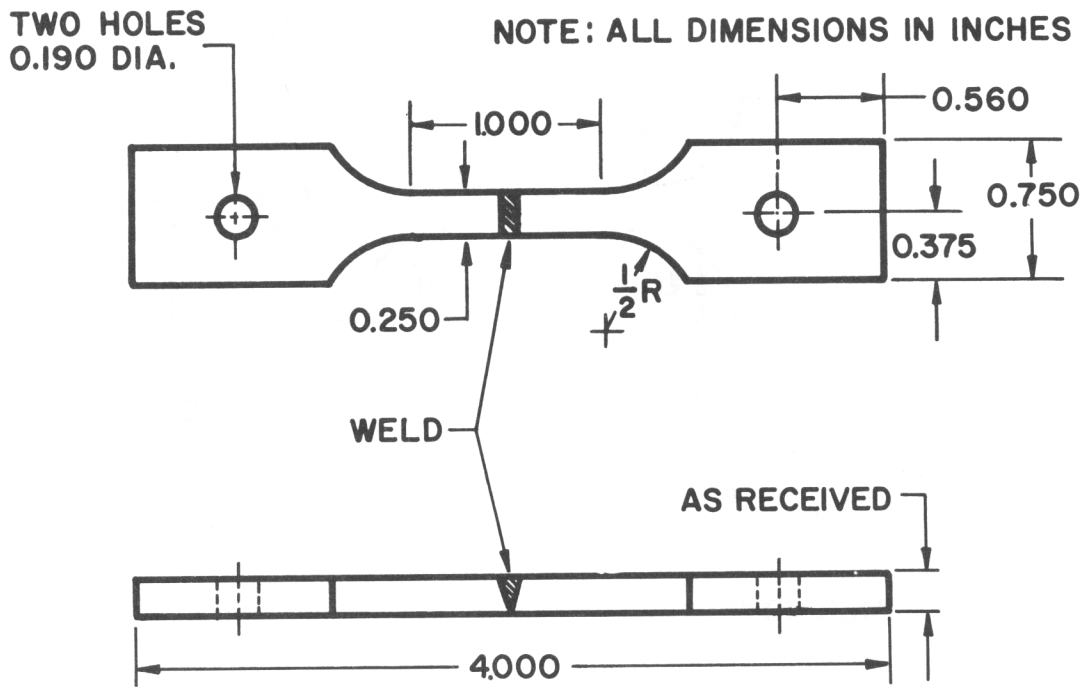
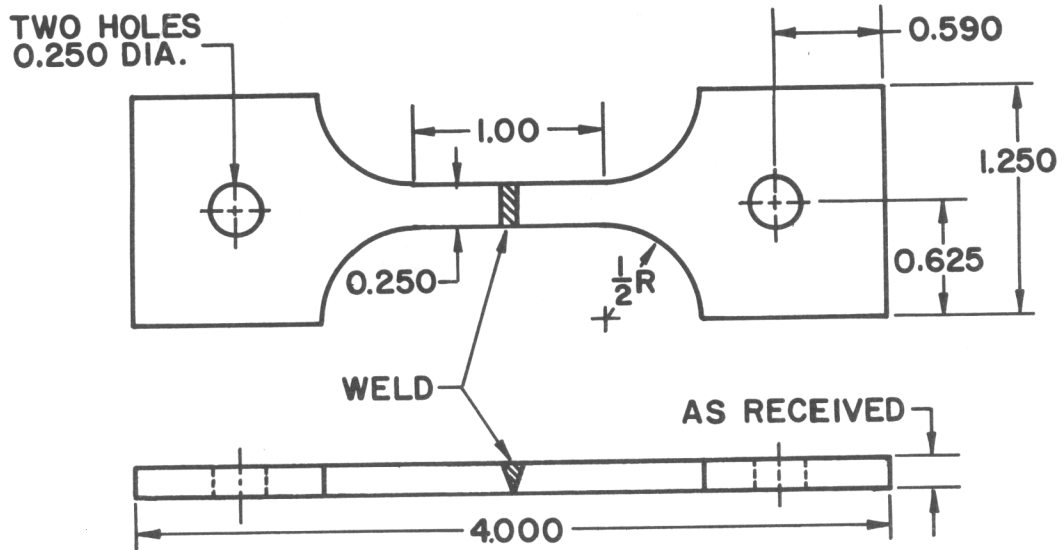


Fig. 1 Molybdenum Tensile Specimen Drawing



Fig. 2 Molybdenum Tensile Specimen



NOTE: ALL DIMENSIONS IN INCHES

Fig. 3 Tungsten Tensile Specimen Drawing



Fig. 4 Tungsten Tensile Specimen

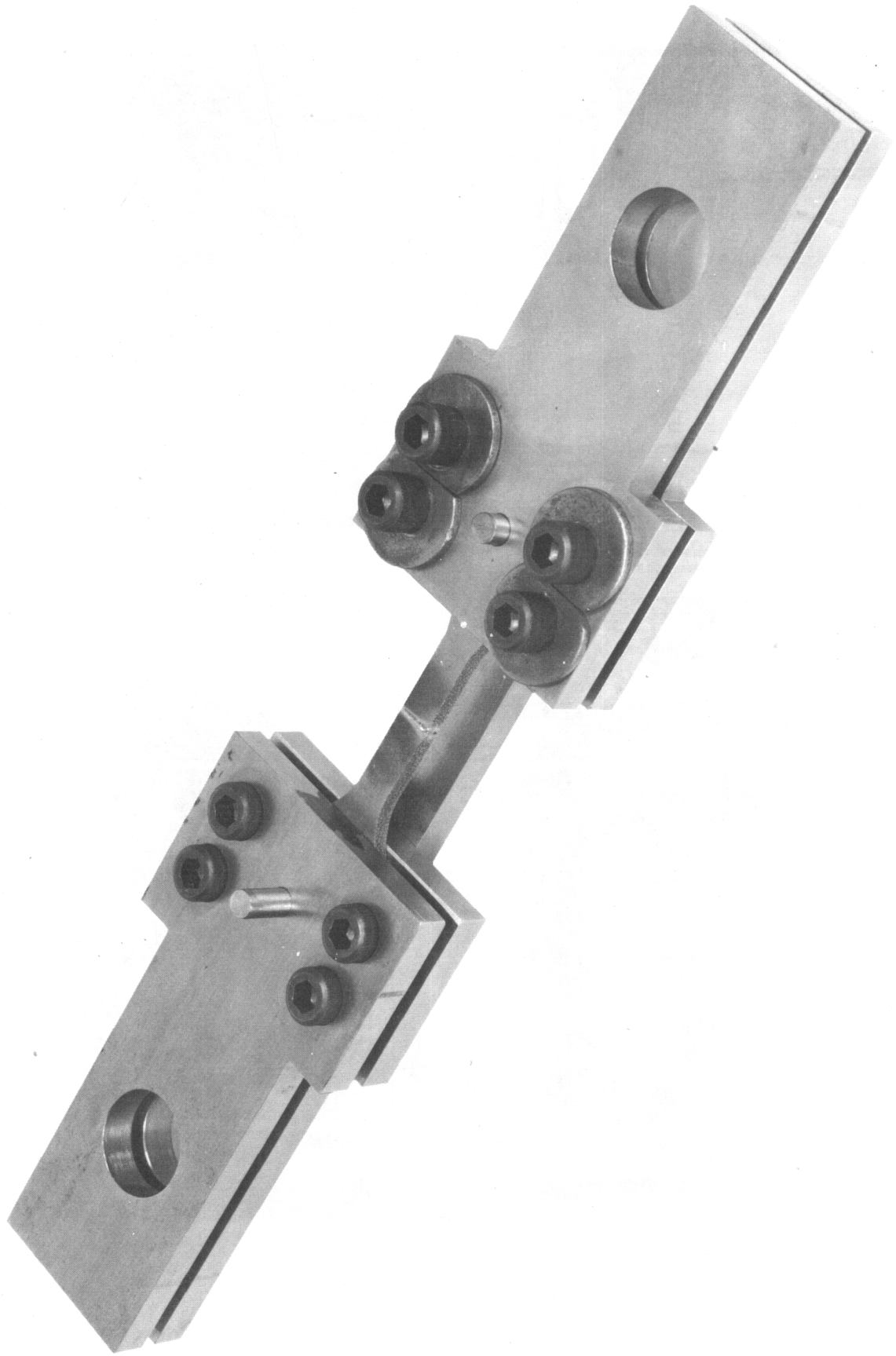


Fig. 5 Room-temperature Tensile Testing Fixture



Fig. 6 Elevated-temperature Tensile Testing Setup

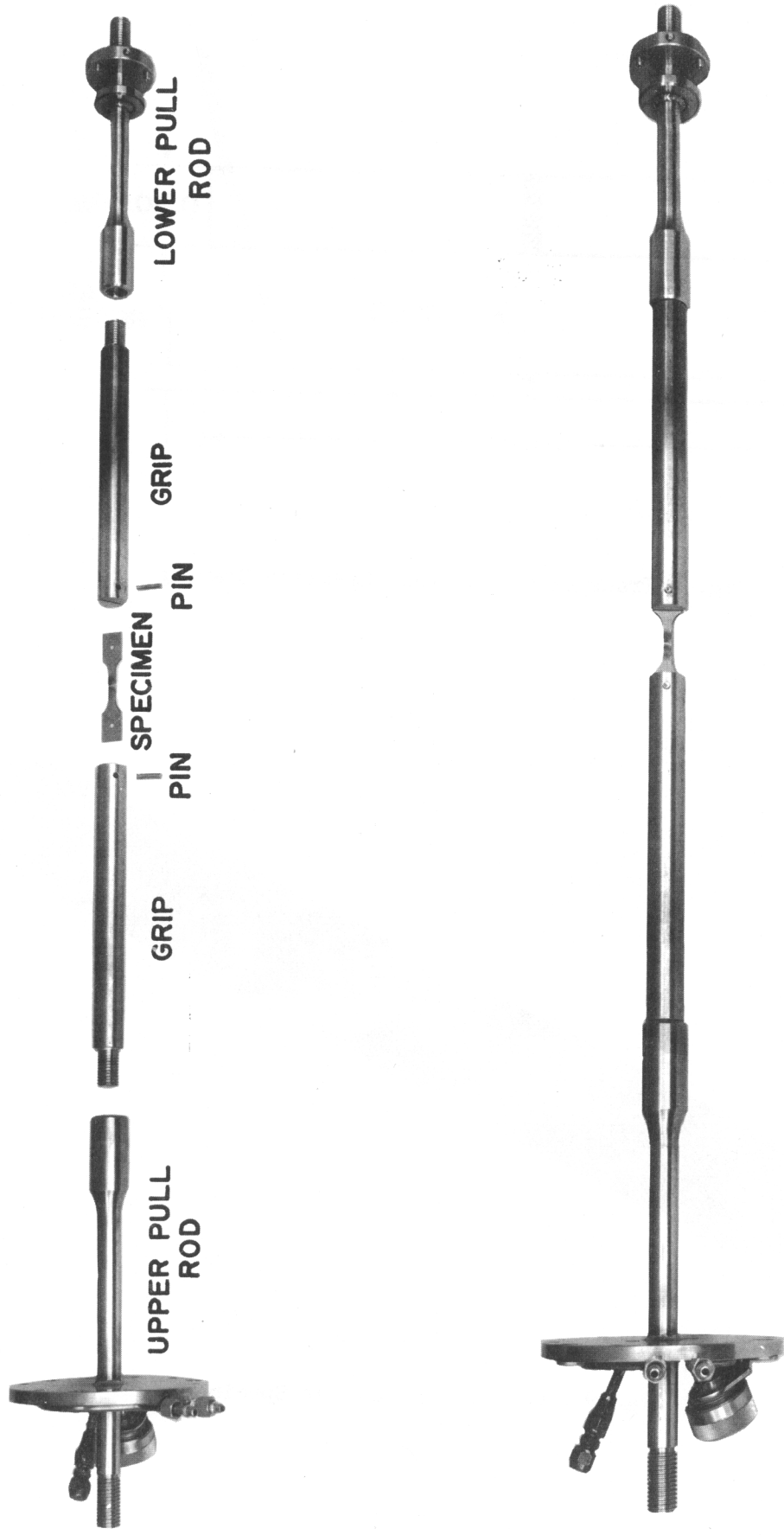


Fig. 7 Elevated-temperature Tensile Pull-rod and Grip Assembly; Exploded and Assembled

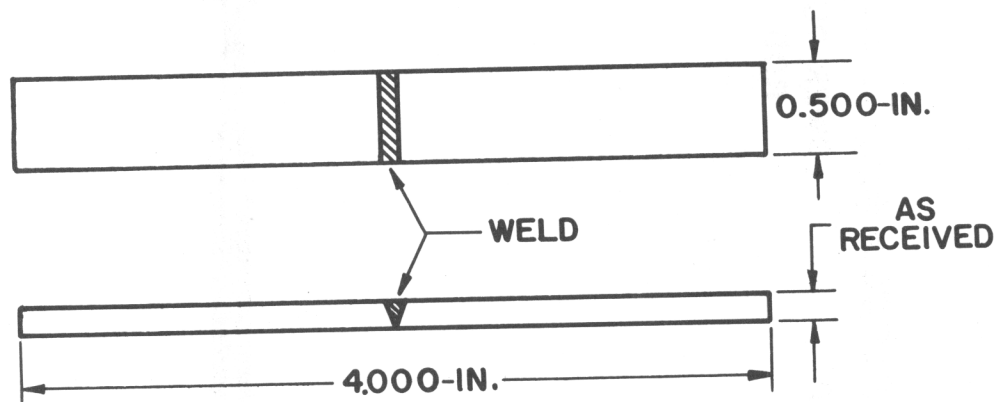


Fig. 8 Transverse Bend-test Specimen Drawing

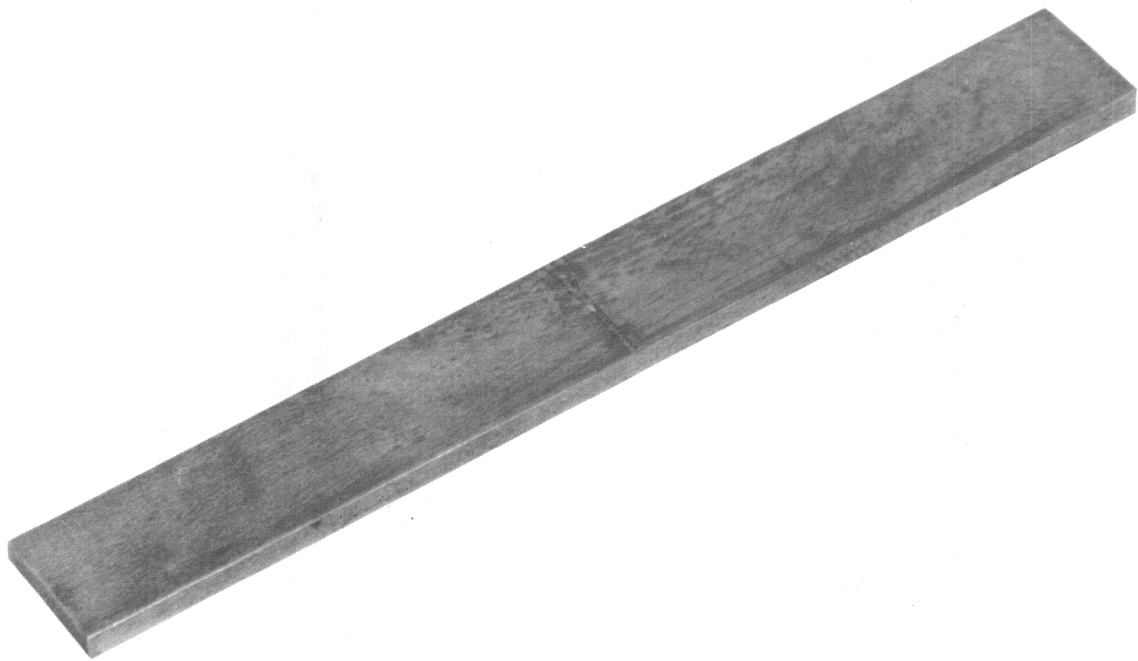


Fig. 9 Transverse Bend-test Specimen

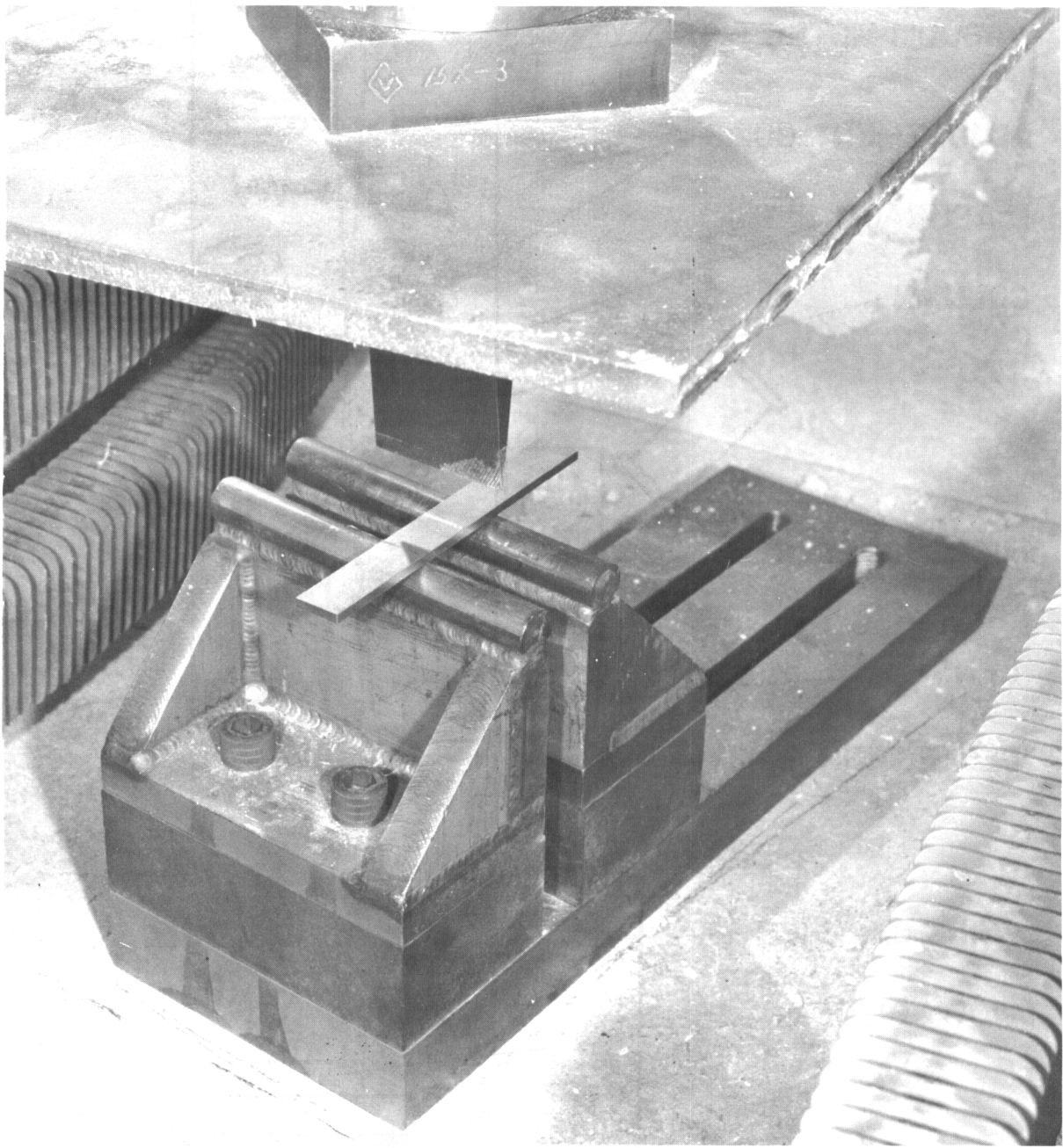


Fig. 10 Elevated-temperature Bend-test Setup

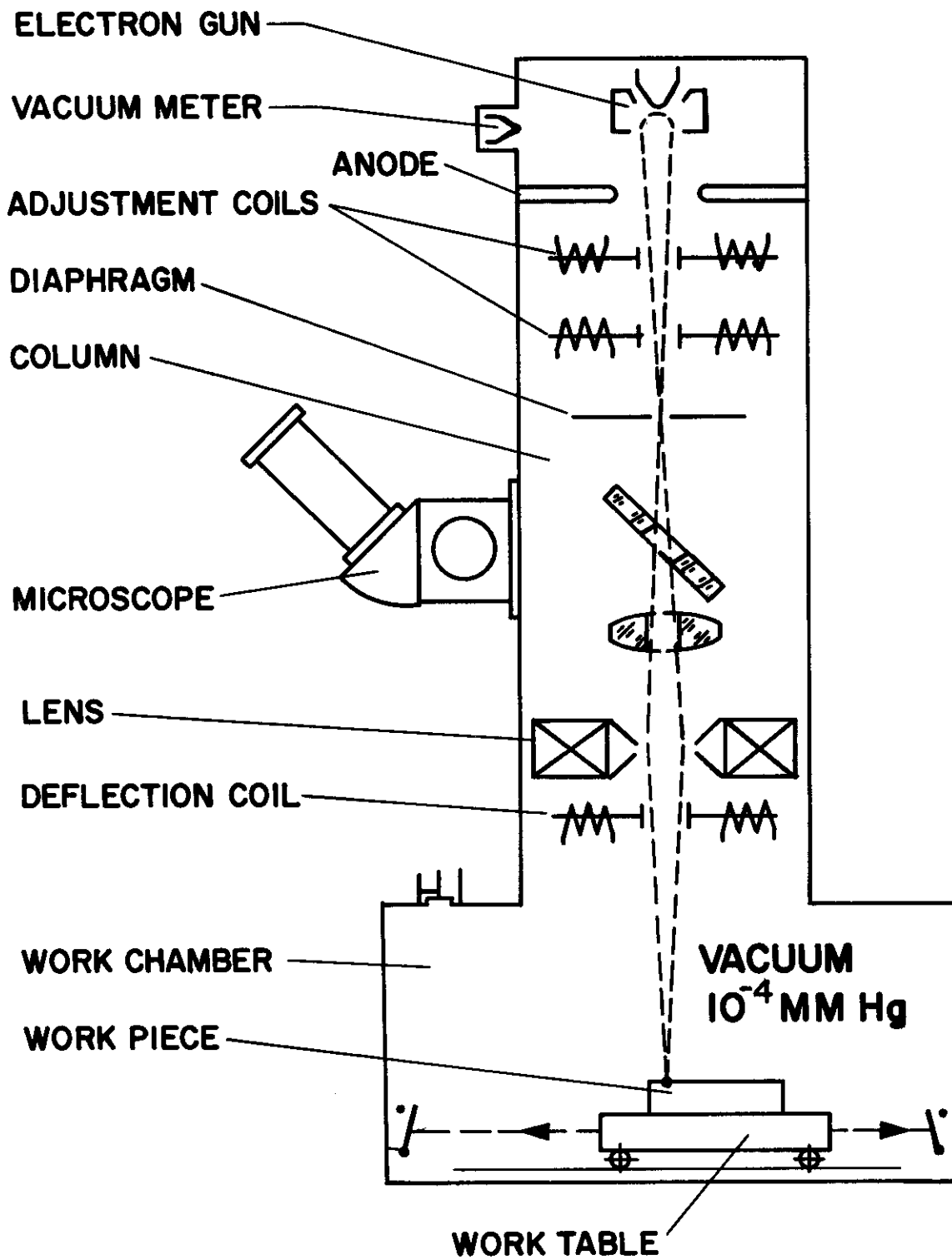


Fig. 11 Electron Beam Welding Machine Schematic

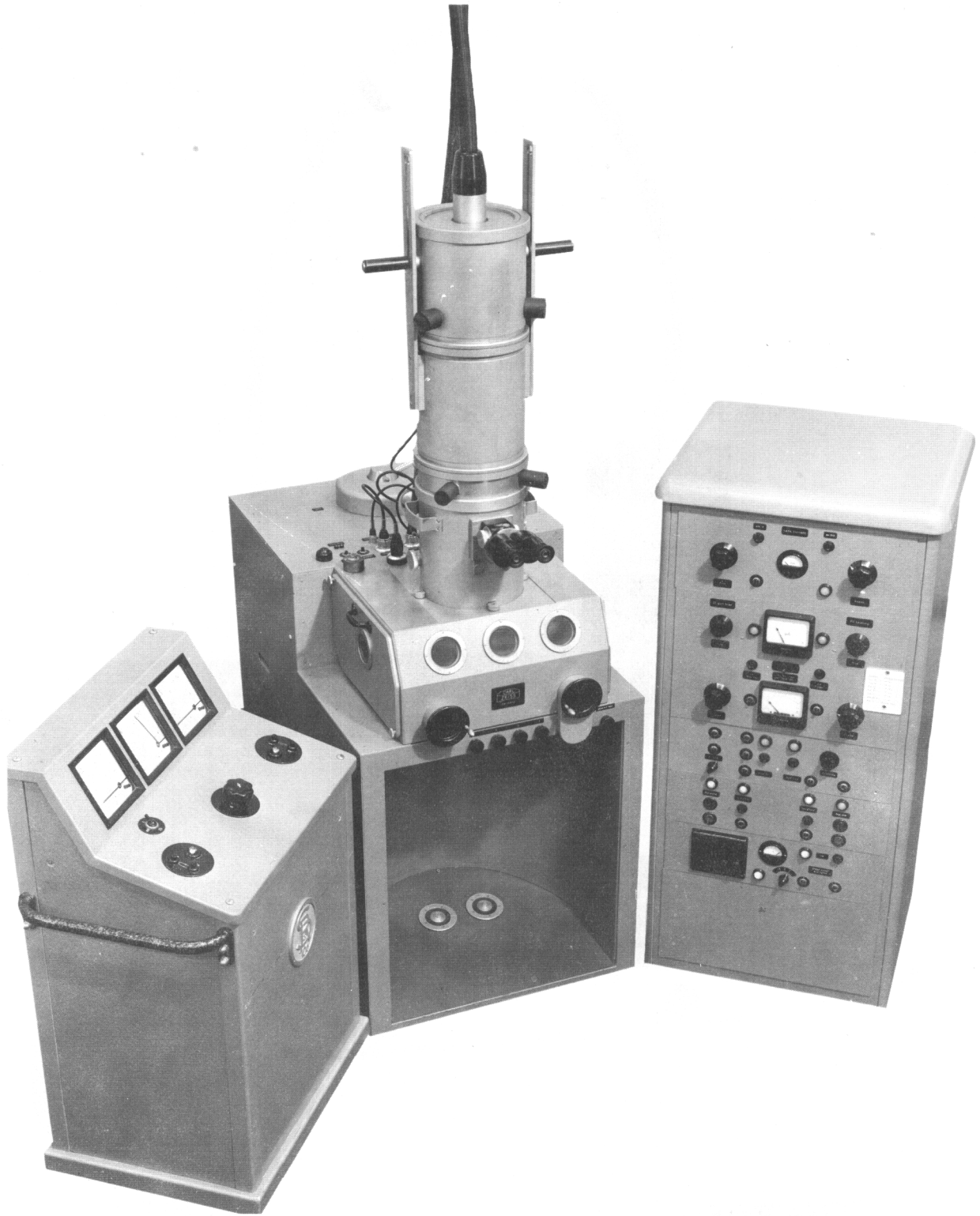


Fig. 12 Zeiss Electron Beam Welding Machine



Fig. 13 Hamilton-Zeiss Electron Beam Welding Machine

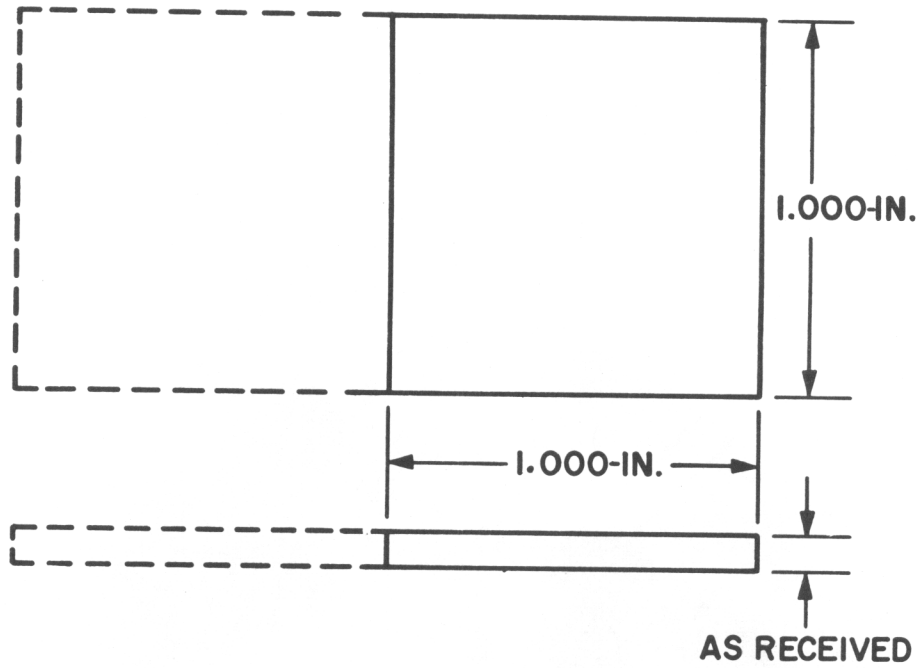


Fig. 14 Trial Butt-weld Specimen Drawing

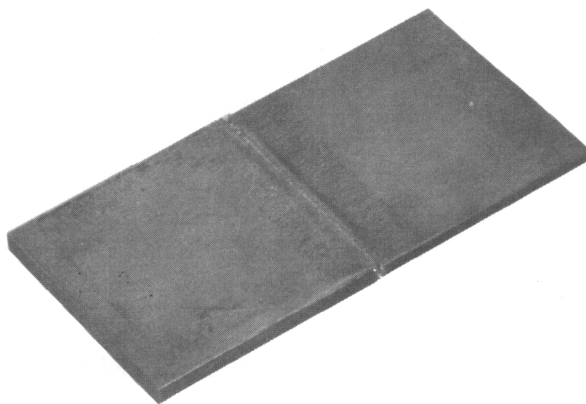


Fig. 15 Trial Butt-weld Specimen

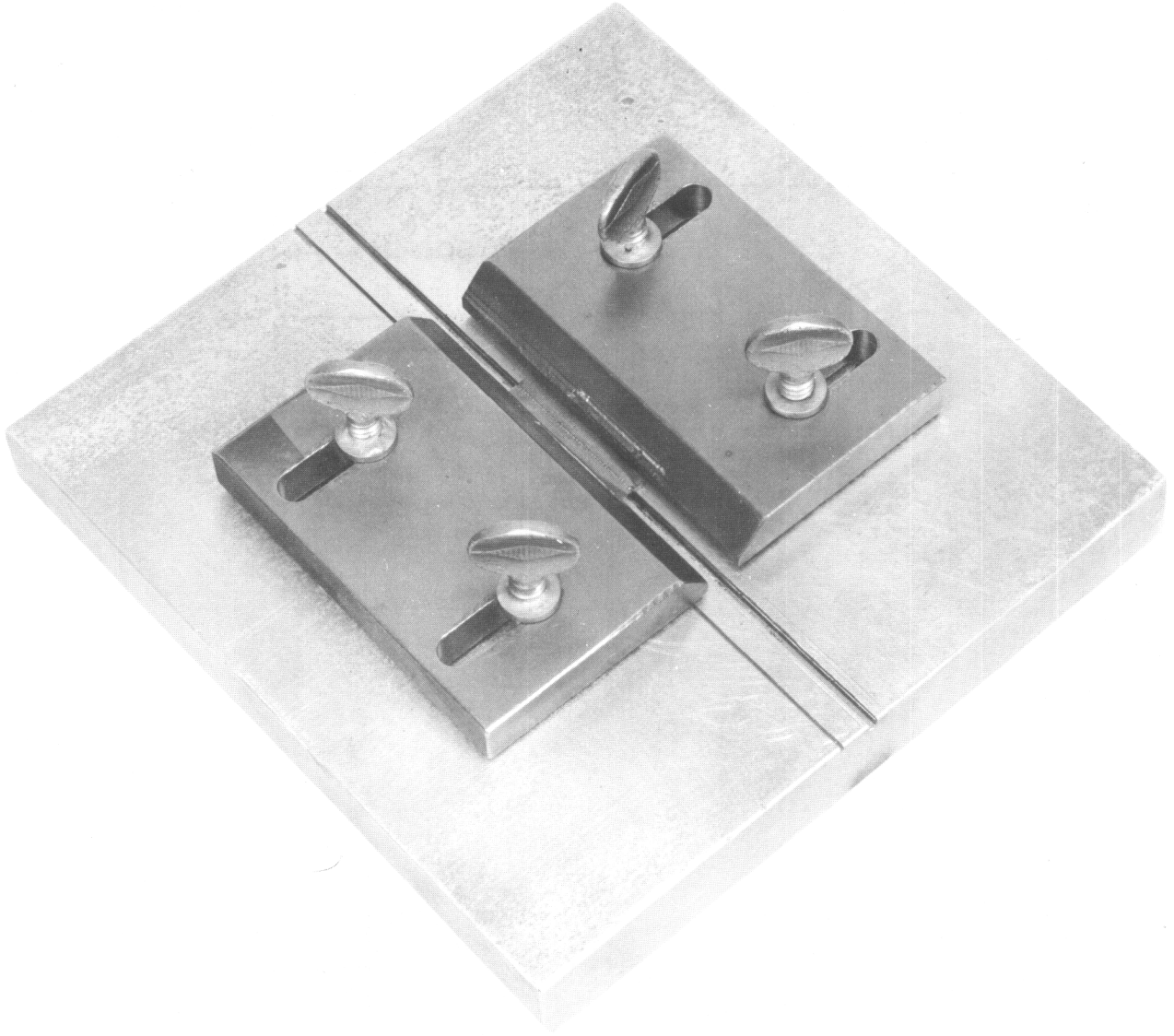


Fig. 16 Typical Welding Fixture

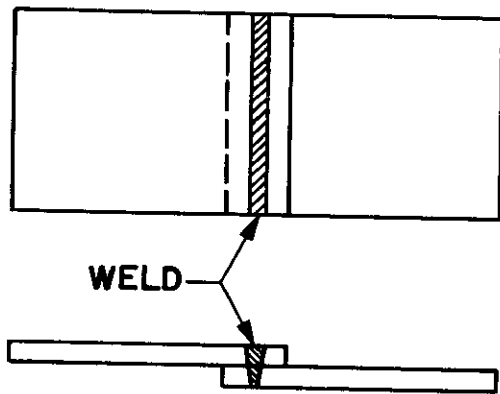


Fig. 17 Seam-weld Specimen Drawing

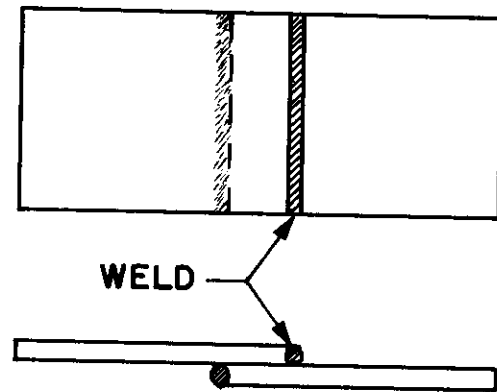


Fig. 18 Lap-weld Specimen Drawing

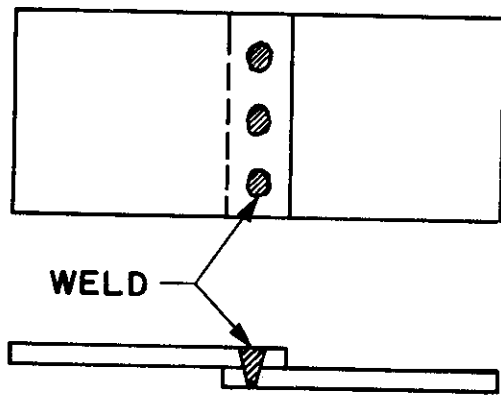


Fig. 19 Spot-weld Specimen Drawing

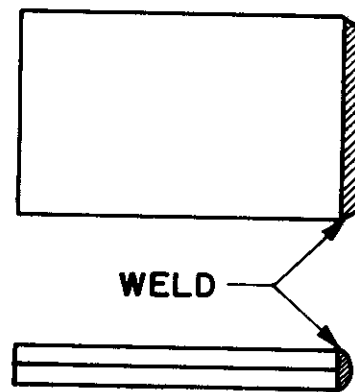


Fig. 20 Edge-weld Specimen Drawing

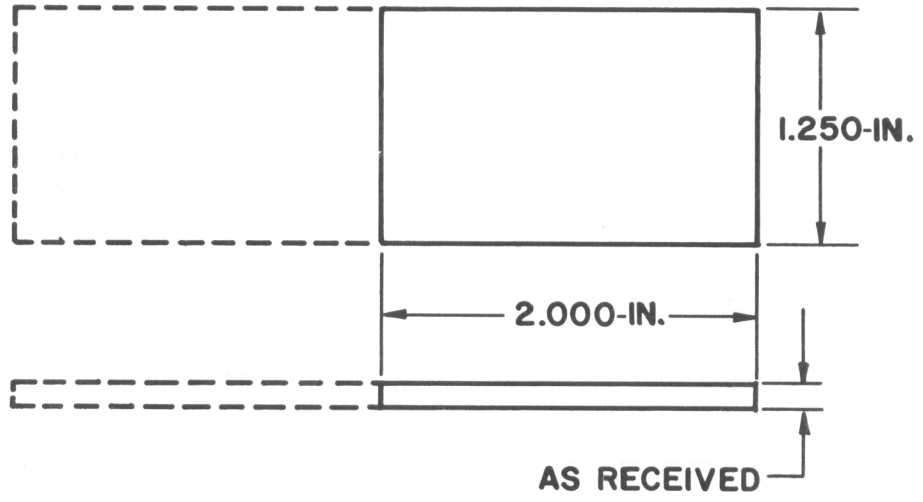


Fig. 21 Final Butt-weld Specimen Drawing

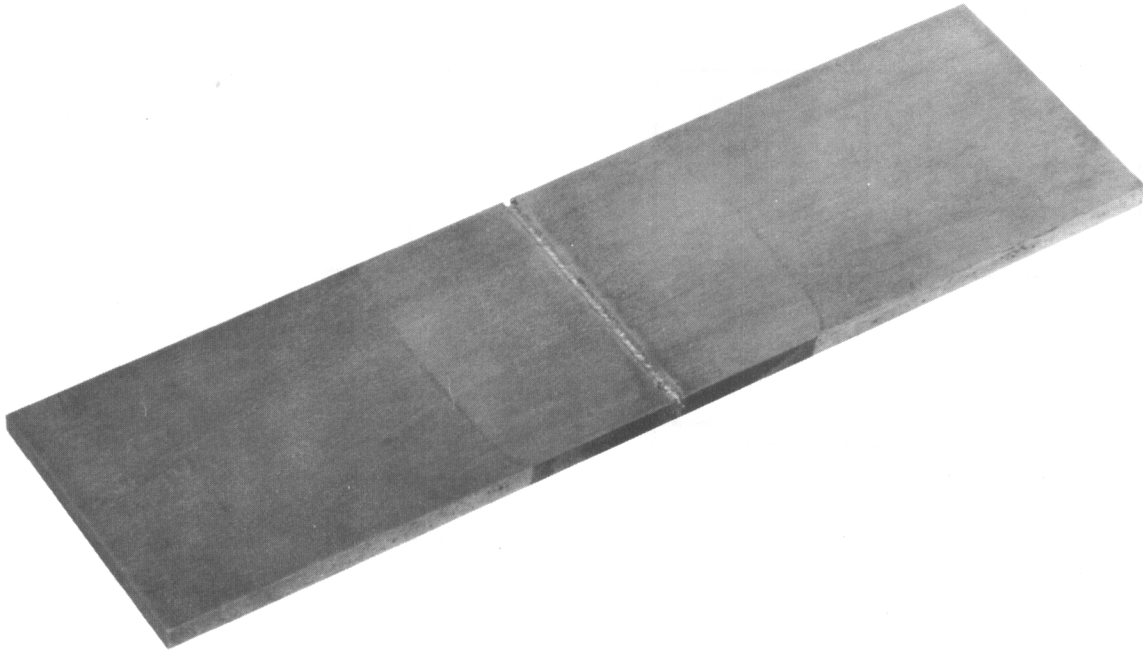


Fig. 22 Final Butt-weld Specimen

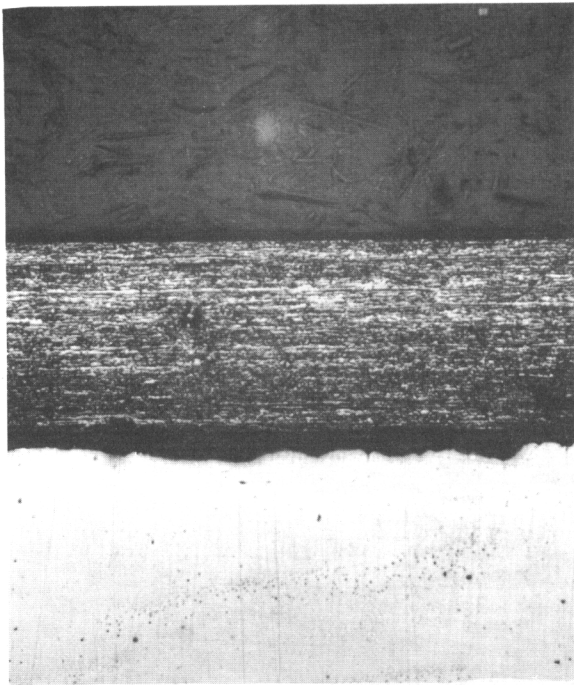


Fig. 23 As-received 0.005-in.
Mo-0.5% Ti; X200

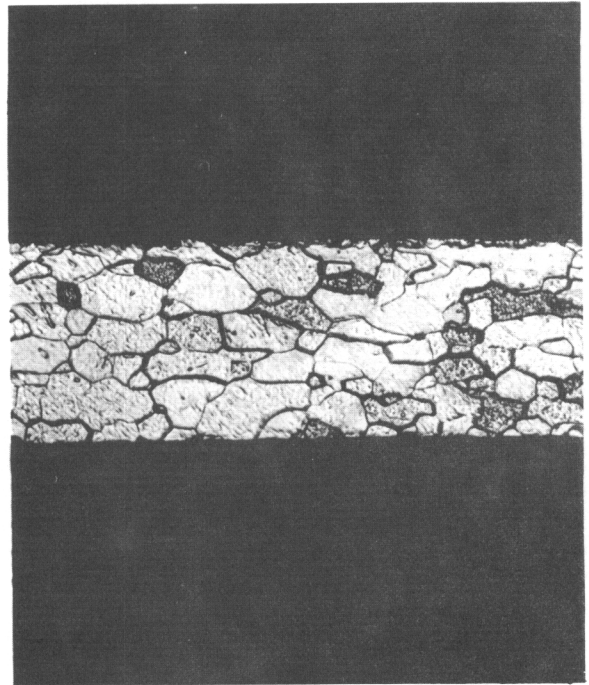


Fig. 24 Recrystallized 0.005-in.
Mo-0.5% Ti; X200



Fig. 25 As-received 0.055-in.
Mo-0.5% Ti; X200

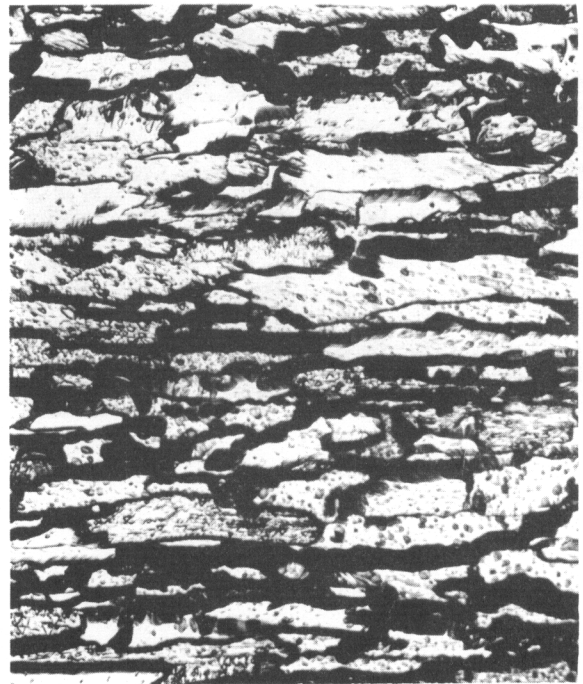


Fig. 26 Recrystallized 0.055-in.
Mo-0.5% Ti; X200



Fig. 27 As-received 0.100-in.
Mo-0.5% Ti; X200

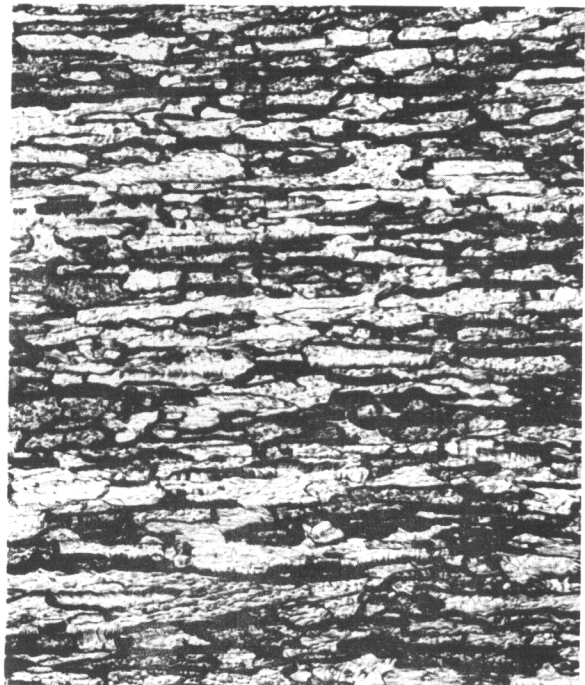


Fig. 28 Recrystallized 0.100-in.
Mo-0.5% Ti; X200



Fig. 29 As-received 0.005-in.
Tungsten; X200

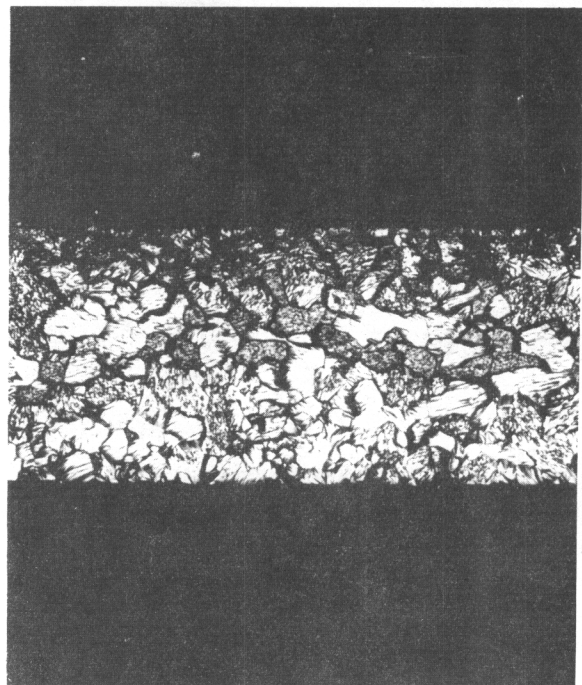


Fig. 30 Recrystallized 0.005-in.
Tungsten; X225



Fig. 31 As-received 0.050-in.
Tungsten; X200

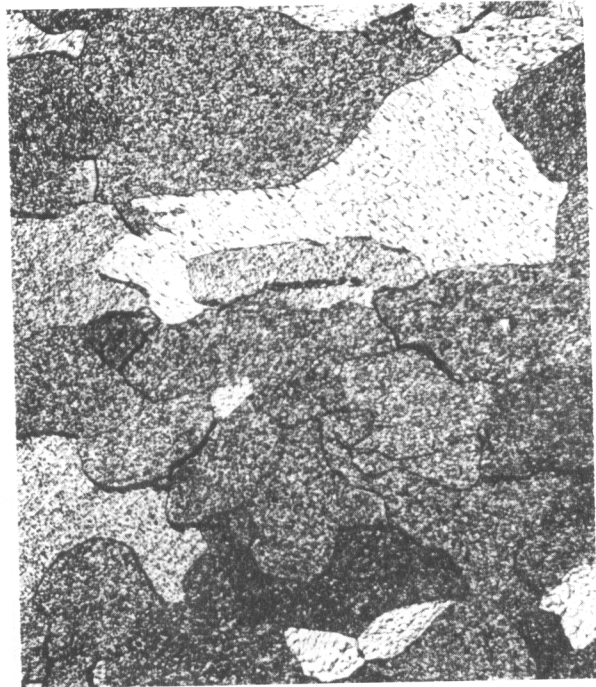


Fig. 32 Recrystallized 0.050-in.
Tungsten; X200

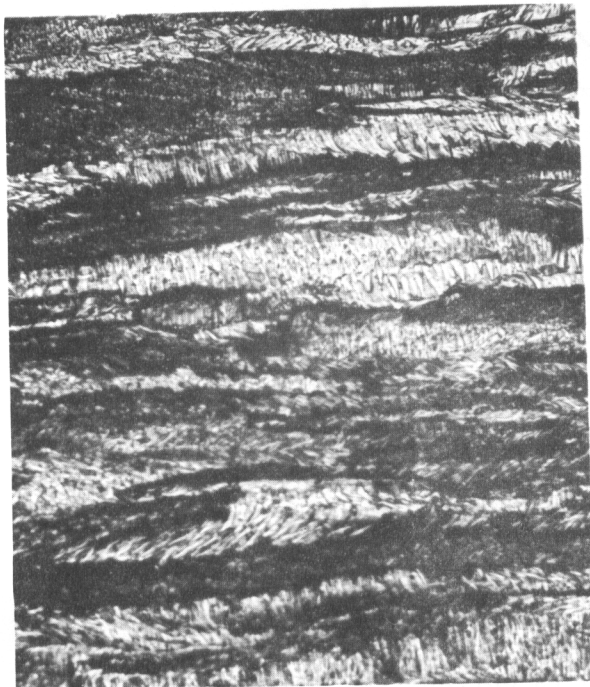


Fig. 33 As-received 0.100-in.
Tungsten; X200



Fig. 34 Recrystallized 0.100-in.
Tungsten; X200

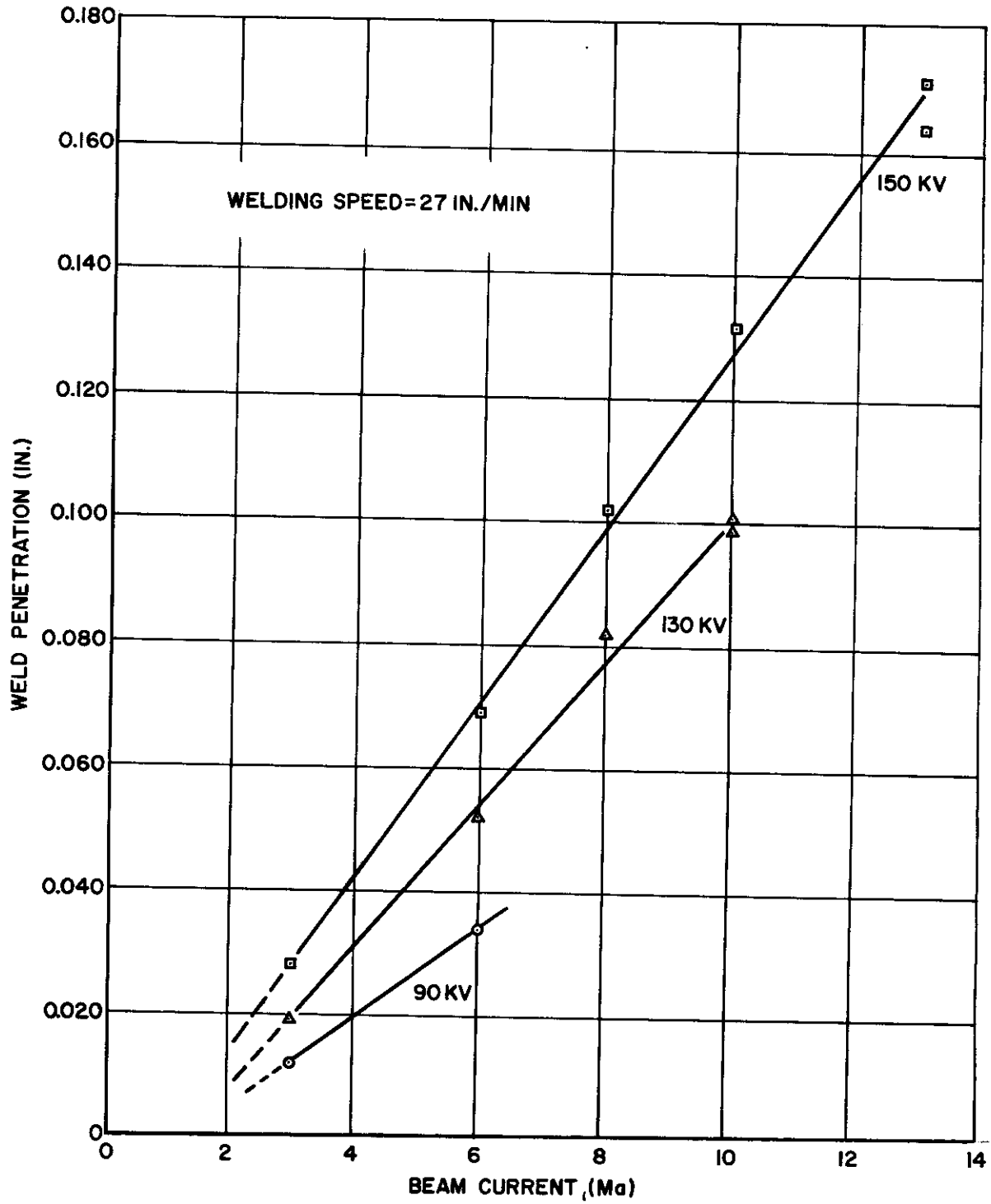


Fig. 35 Molybdenum Weld Penetration vs Current and Voltage

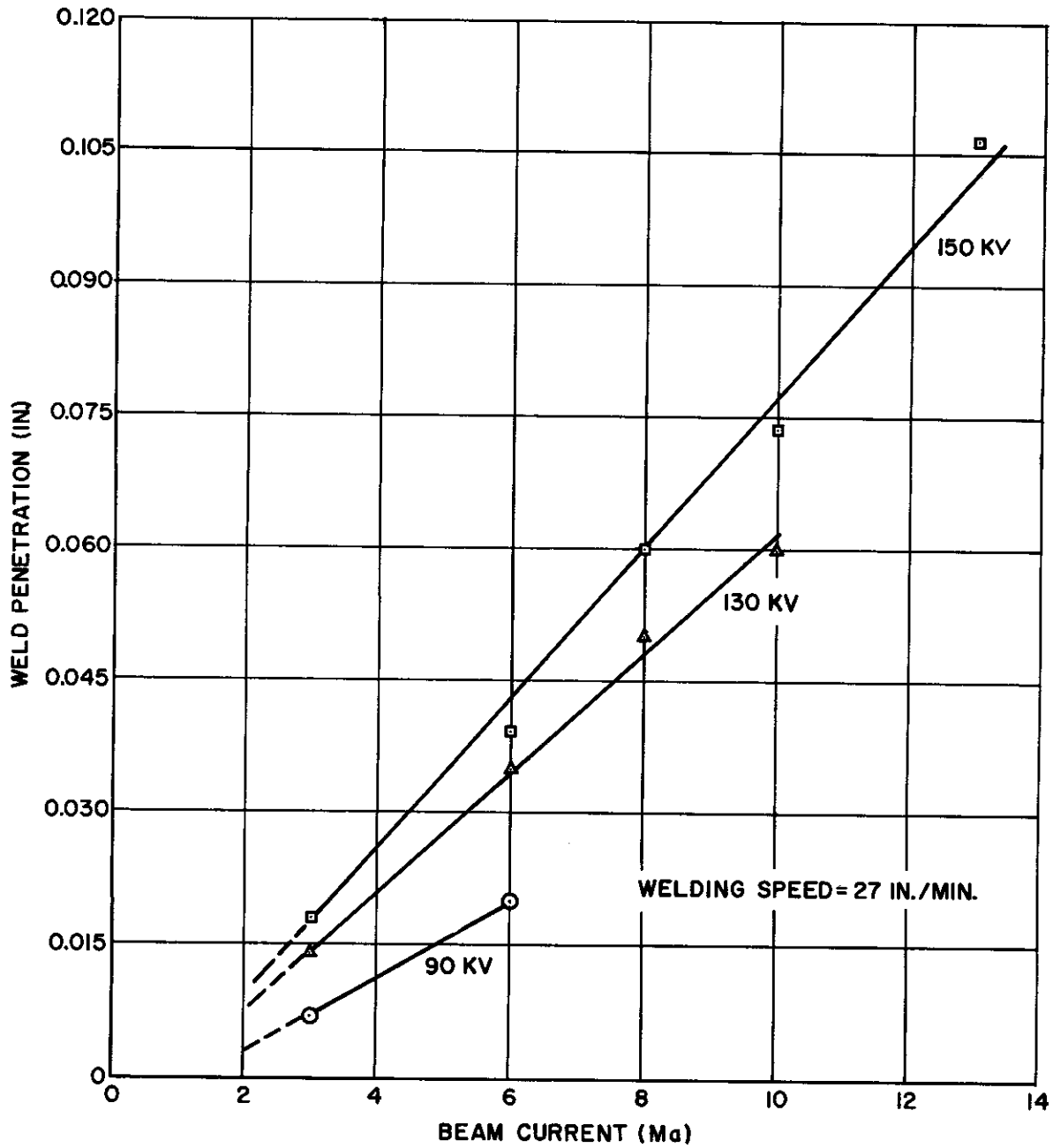


Fig. 36 Tungsten Weld Penetration vs Current and Voltage

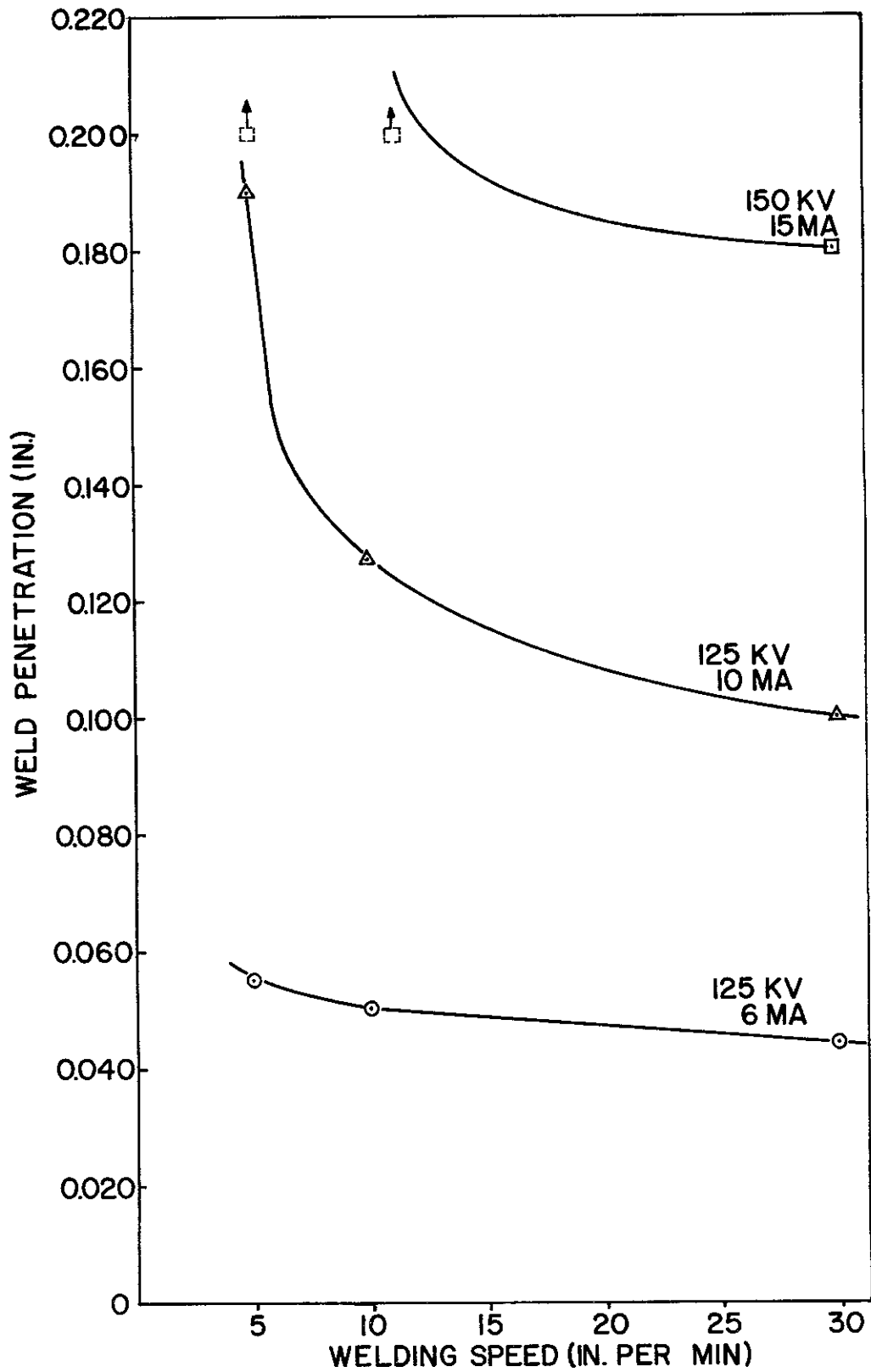


Fig. 37 Molybdenum Weld Penetration vs Welding Speed

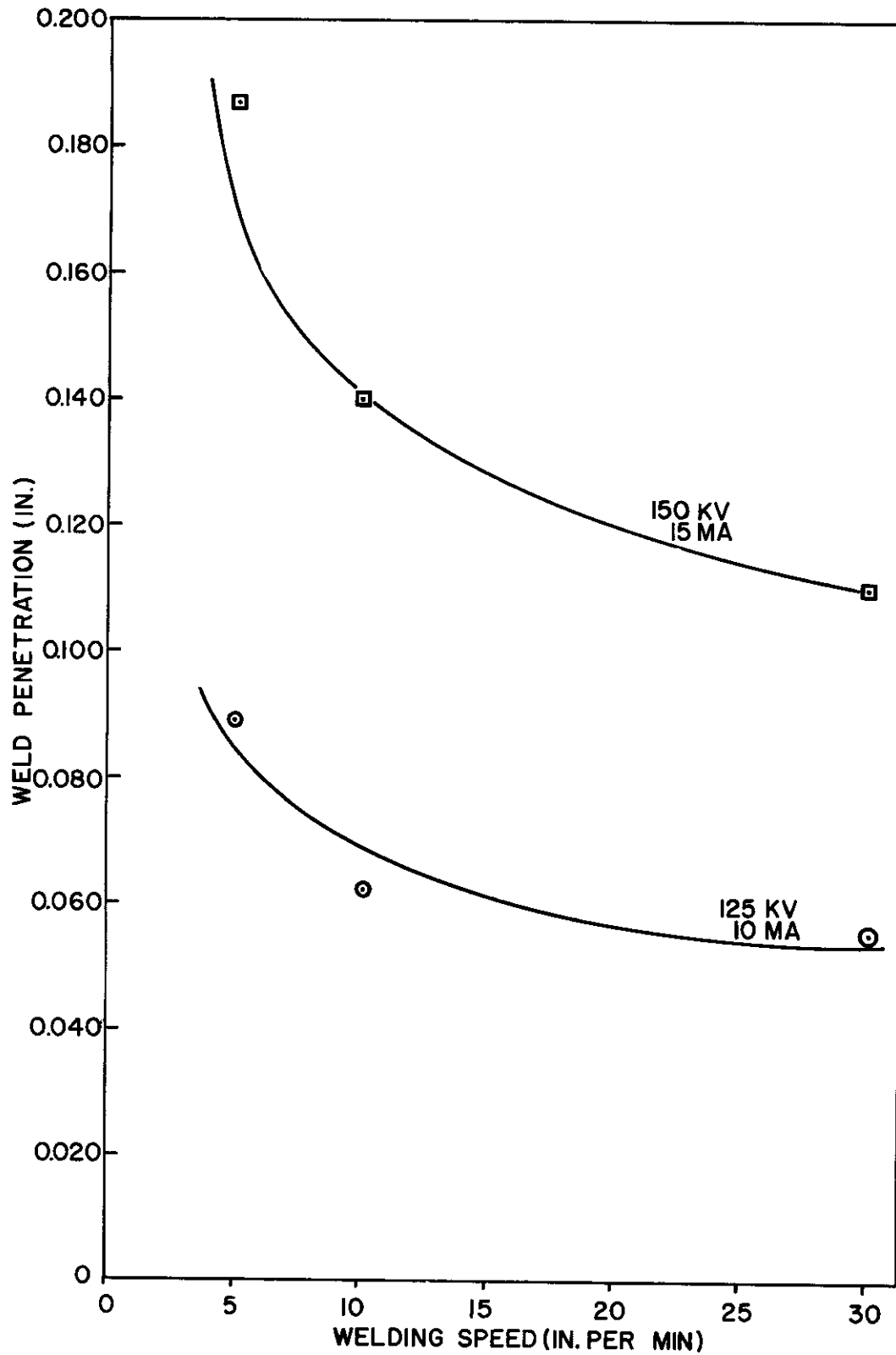


Fig. 38 Tungsten Weld Penetration vs Welding Speed

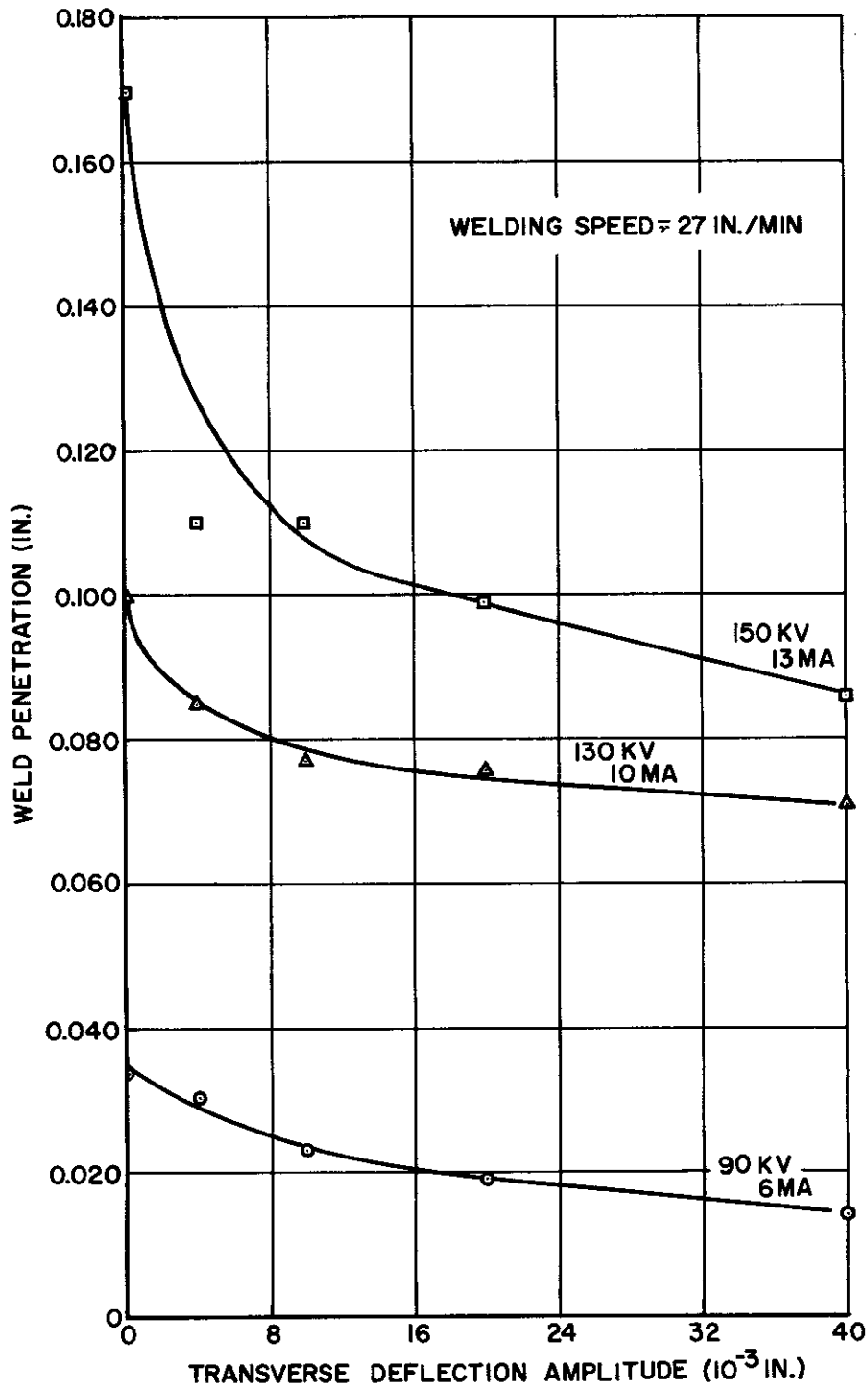


Fig. 39 Molybdenum Weld Penetration vs Transverse Oscillation

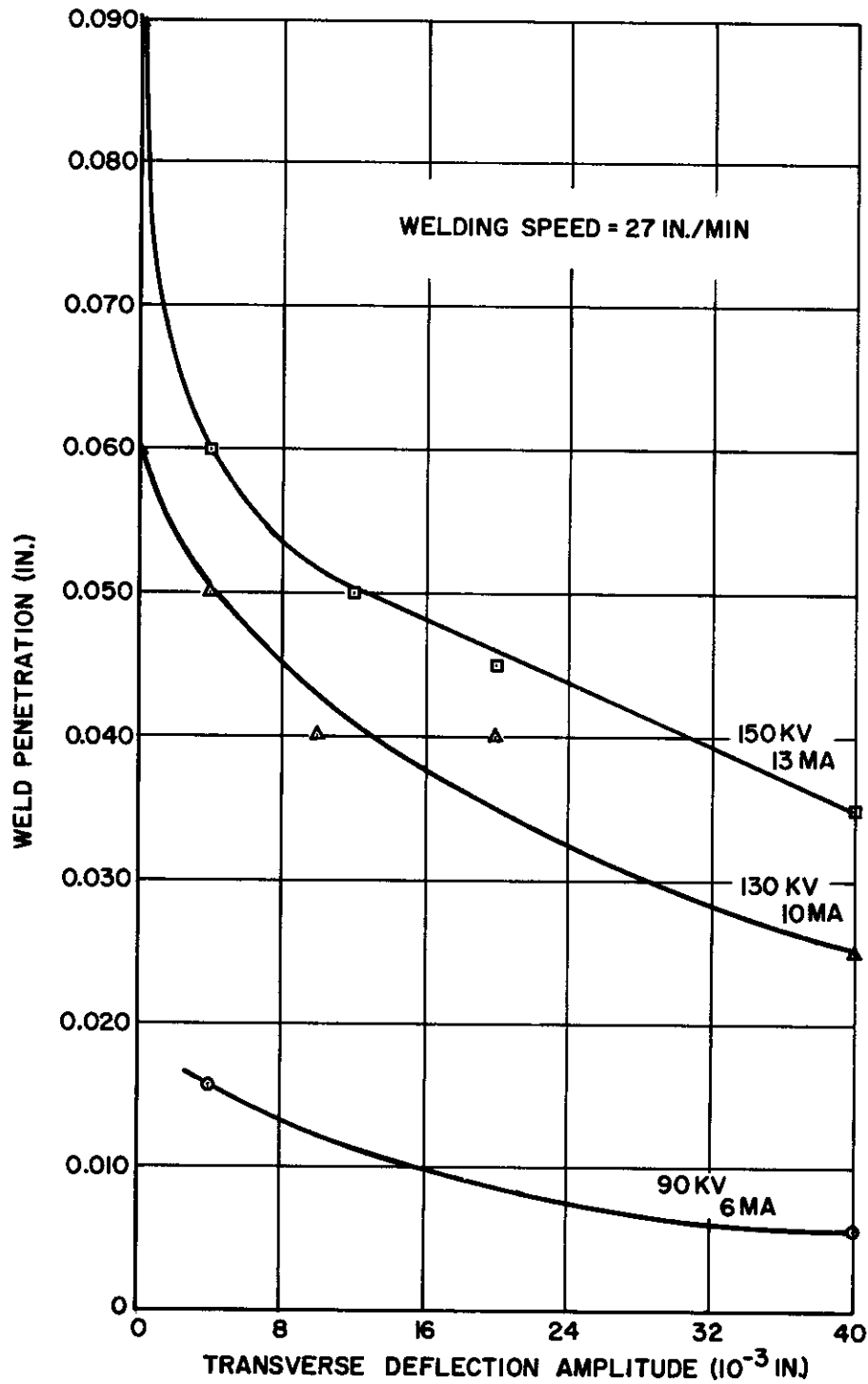


Fig. 40 Tungsten Weld Penetration vs Transverse Oscillation

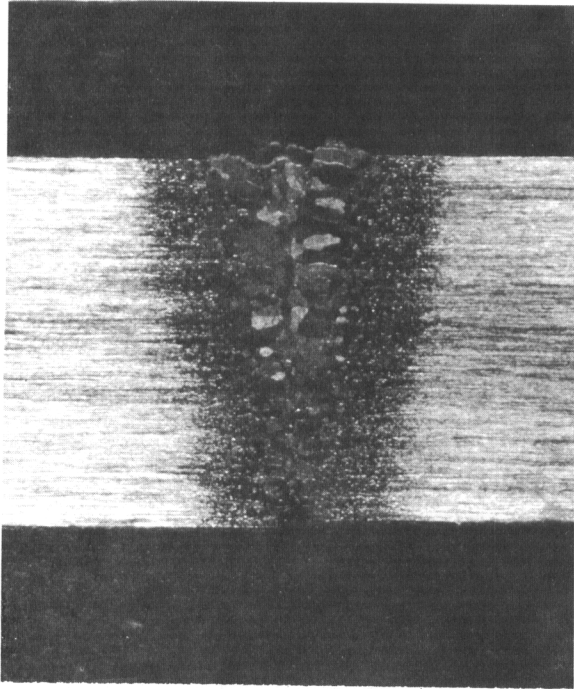


Fig. 41 Trial Weld Cross-section;
X20; 0.100-in. Mo-0.5% Ti; 100KV,
10ma, 7ipm

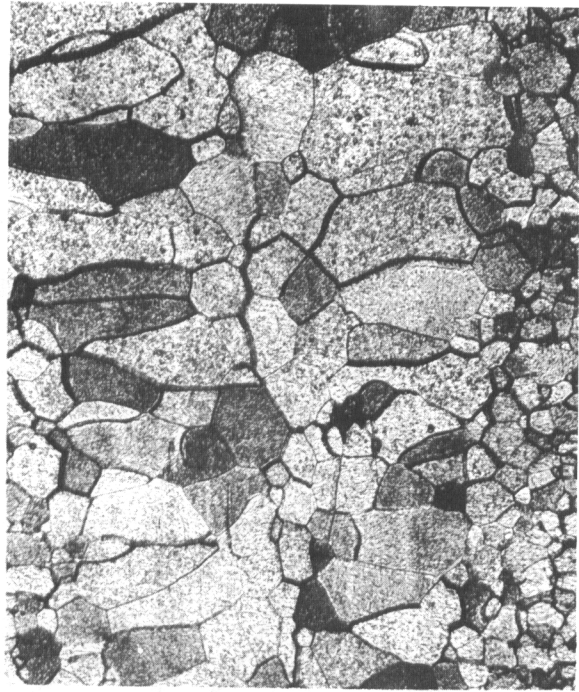


Fig. 42 Trial Weld Microstructure;
X100; 0.100-in. Mo-0.5% Ti; 100KV,
10ma, 7ipm

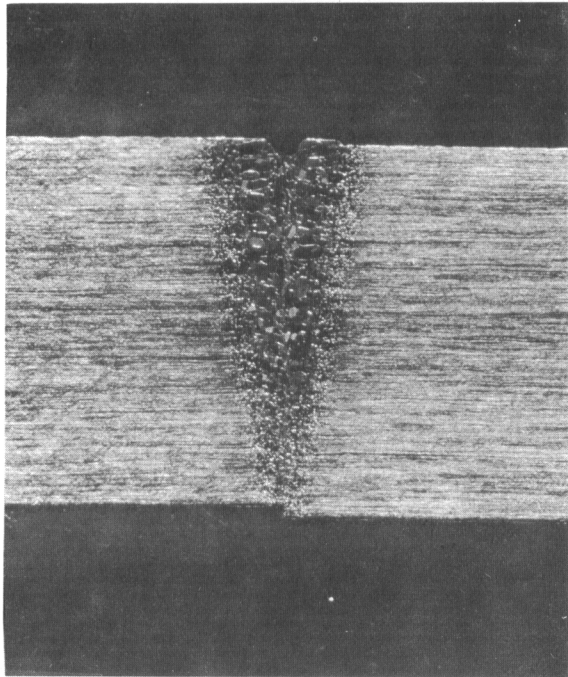


Fig. 43 Trial Weld Cross-section;
X20; 0.100-in. Mo-0.5% Ti; 135KV,
11ma, 27ipm

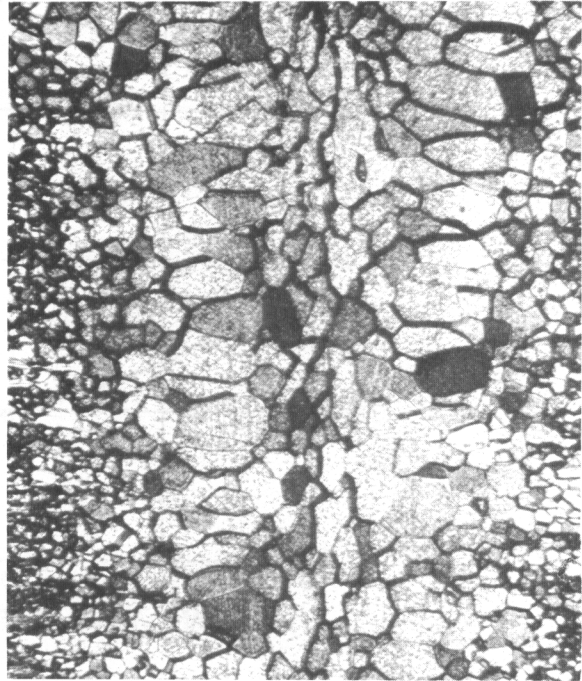


Fig. 44 Trial Weld Microstructure;
X100; 0.100-in. Mo-0.5% Ti; 135KV,
11ma, 27ipm

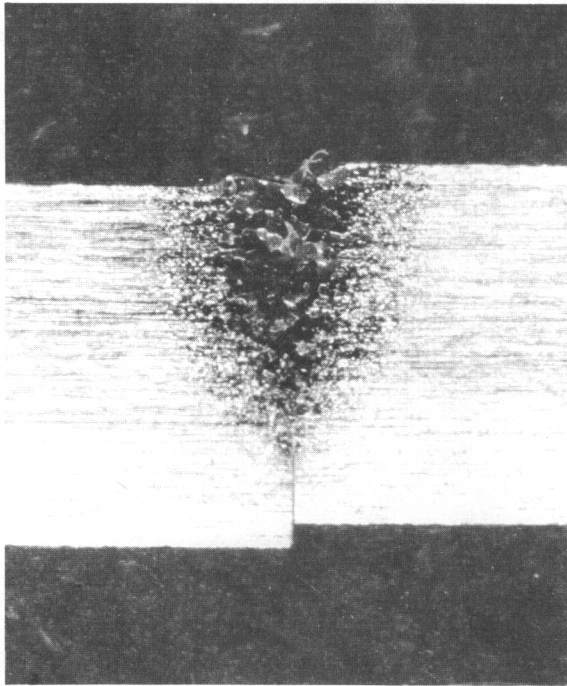


Fig. 45 Trial Weld Cross-section;
X20; 0.100-in. Mo-0.5% Ti; 120KV,
12ma, 4ipm, 300cps, 2ms on-time

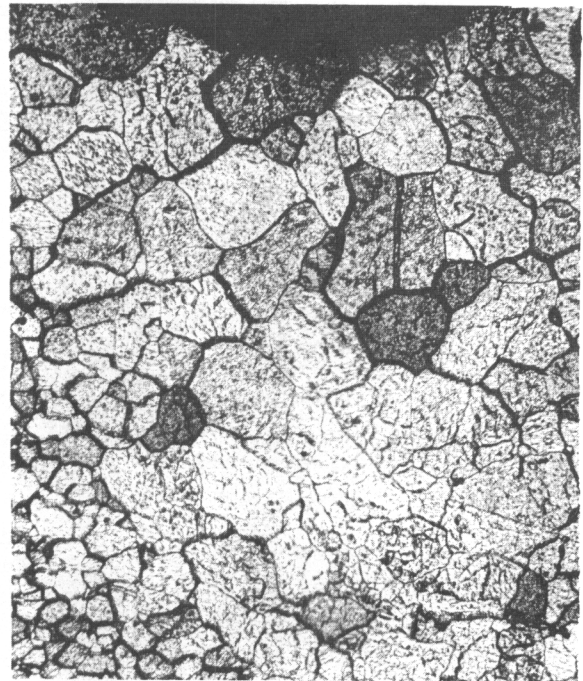


Fig. 46 Trial Weld Microstructure;
X100; 0.100-in. Mo-0.5% Ti; 120KV,
12ma, 4ipm, 300cps, 2ms on-time

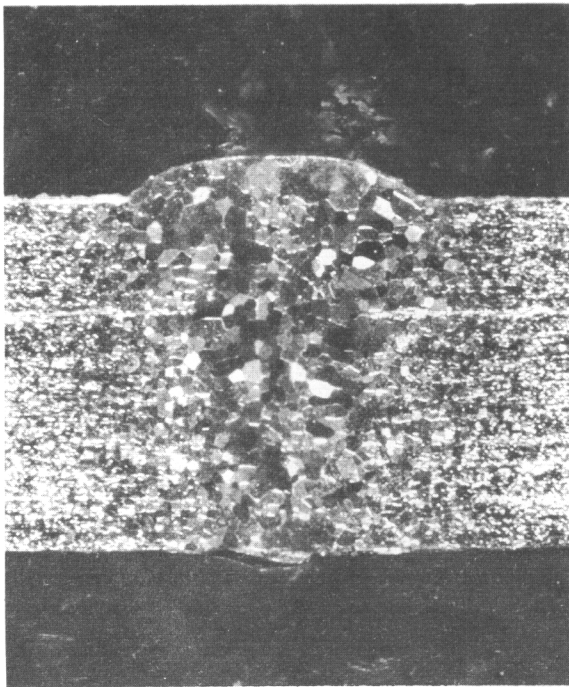


Fig. 47 Trial Weld Cross-section;
X20; 0.100-in. Mo-0.5% Ti; 110KV,
8ma, 10ipm, defocused

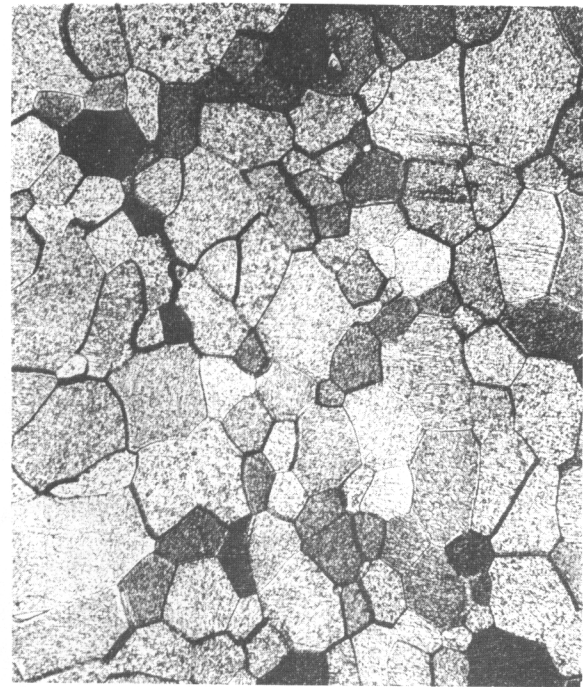


Fig. 48 Trial Weld Microstructure;
X100; 0.100-in. Mo-0.5% Ti; 110KV,
8ma, 10ipm, defocused

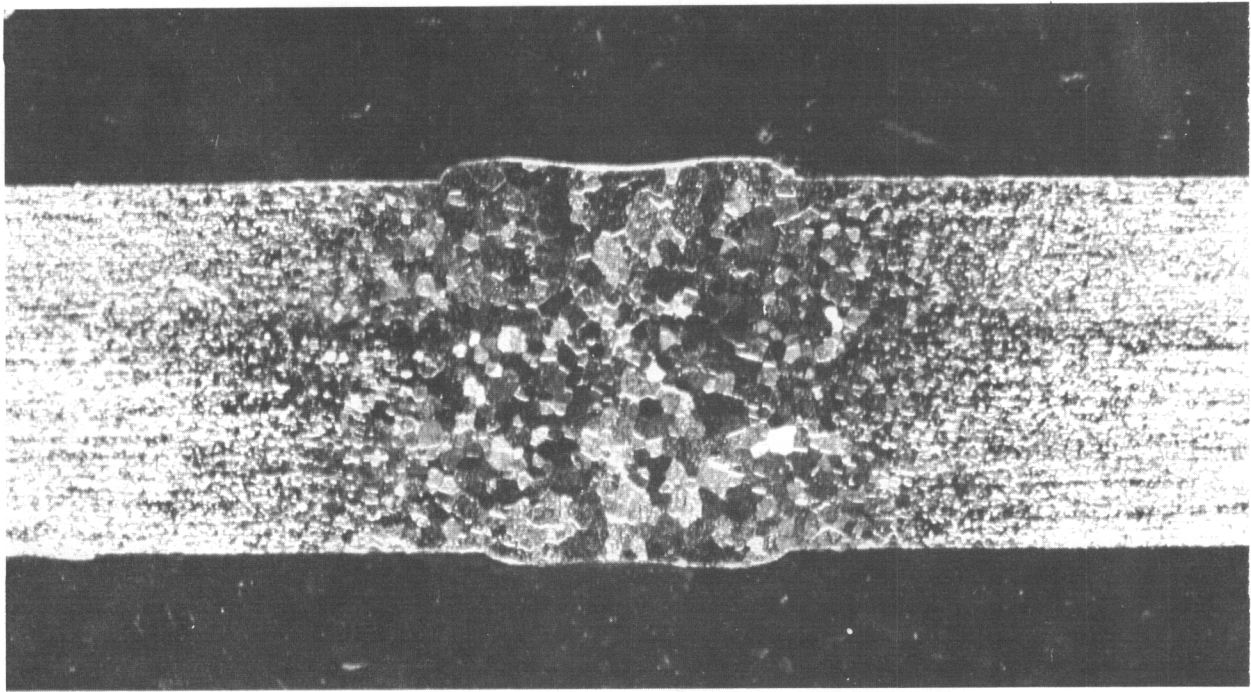


Fig. 49 Trial Weld Cross-section; X20; 0.100-in. Mo-0.5% Ti; 115KV, 11ma, 14ipm, 0.020-in. Y oscillation

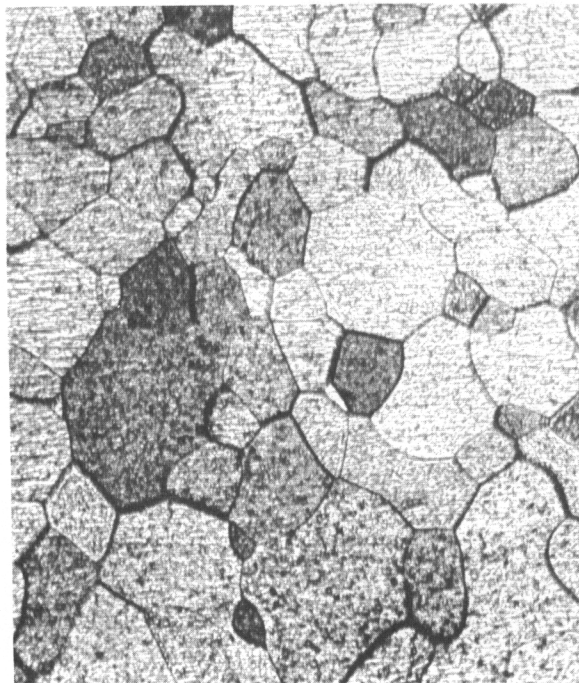


Fig. 50 Trial Weld Microstructure; X100; 0.100-in. Mo-0.5% Ti; 115KV, 11ma, 14ipm, 0.020-in. Y oscillation

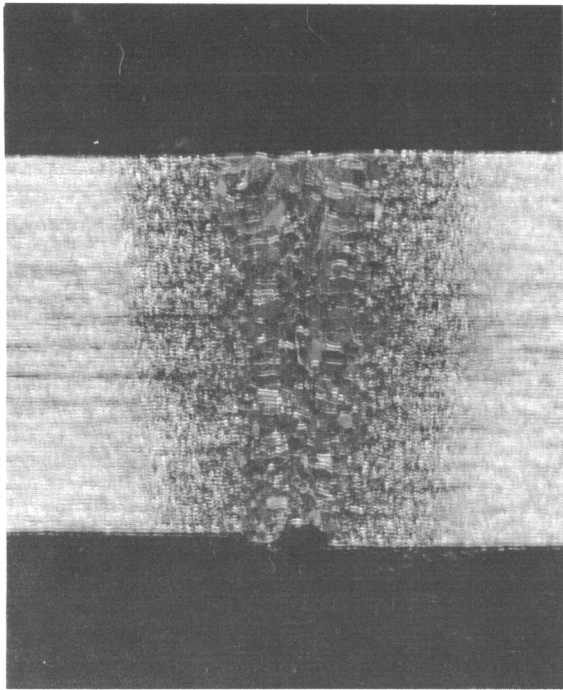


Fig. 51 Trial Weld Cross-section;
X20; 0.100-in. Mo-0.5% Ti; 135KV,
12ma, 27ipm, 0.020-in. X oscillation

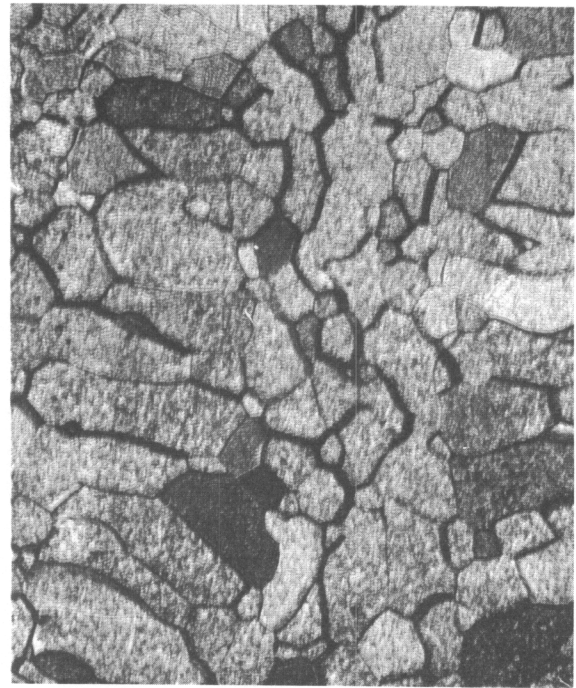


Fig. 52 Trial Weld Microstructure;
X100; 0.100-in. Mo-0.5% Ti; 135KV,
12ma, 27ipm, 0.020-in. X oscillation

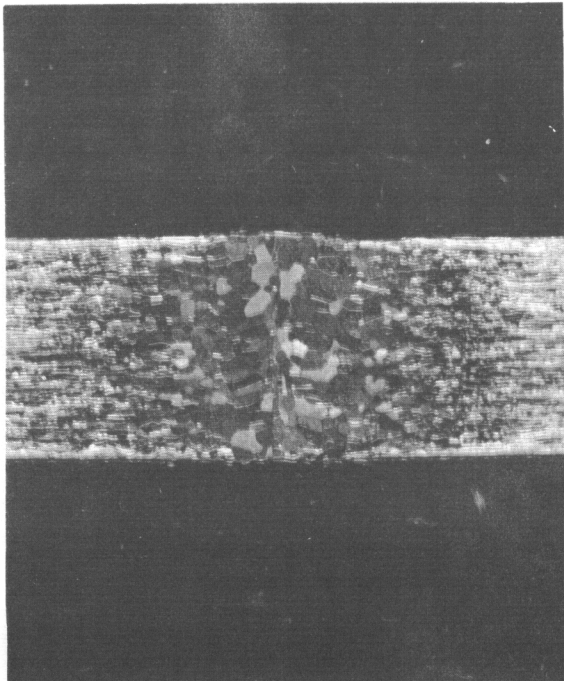


Fig. 53 Trial Weld Cross-section;
X20; 0.055-in. Mo-0.5% Ti; 120KV,
7ma, 27ipm, 0.050-in. X oscillation

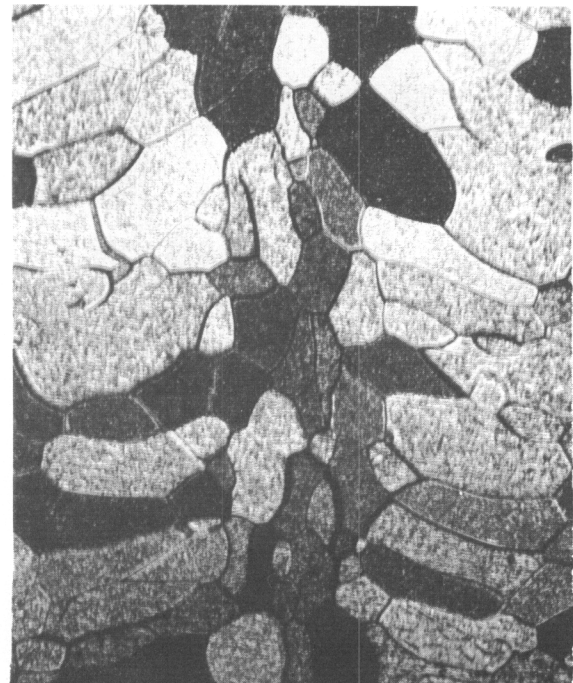


Fig. 54 Trial Weld Microstructure;
X100; 0.055-in. Mo-0.5% Ti; 120KV,
7ma, 27ipm, 0.050-in. X oscillation

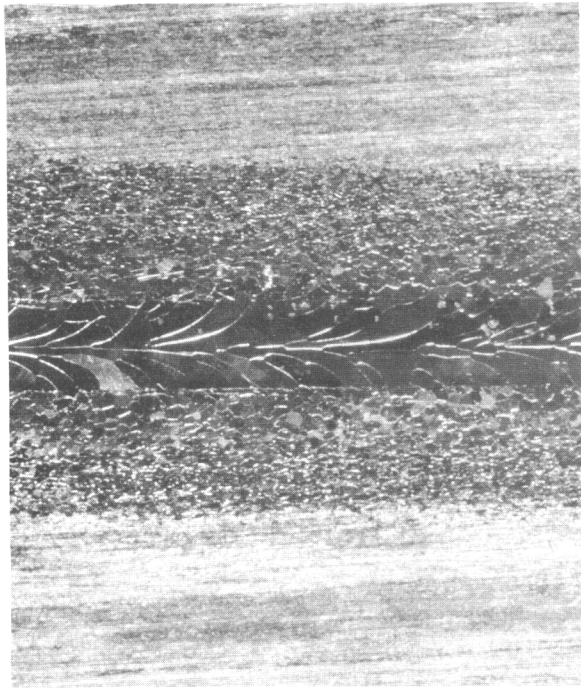


Fig. 55 Trial Weld Bead; X20;
0.005-in. Mo-0.5% Ti; 70KV, 1.2ma,
7ipm

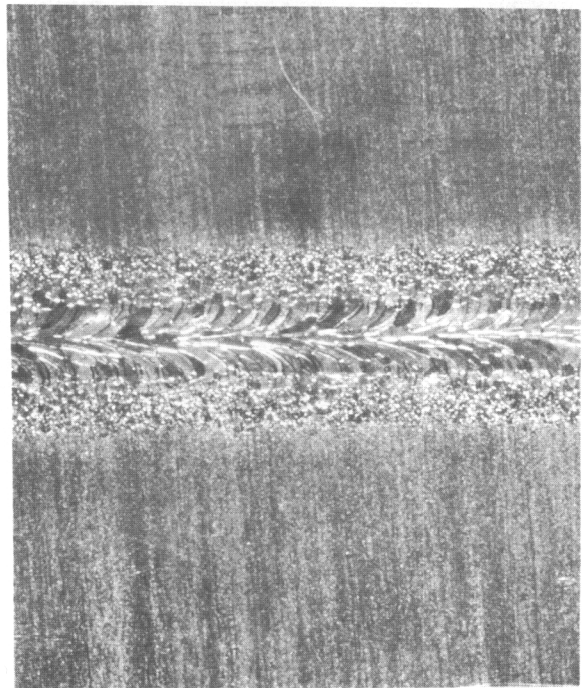


Fig. 56 Trial Weld Bead; X20;
0.005-in. Mo-0.5% Ti; 80KV, 1.5ma,
27ipm

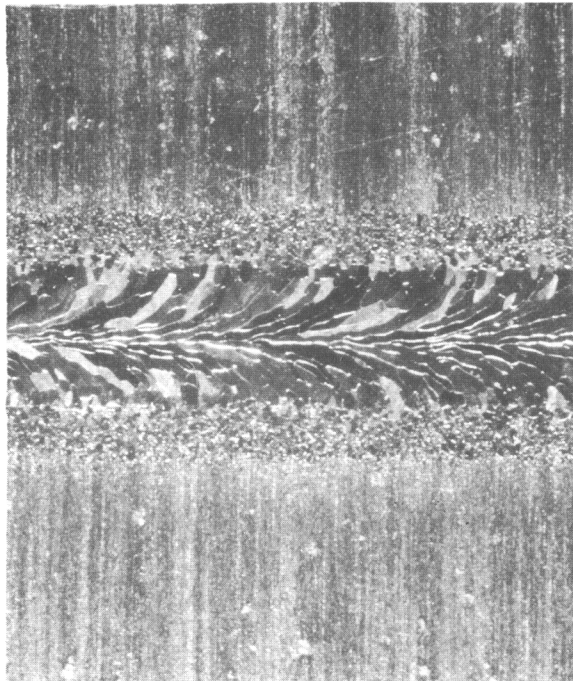


Fig. 57 Trial Weld Bead; X20;
0.005-in. Mo-0.5% Ti; 85KV, 1.3ma,
27ipm, 0.020-in. Y oscillation

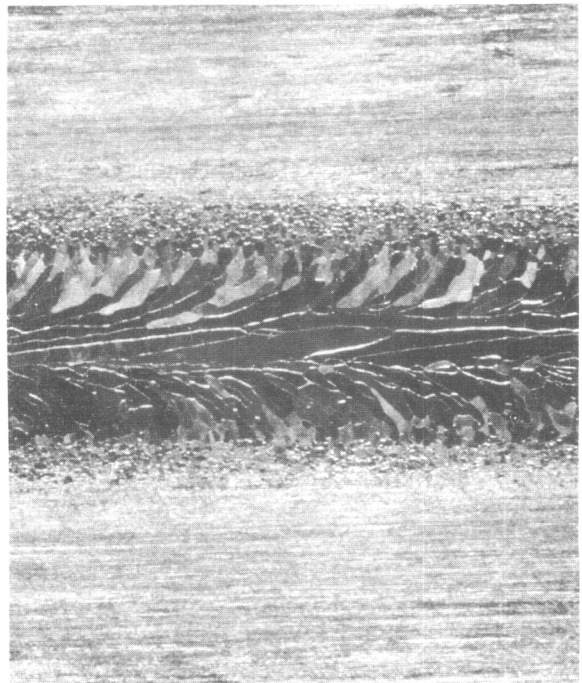


Fig. 58 Trial Weld Bead; X20;
0.005-in. Mo-0.5% Ti; 85KV, 1.6ma,
27ipm, 0.040-in. Y oscillation

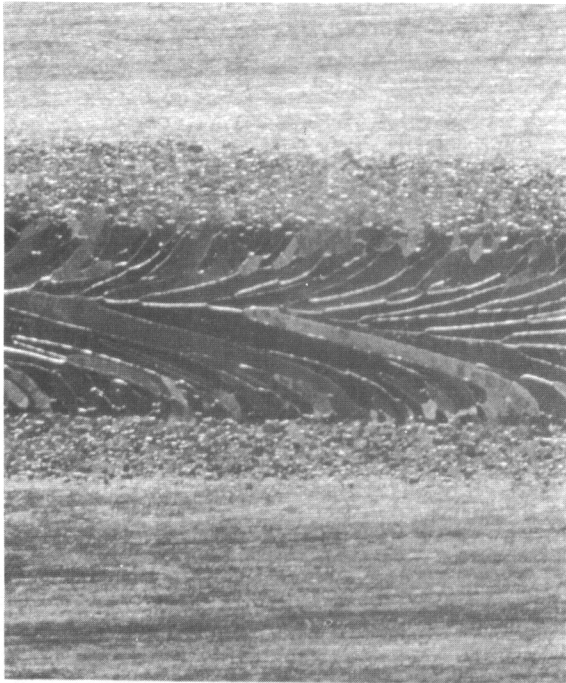


Fig. 59 Trial Weld Bead; X20;
0.005-in. Mo-0.5% Ti; 85KV, 1.2ma,
14ipm, 0.040-in. Y oscillation

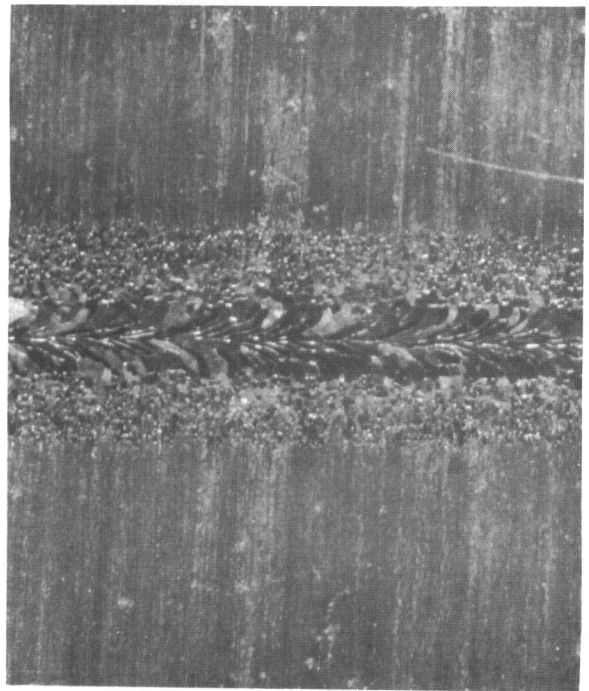


Fig. 60 Trial Weld Bead; X20;
0.005-in. Mo-0.5% Ti; 85KV, 1.3ma,
27ipm, 0.050-in. X oscillation

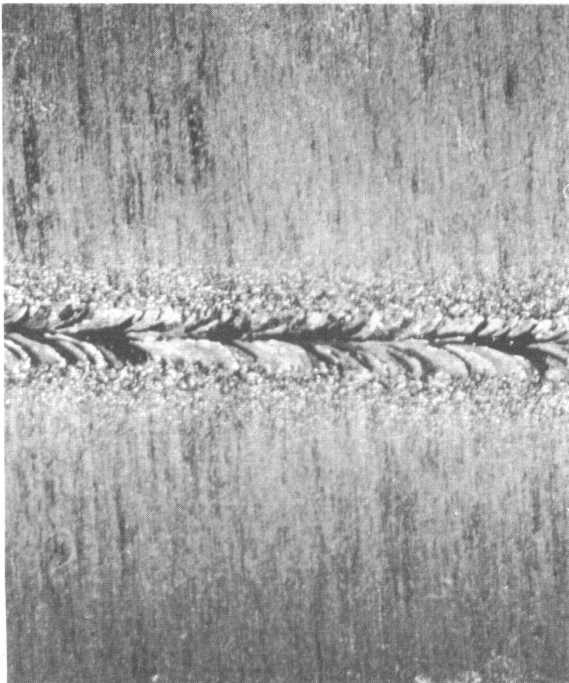


Fig. 61 Trial Weld Bead; X20;
0.005-in. Mo-0.5% Ti; 90KV, 1.2ma,
7ipm, 30cps, 10ms on-time

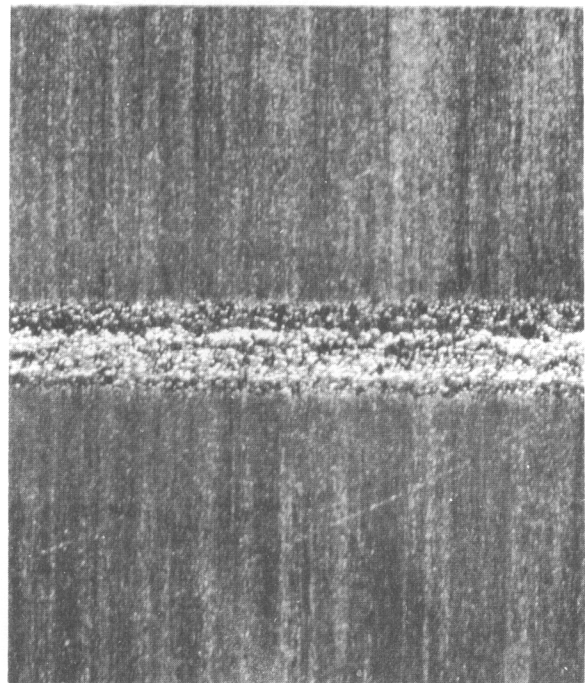


Fig. 62 Trial Weld Bead; X20; 0.005-in.
Mo-0.5% Ti; 85KV, 1.2ma, 27ipm,
0.020-in. X oscillation, chilled

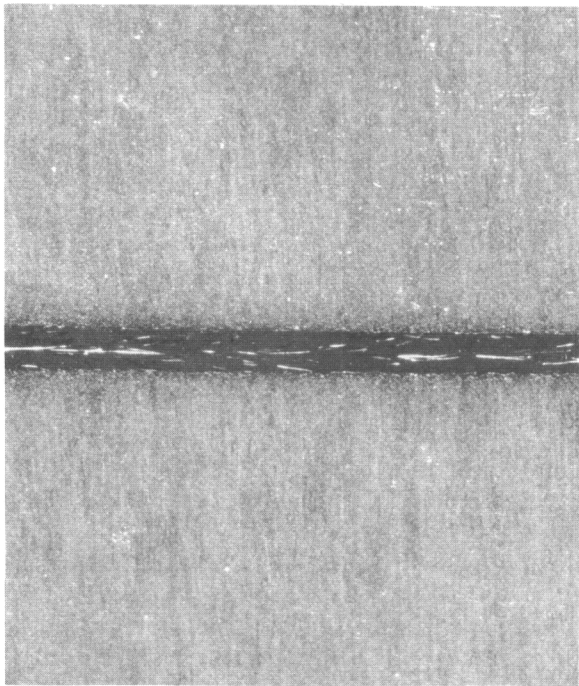


Fig. 63 Tungsten Weld Bead;
Unetched; X20; 90KV, 1.0ma, 7ipm

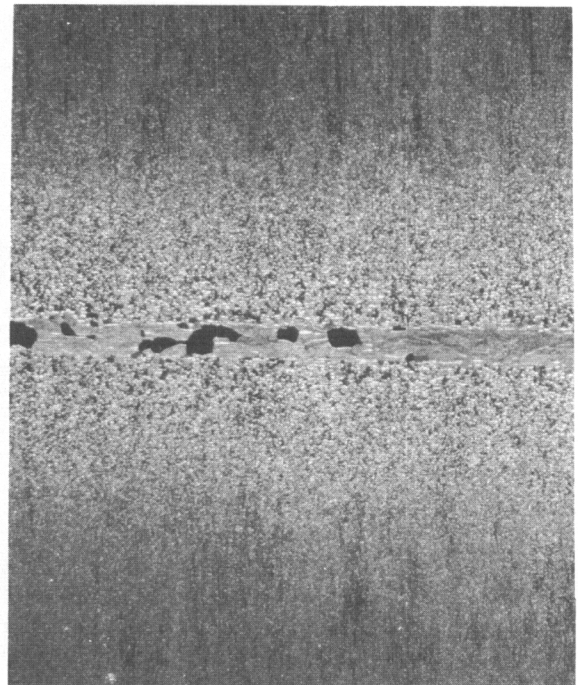


Fig. 64 Tungsten Weld Bead; Etched;
X20; 90KV, 1.0ma, 7ipm

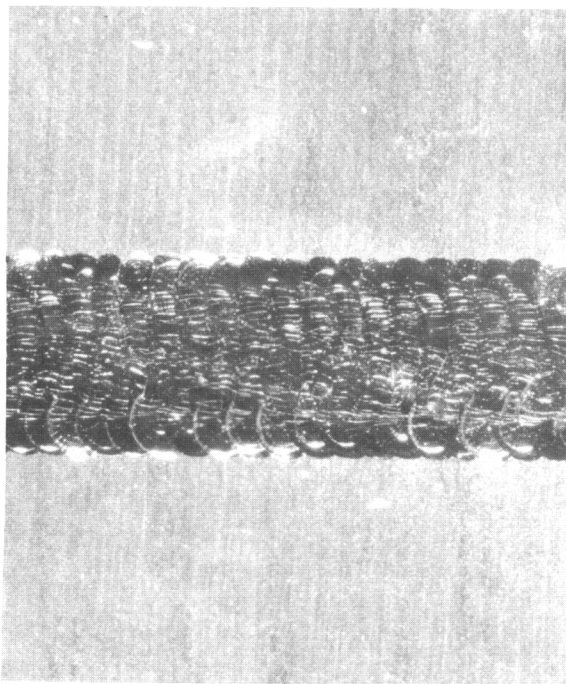


Fig. 65 Tungsten Weld Bead;
Unetched; X20; 90KV, 2.0ma, 27ipm,
0.040-in. Y oscillation

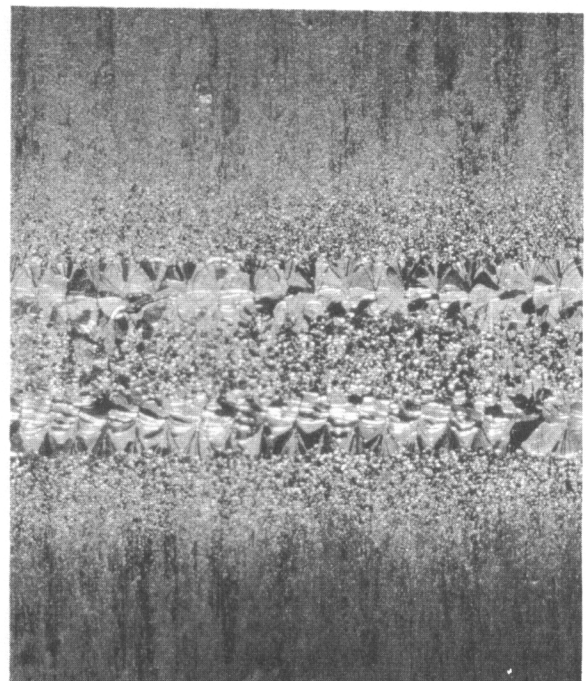


Fig. 66 Tungsten Weld Bead; Etched;
X20; 90KV, 2.0ma, 27ipm, 0.040-in.
Y oscillation

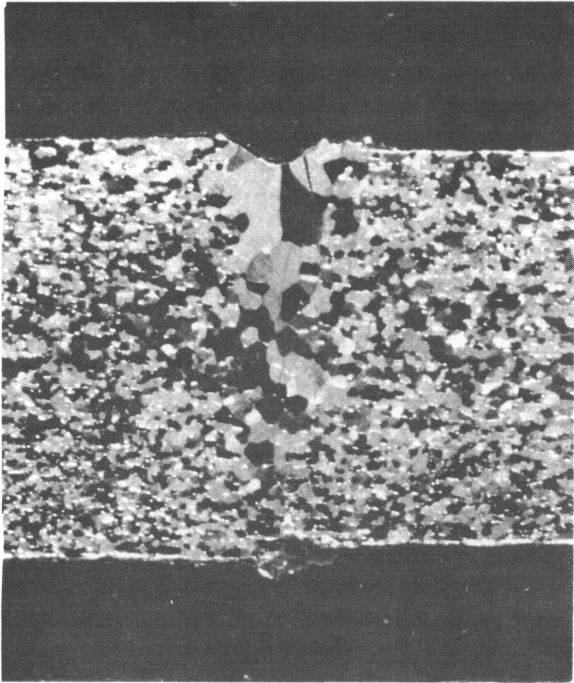


Fig. 67 Trial Weld Cross-section;
X20; 0.100-in. Tungsten; 135KV, 8ma,
4ipm

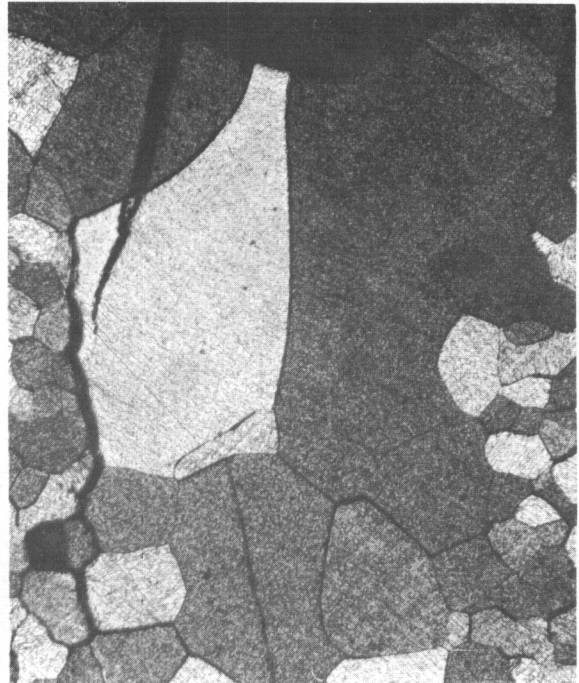


Fig. 68 Trial Weld Microstructure;
X100; 0.100-in. Tungsten; 135KV,
8ma, 4ipm

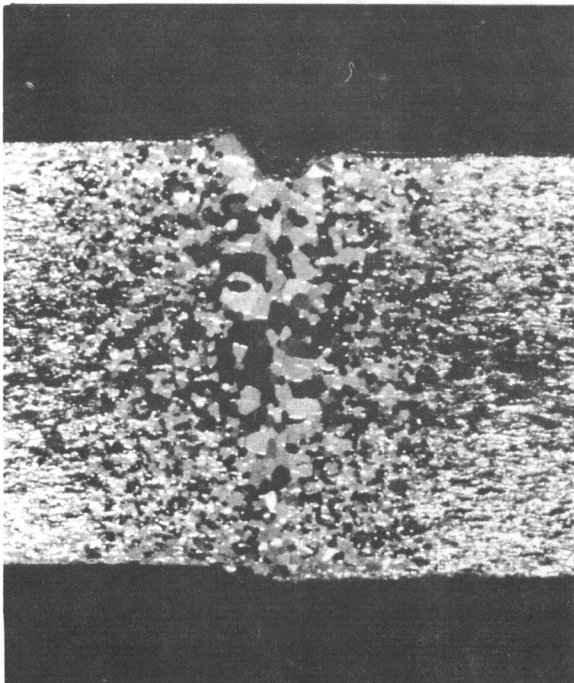


Fig. 69 Trial Weld Cross-section;
X20; 0.100-in. Tungsten; 135KV,
10ma, 10ipm

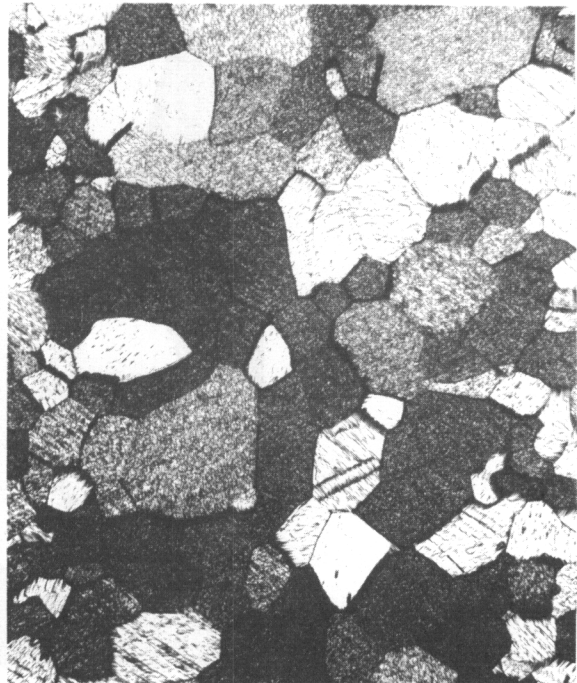


Fig. 70 Trial Weld Microstructure;
X100; 0.100-in. Tungsten; 135KV,
10ma, 10ipm

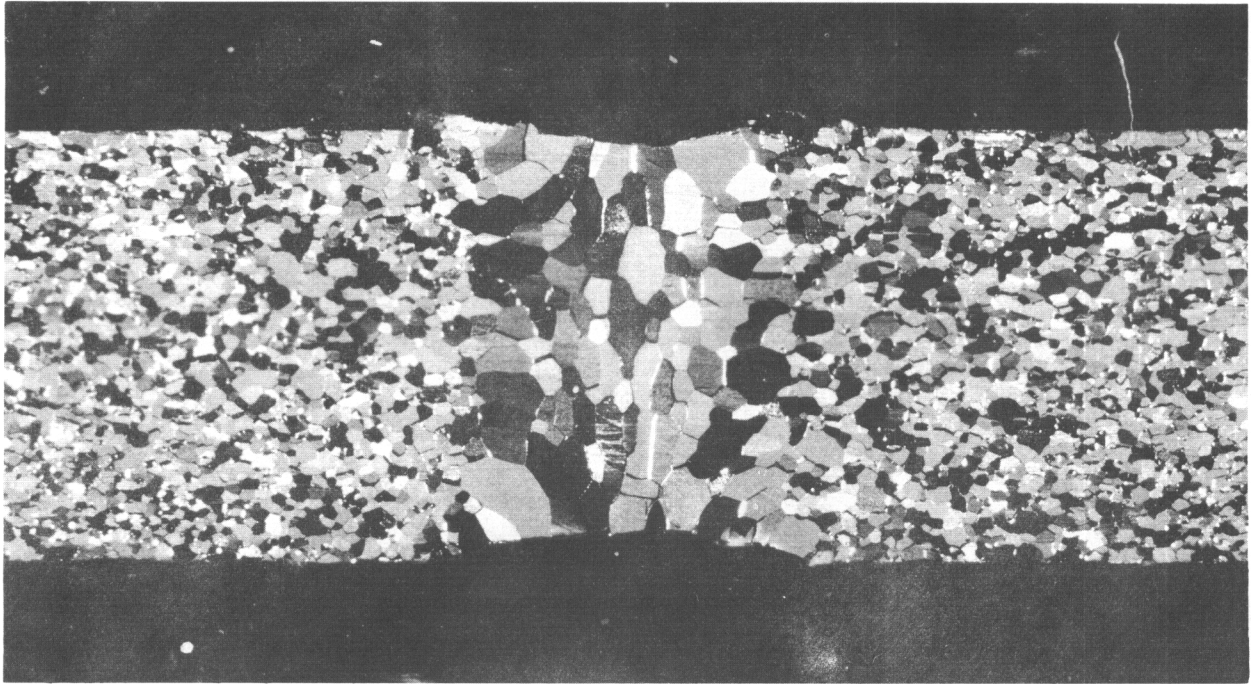


Fig. 71 Trial Weld Cross-section; X20; 0.100-in. Tungsten; 150KV, 10ma, 7ipm, 0.040-in. Y oscillation

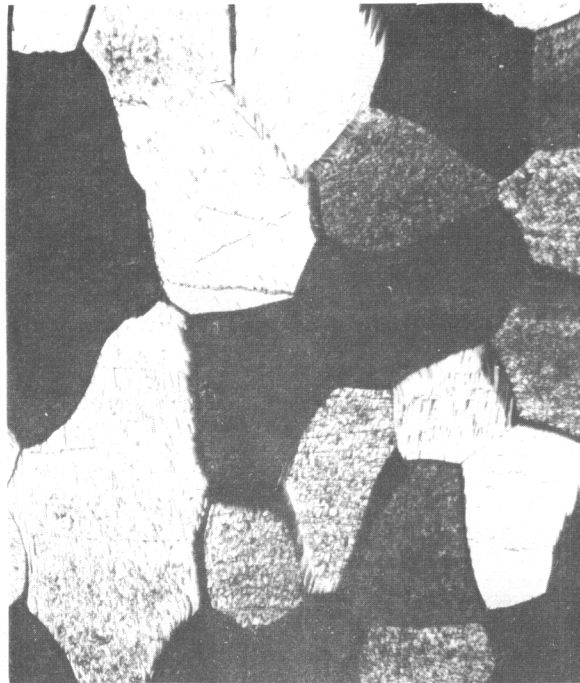


Fig. 72 Trial Weld Microstructure; X100; 0.100-in. Tungsten; 150KV, 10ma, 7ipm, 0.040-in. Y oscillation

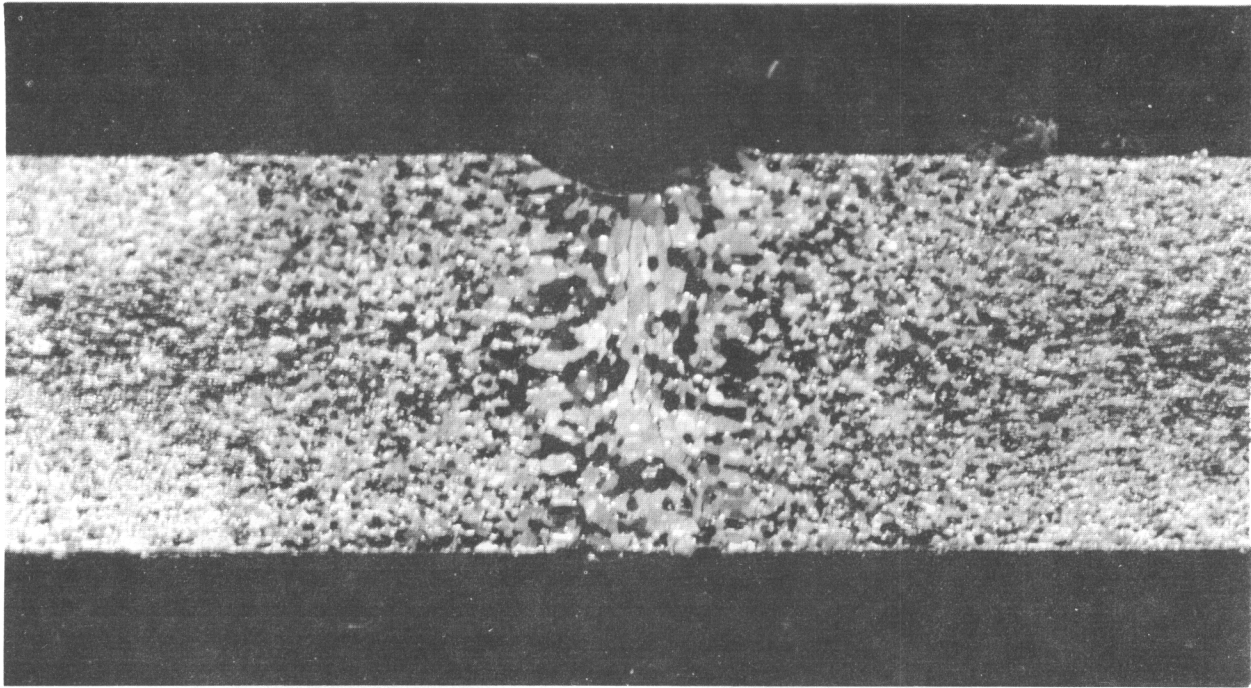


Fig. 73 Trial Weld Cross-section; X20; 0.100-in. Tungsten; 135KV, 11ma, 14ipm, 0.020-in. Y oscillation

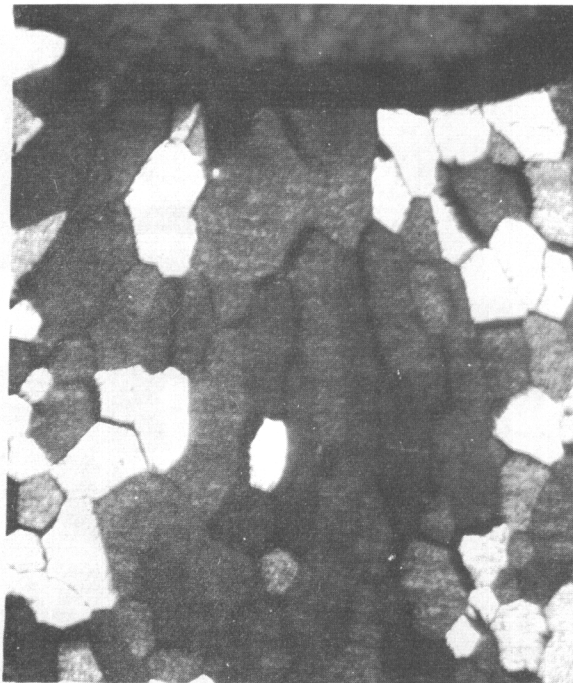


Fig. 74 Trial Weld Microstructure; X100; 0.100-in. Tungsten; 135KV, 11ma, 14ipm, 0.020-in. Y oscillation

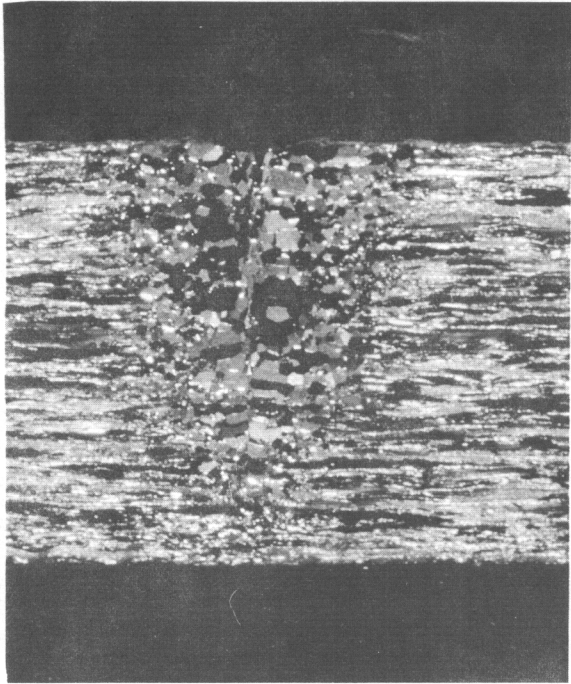


Fig. 75 Trial Weld Cross-section;
X20; 0.100-in. Tungsten; 135KV,
11ma, 14ipm, 0.025-in. X oscillation

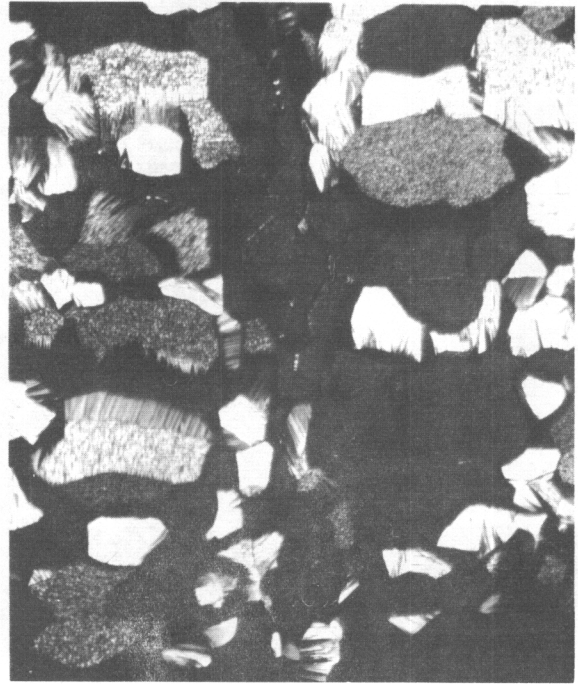


Fig. 76 Trial Weld Microstructure;
X100; 0.100-in. Tungsten; 135KV,
11ma, 14ipm, 0.025-in. X oscillation

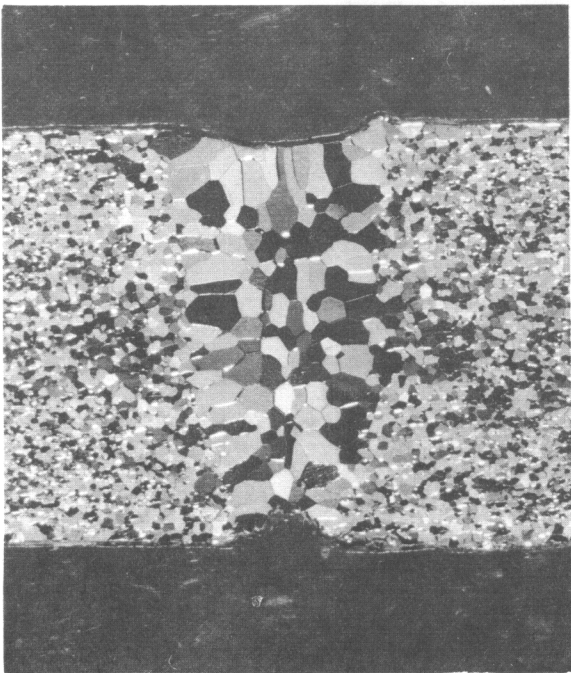


Fig. 77 Trial Weld Cross-section;
X20; 0.100-in. Tungsten; 150KV,
16ma, 20ipm, 0.050-in. X oscillation,
defocused

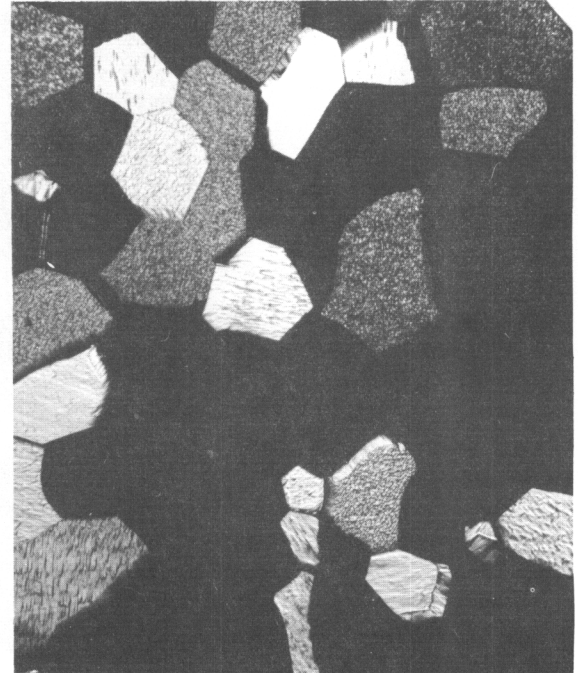


Fig. 78 Trial Weld Microstructure;
X100; 0.100-in. Tungsten; 150KV,
16ma, 20ipm, 0.050-in. X oscillation,
defocused

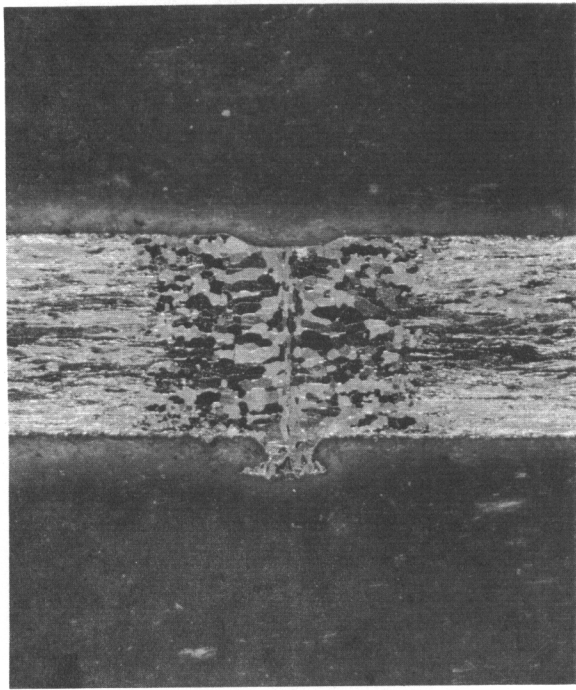


Fig. 79 Trial Weld Cross-section;
X20; 0.050-in. Tungsten; 135KV,
12ma, 27ipm, 0.060-in. X oscillation

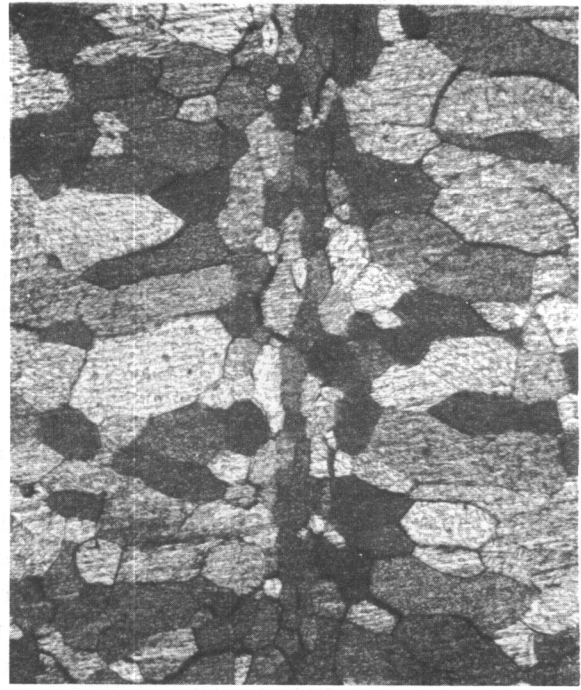


Fig. 80 Trial Weld Microstructure;
X100; 0.050-in. Tungsten; 135KV,
12ma, 27ipm, 0.060-in. X oscillation

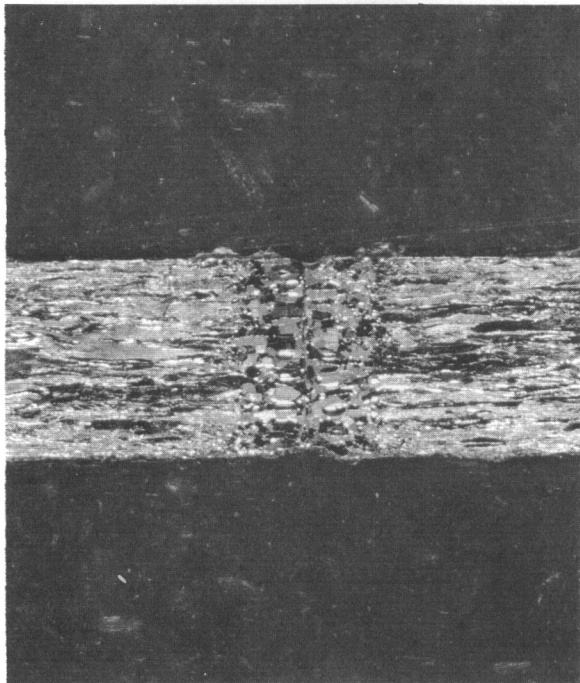


Fig. 81 Trial Weld Cross-section;
X20; 0.050-in. Tungsten; 145KV,
16ma, 100ipm, 0.065-in. X oscillation

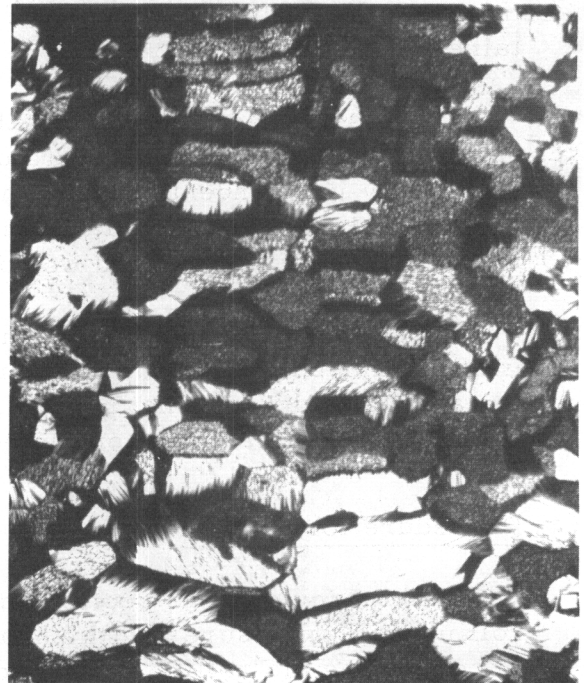


Fig. 82 Trial Weld Microstructure;
X100; 0.050-in. Tungsten; 145KV,
16ma, 100ipm, 0.065-in. X oscillation

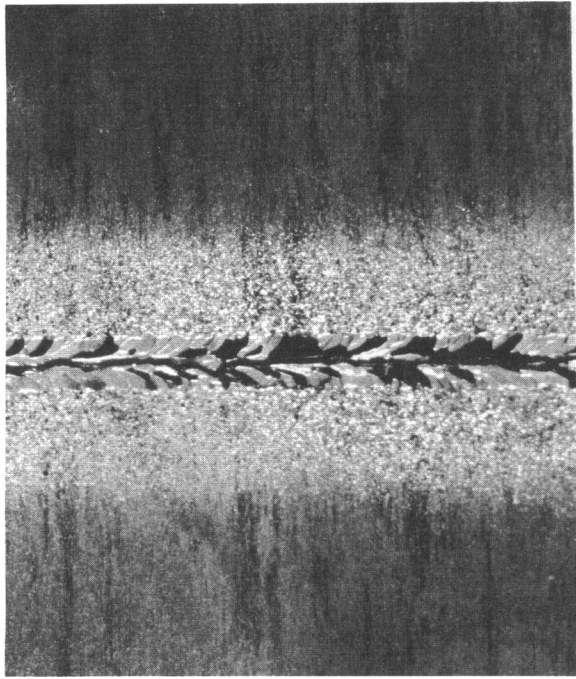


Fig. 83 Trial Weld Bead; X20;
0.005-in. Tungsten; 90KV, 1.5ma,
27ipm

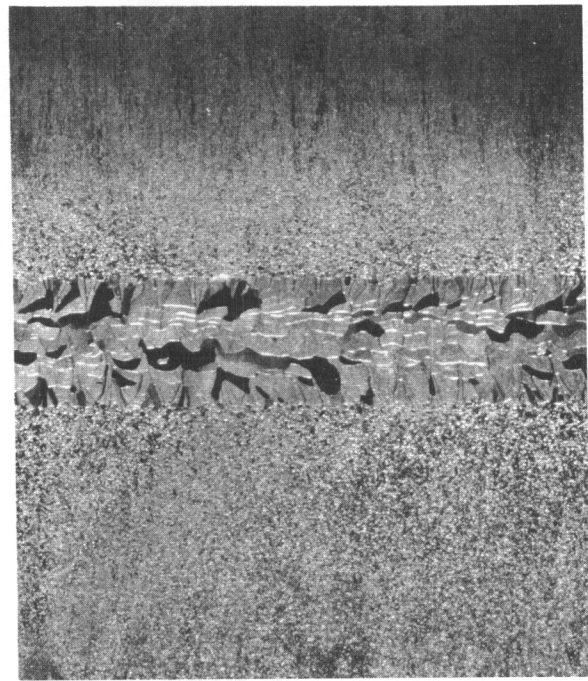


Fig. 84 Trial Weld Bead; X20;
0.005-in. Tungsten; 90KV, 1.7ma,
27ipm, 0.020-in. Y oscillation

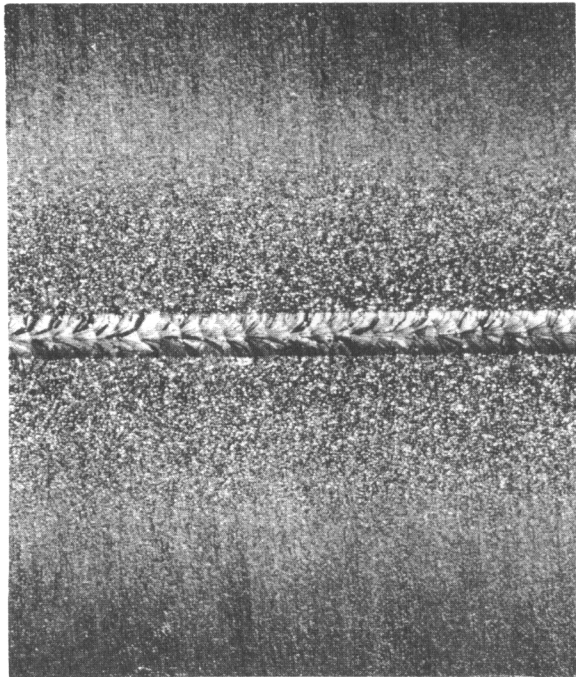


Fig. 85 Trial Weld Bead; X20;
0.005-in. Tungsten; 90KV, 2.4ma,
27ipm, 0.200-in. X oscillation

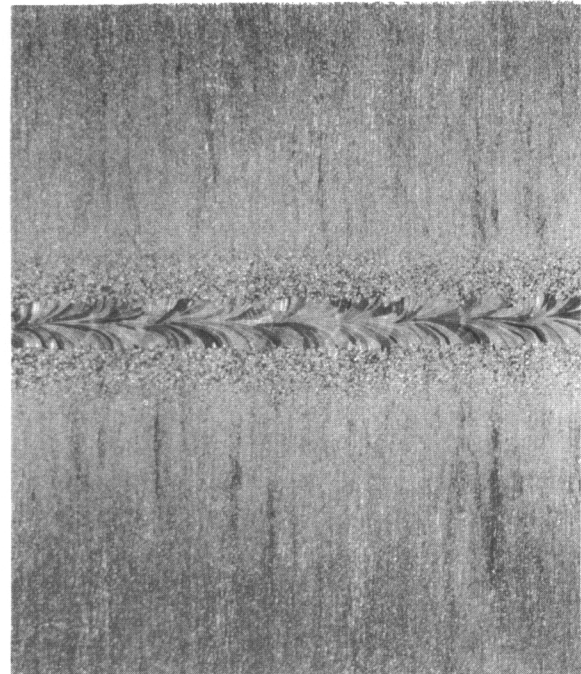


Fig. 86 Trial Weld Bead; X20;
0.005-in. Tungsten; 90KV, 2.9ma,
100ipm

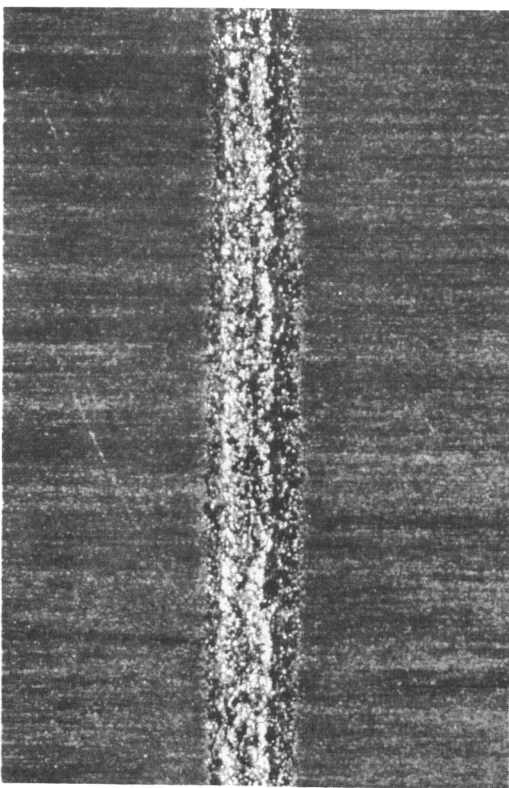


Fig. 88 Final Weld Bead; X20;
0.005-in. Mo-0.5% Ti

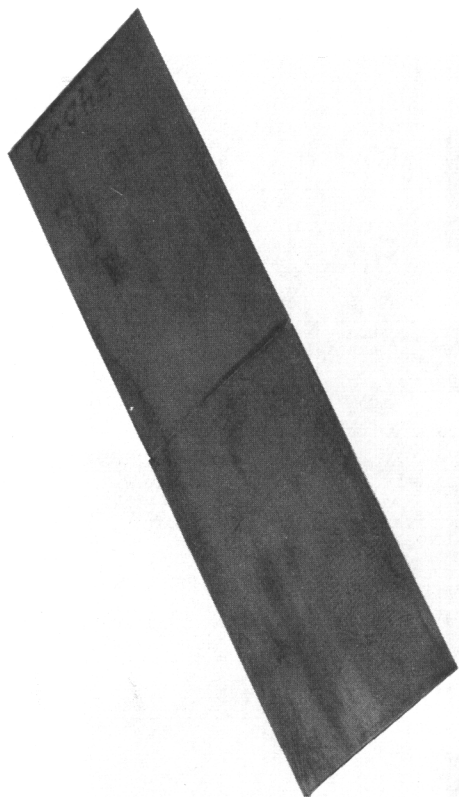


Fig. 87 Final Weld Specimen;
0.005-in. Mo-0.5% Ti

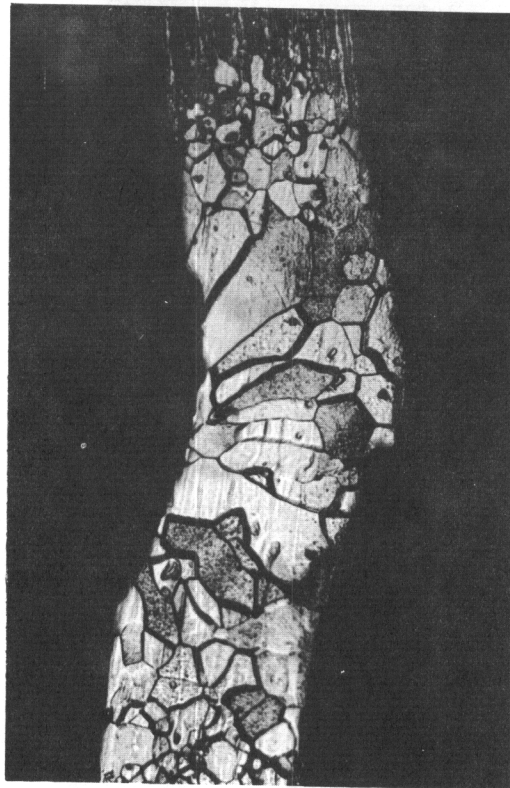


Fig. 89 Final Weld Microstructure;
X200; 0.005-in. Mo-0.5% Ti

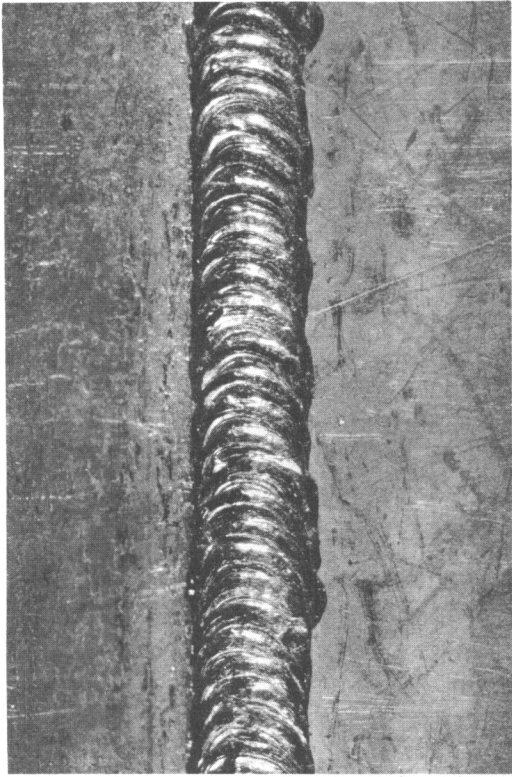


Fig. 91 Final Weld Bead; X20;
0.055-in. Mo-0.5% Ti

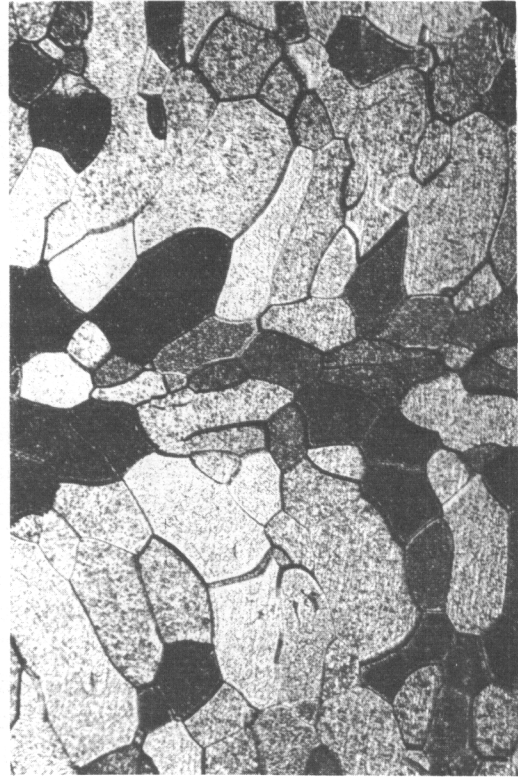


Fig. 93 Final Weld Microstructure;
X100; 0.055-in. Mo-0.5% Ti

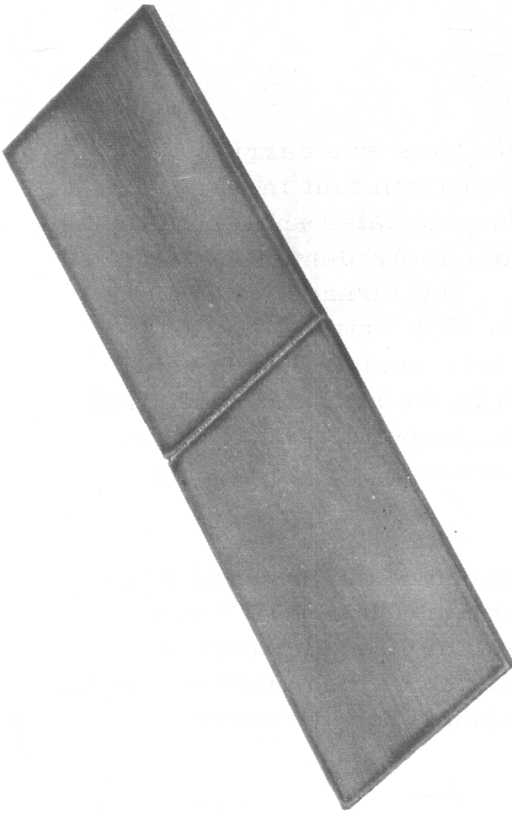


Fig. 90 Final Weld Specimen;
0.055-in. Mo-0.5% Ti

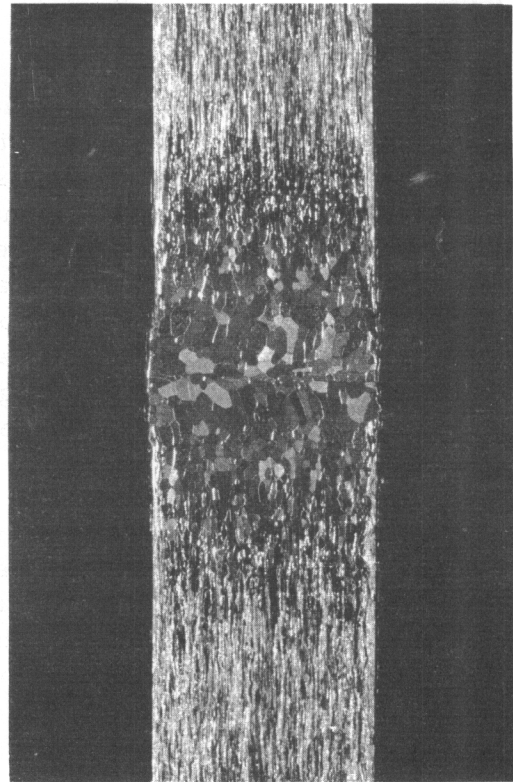


Fig. 92 Final Weld Cross-section;
X20; 0.055-in. Mo-0.5% Ti

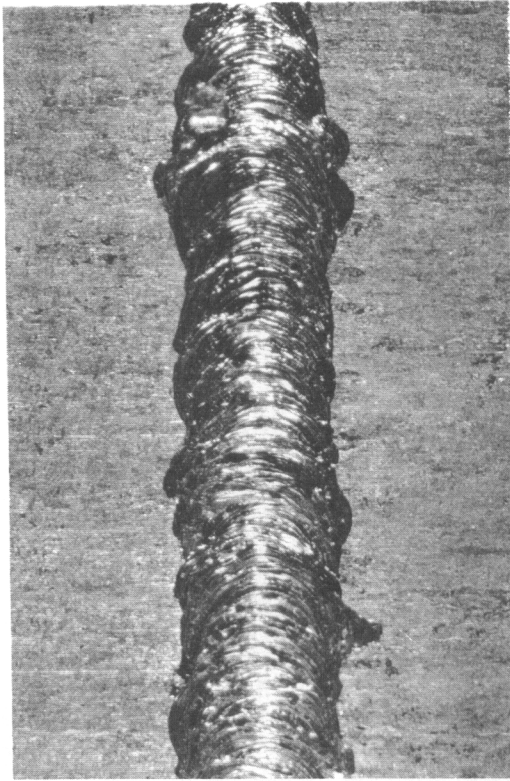


Fig. 95 Final Weld Bead; X20;
0.100-in. Mo-0.5% Ti

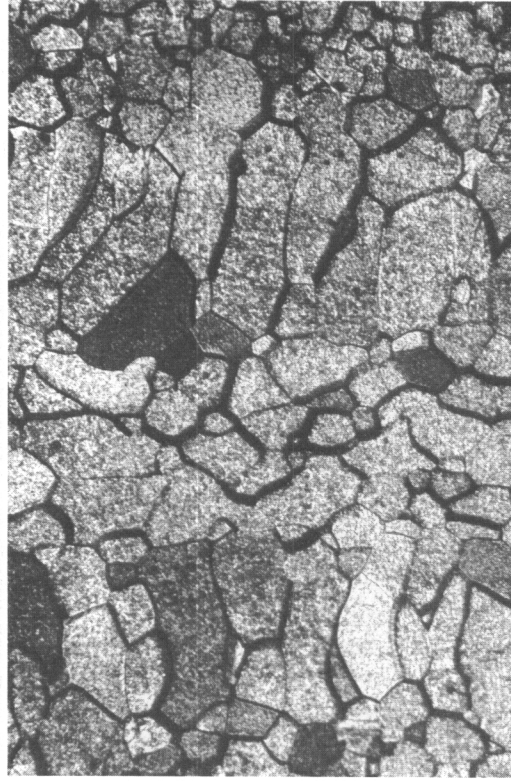


Fig. 97 Final Weld Microstructure;
X100; 0.100-in. Mo-0.5% Ti

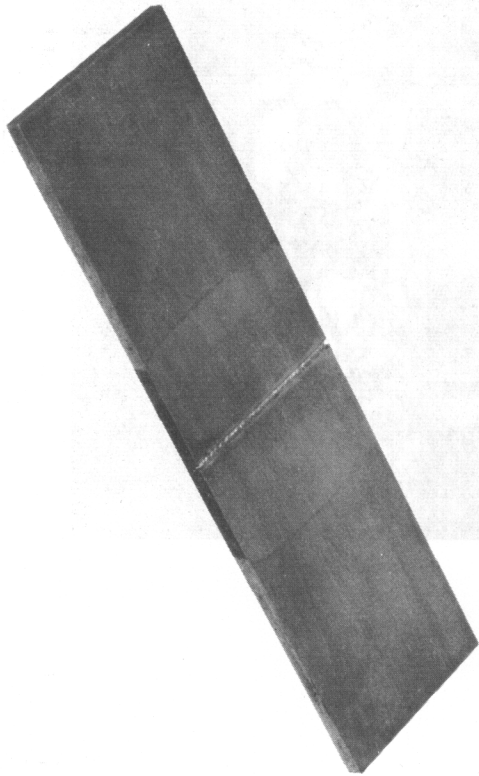


Fig. 94 Final Weld Specimen;
0.100-in. Mo-0.5% Ti

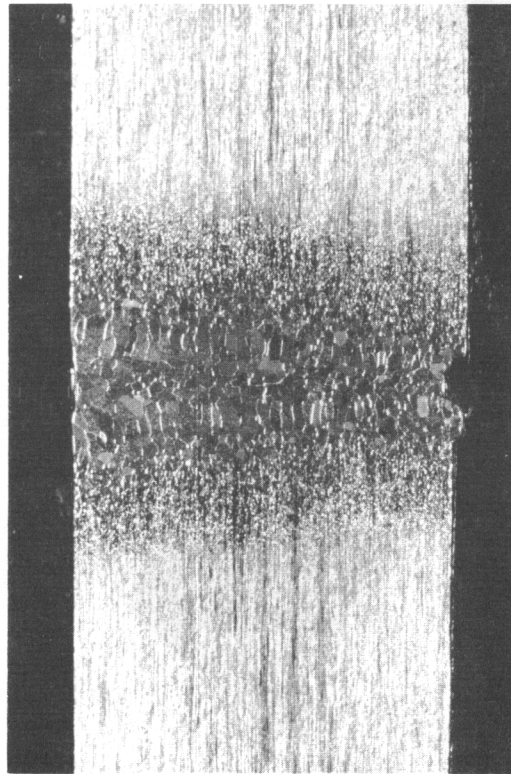


Fig. 96 Final Weld Cross-section;
X20; 0.100-in. Mo-0.5% Ti

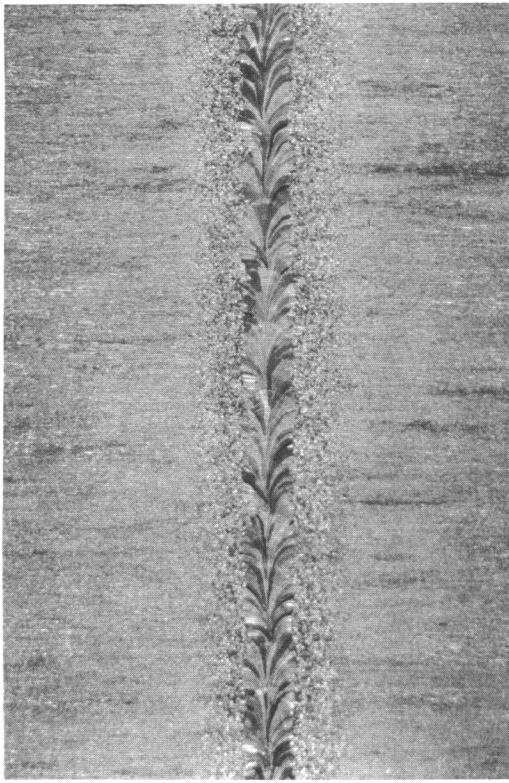


Fig. 99 Final Weld Bead; X20;
0.005-in. Tungsten

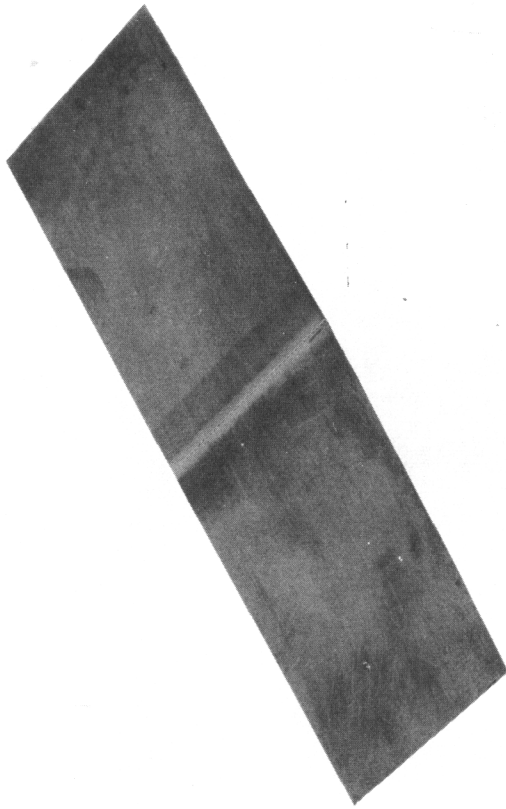


Fig. 98 Final Weld Specimen;
0.005-in. Tungsten

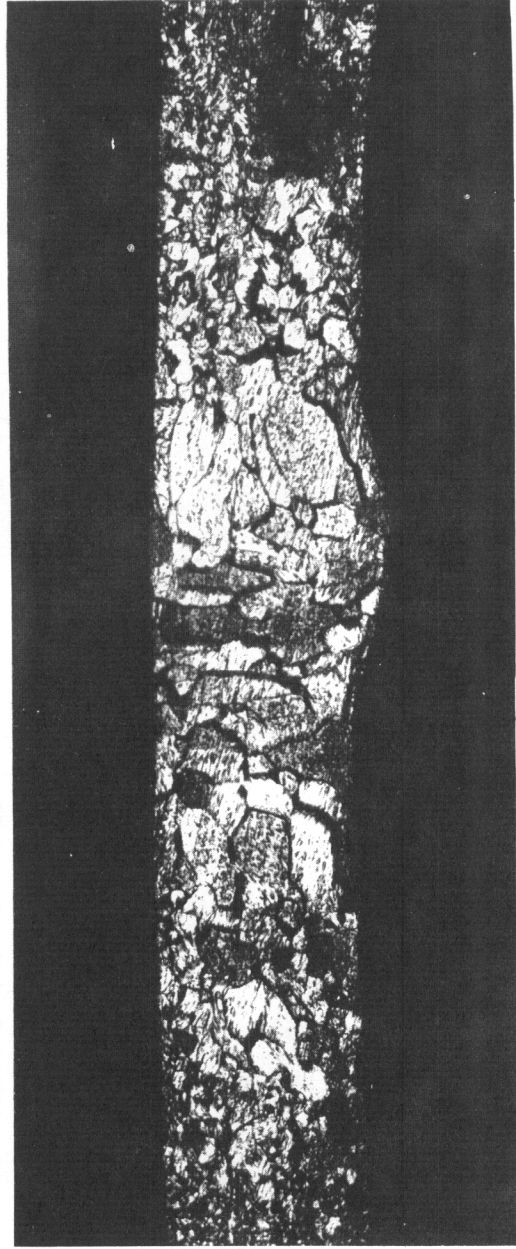


Fig. 100 Final Weld Microstructure;
X200; 0.005-in. Tungsten

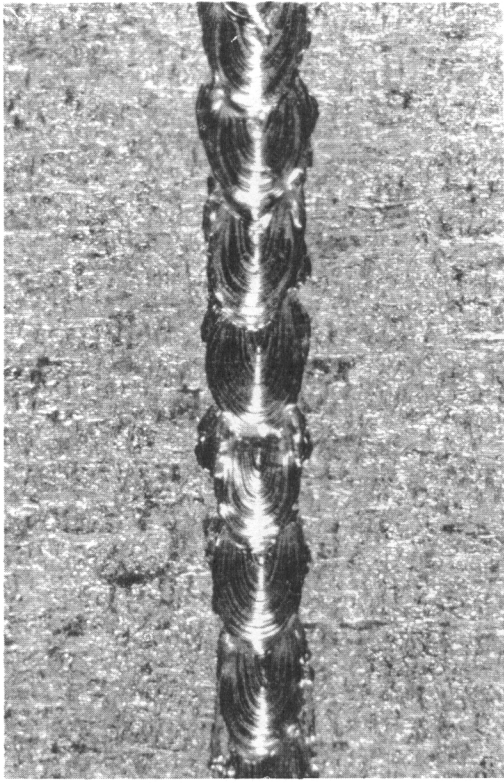


Fig. 102 Final Weld Bead; X20;
0.050-in. Tungsten



Fig. 104 Final Weld Microstructure;
X100; 0.050-in. Tungsten

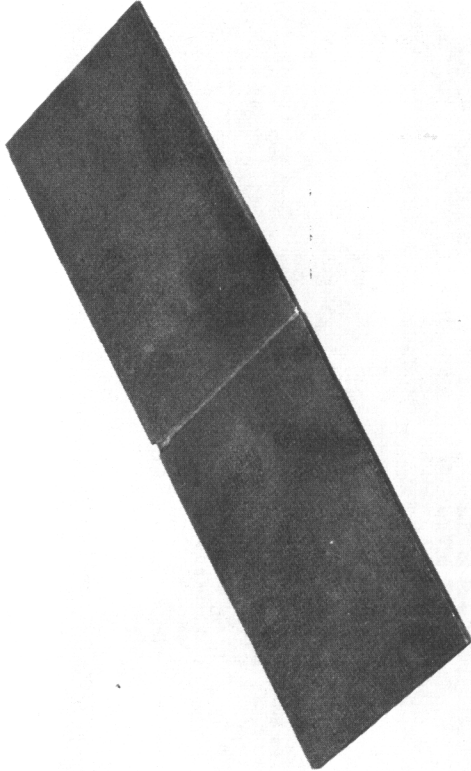


Fig. 101 Final Weld Specimen;
0.050-in. Tungsten

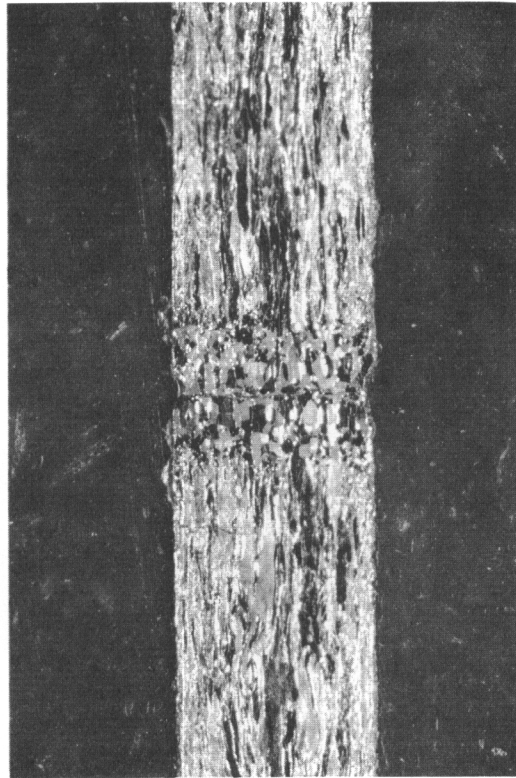


Fig. 103 Final Weld Cross-section;
X20; 0.050-in. Tungsten

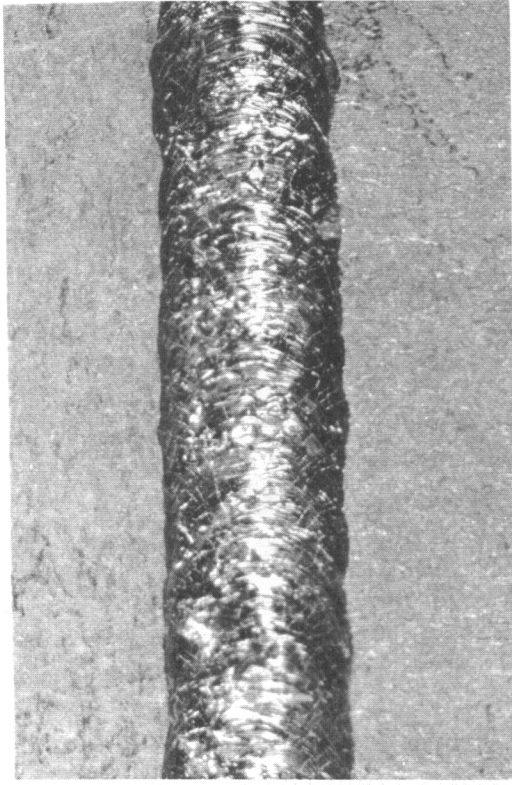


Fig. 106 Final Weld Bead; X10;
0.100-in. Tungsten

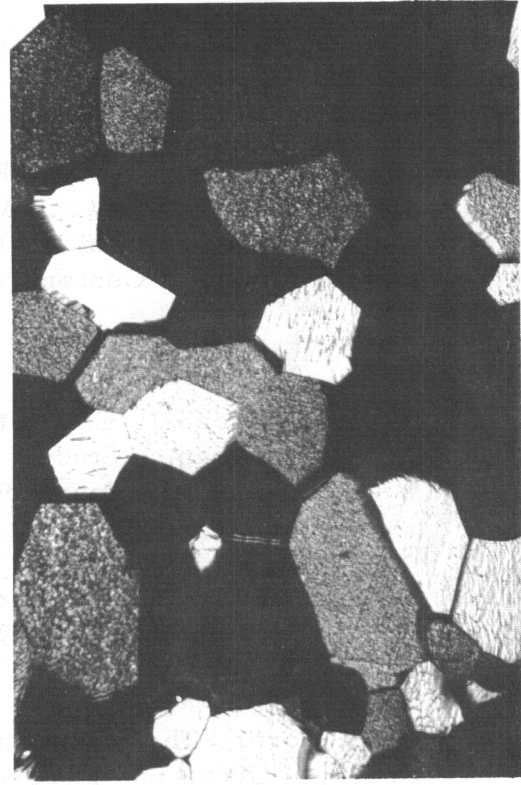


Fig. 108 Final Weld Microstructure;
X100; 0.100-in. Tungsten

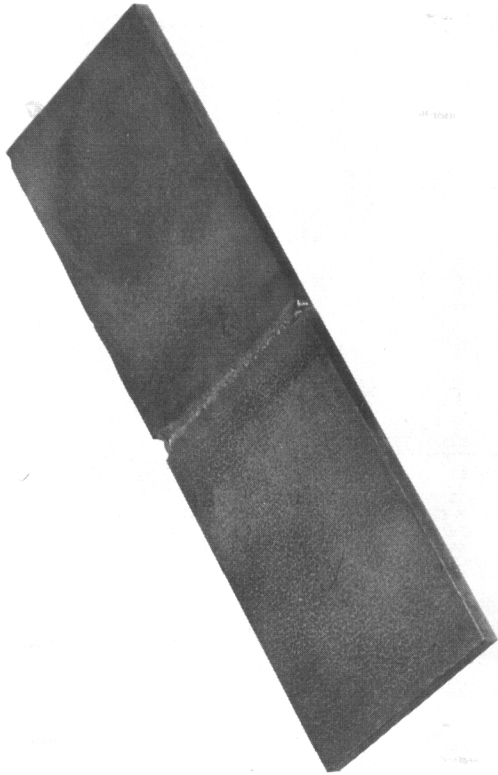


Fig. 105 Final Weld Specimen;
0.100-in. Tungsten

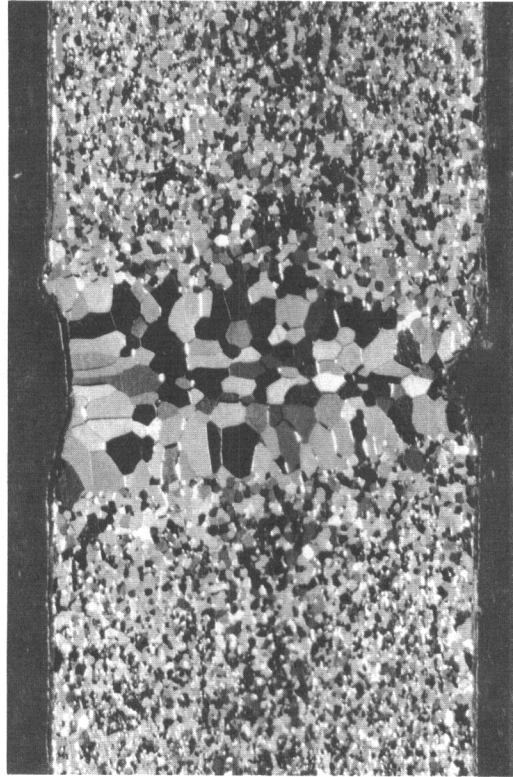


Fig. 107 Final Weld Cross-section;
X20; 0.100-in. Tungsten

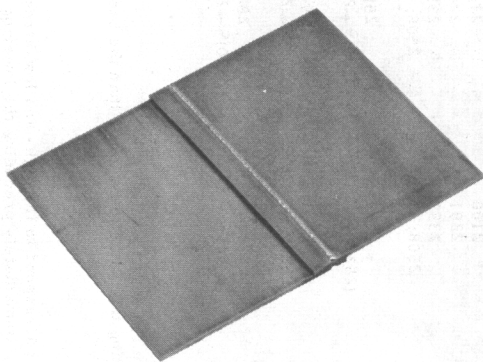


Fig. 109 Seam Weld; 0.055-in.
Mo-0.5% Ti

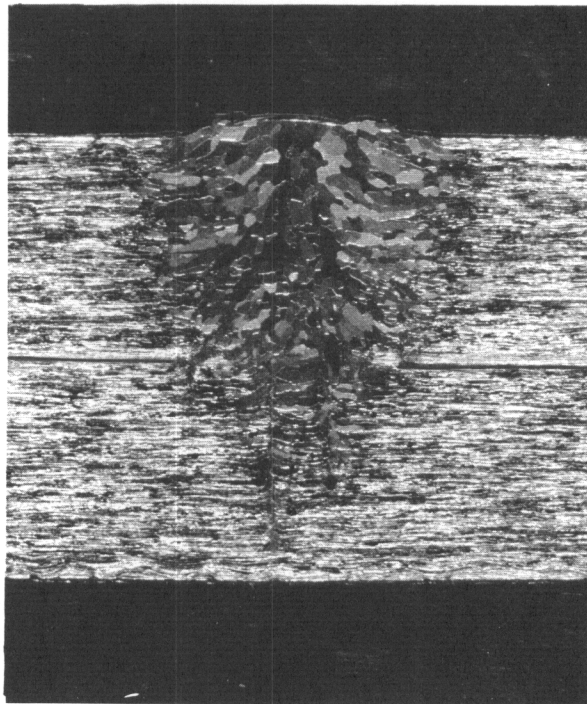


Fig. 110 Seam-weld Cross-section;
X20; 0.055-in. Mo-0.5% Ti

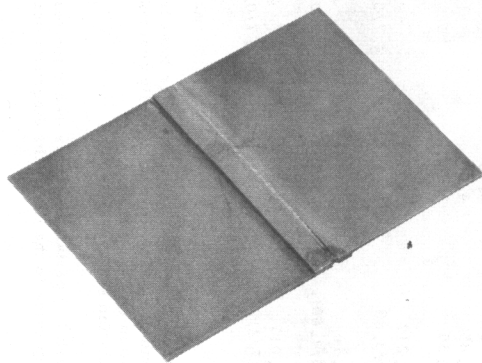


Fig. 111 Seam Weld; 0.050-in.
Tungsten

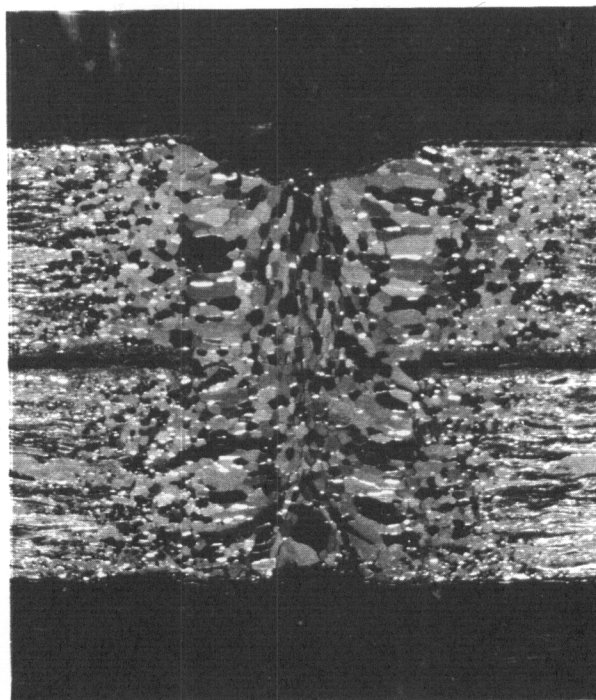


Fig. 112 Seam-weld Cross-section;
X20; 0.050-in. Tungsten

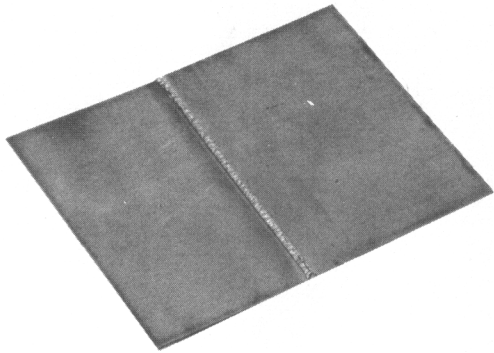


Fig. 113 Lap Weld; 0.055-in.
Mo-0.5% Ti



Fig. 114 Lap-weld Cross-section;
X20; 0.055-in. Mo-0.5% Ti

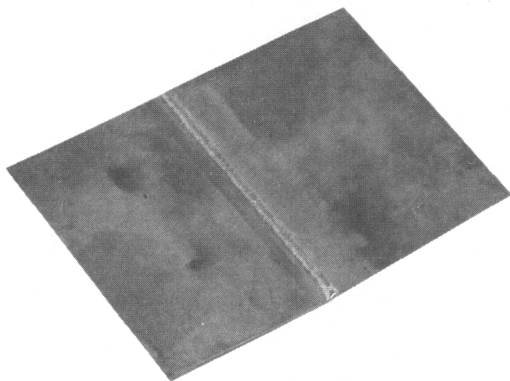


Fig. 115 Lap Weld; 0.050-in.
Tungsten

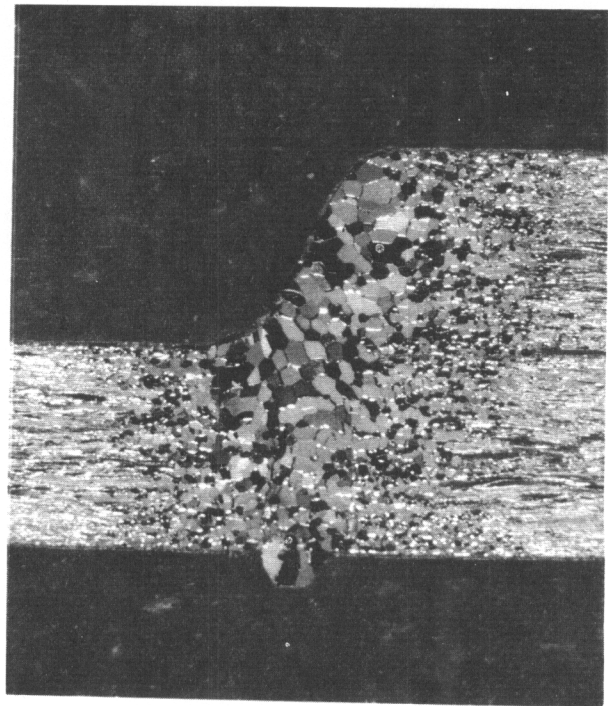


Fig. 116 Lap-weld Cross-section;
X20; 0.050-in. Tungsten

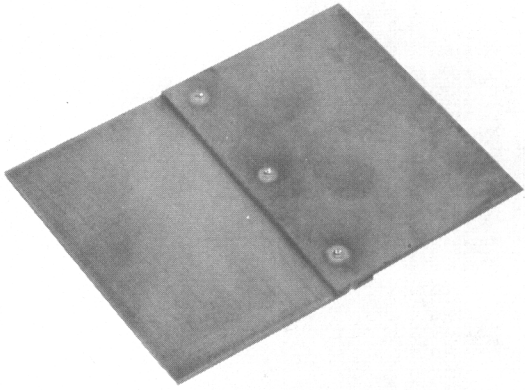


Fig. 117 Spot Weld; 0.055-in.
Mo-0.5% Ti

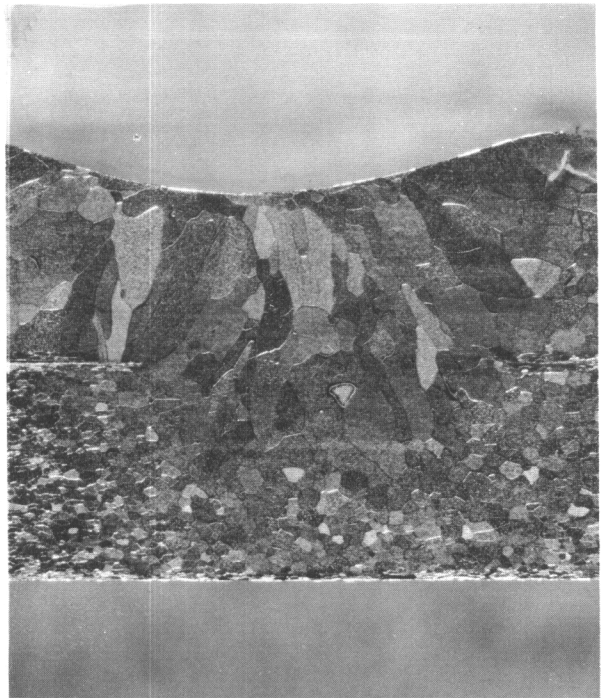


Fig. 118 Spot-weld Cross-section;
X20; 0.055-in. Mo-0.5% Ti

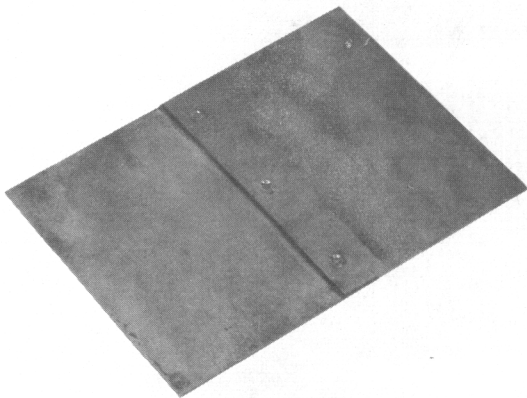


Fig. 119 Spot Weld; 0.050-in.
Tungsten

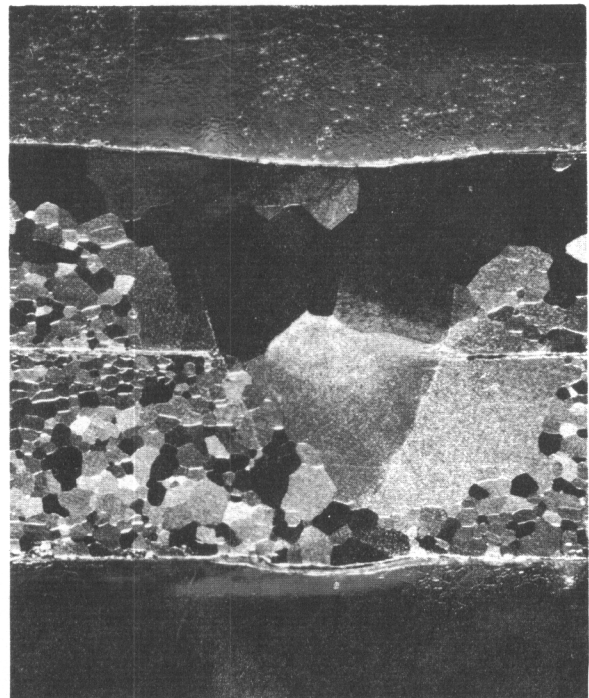


Fig. 120 Spot-weld Cross-section;
X20; 0.050-in. Tungsten

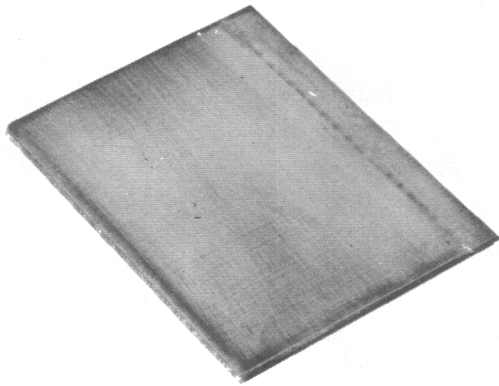


Fig. 121 Edge Weld; 0.055-in.
Mo-0.5% Ti

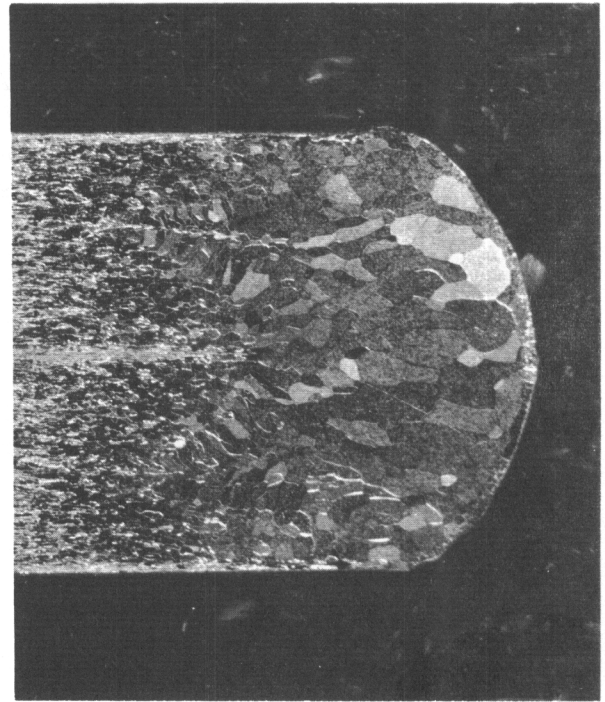


Fig. 122 Edge-weld Cross-section;
X20; 0.055-in. Mo-0.5% Ti

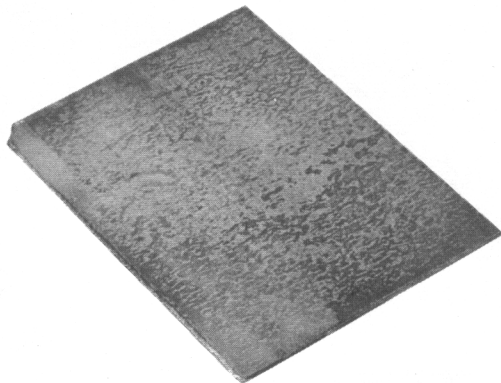


Fig. 123 Edge Weld; 0.050-in.
Tungsten

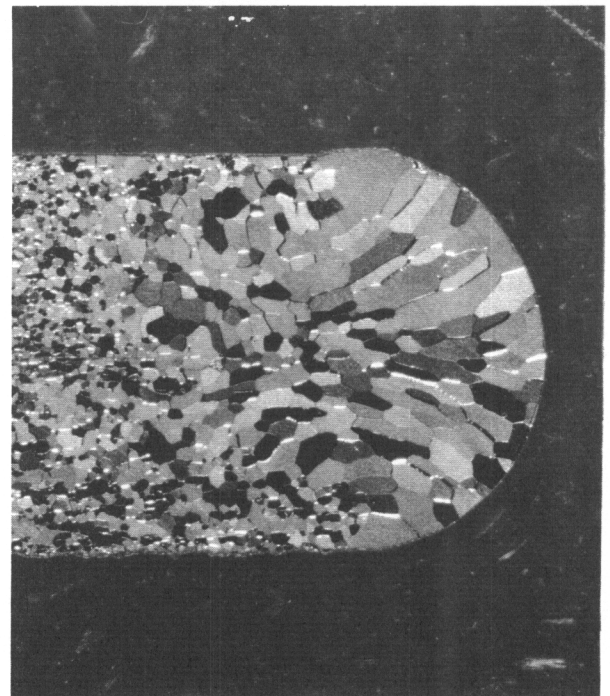


Fig. 124 Edge-weld Cross-section;
X20; 0.050-in. Tungsten

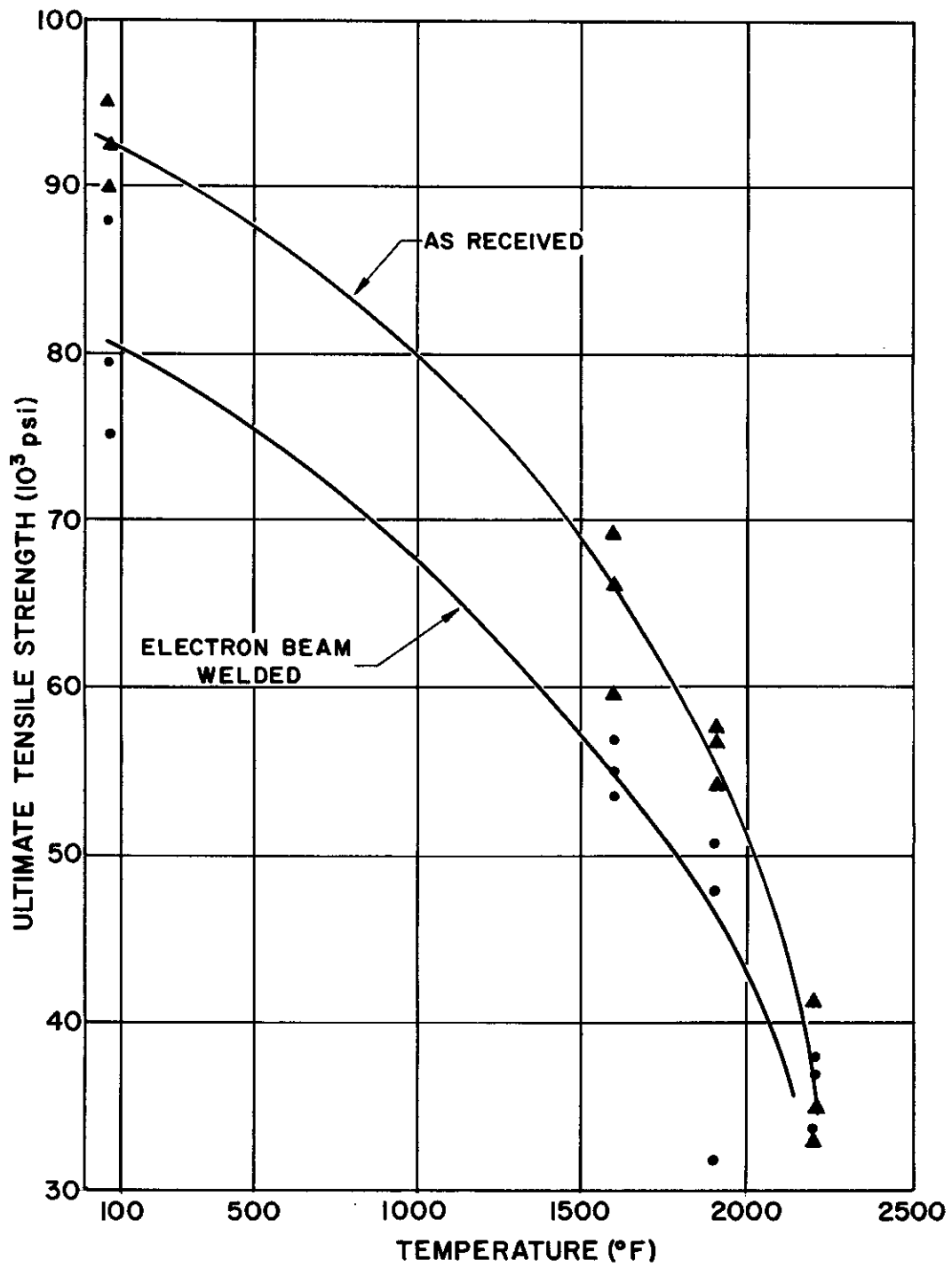


Fig. 125 Ultimate Strength vs Temperature; 0.055-in. Mo-0.5% Ti Welds



Fig. 126 Room-temperature weld-zone Failure; X50; 0.055-in. Mo-0.5% Ti Weld

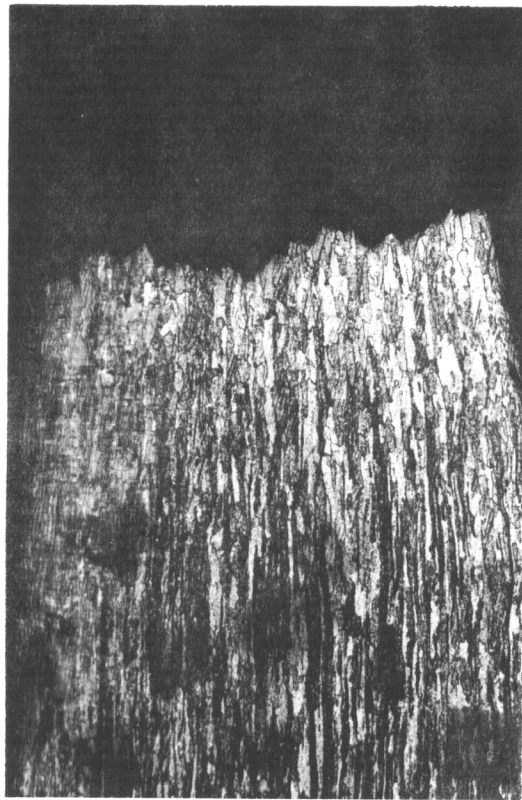


Fig. 127 1600°F Weld-zone Failure; X50; 0.055-in. Mo-0.5% Ti Weld

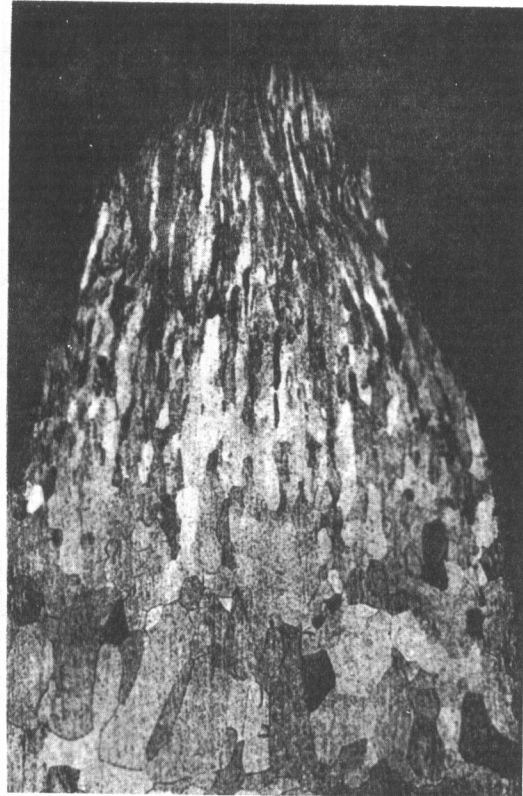


Fig. 128 2200°F Base-metal Failure; X50; 0.055-in. Mo-0.5% Ti Weld

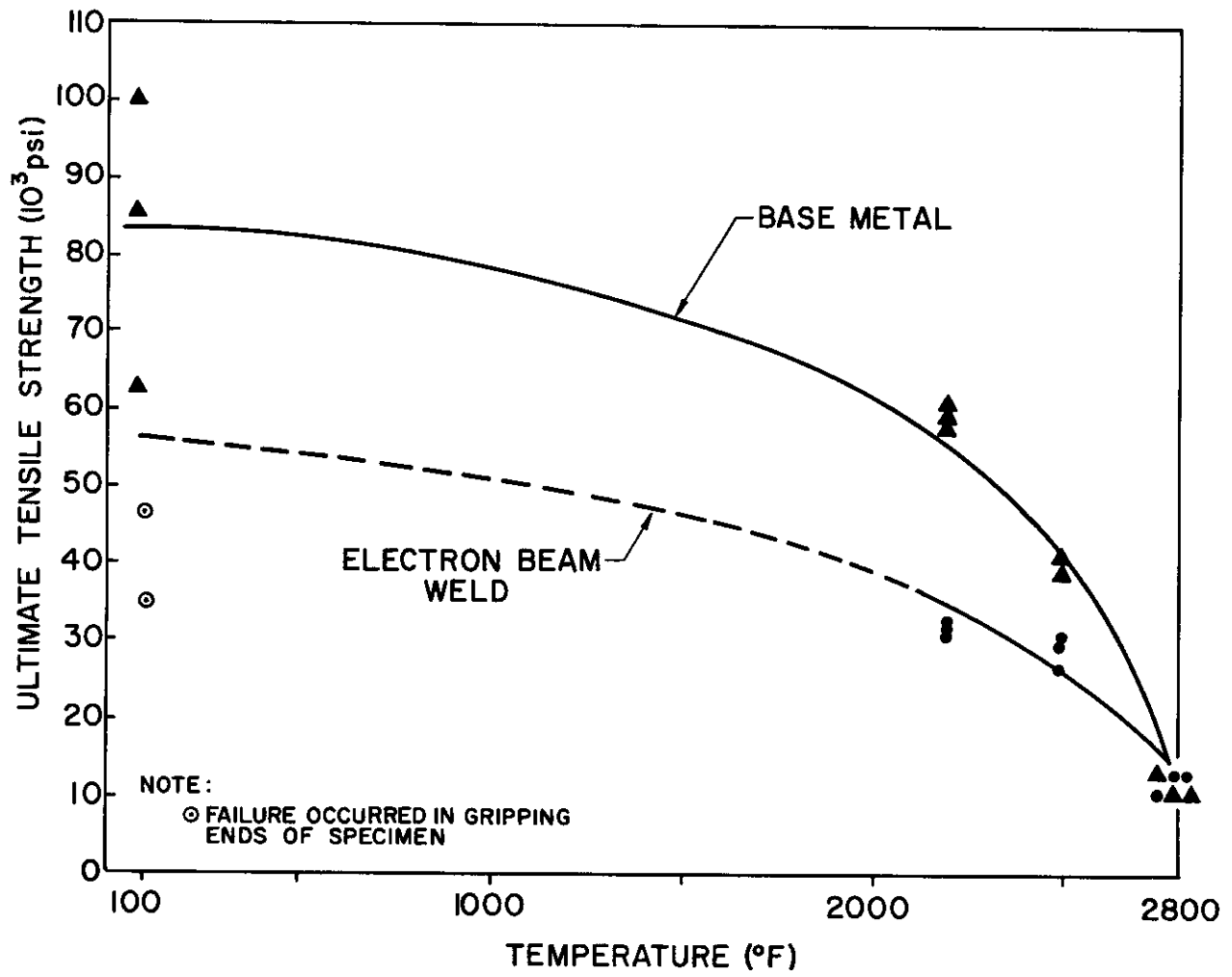


Fig. 129 Ultimate Strength vs Temperature; 0.050-in. Tungsten Welds

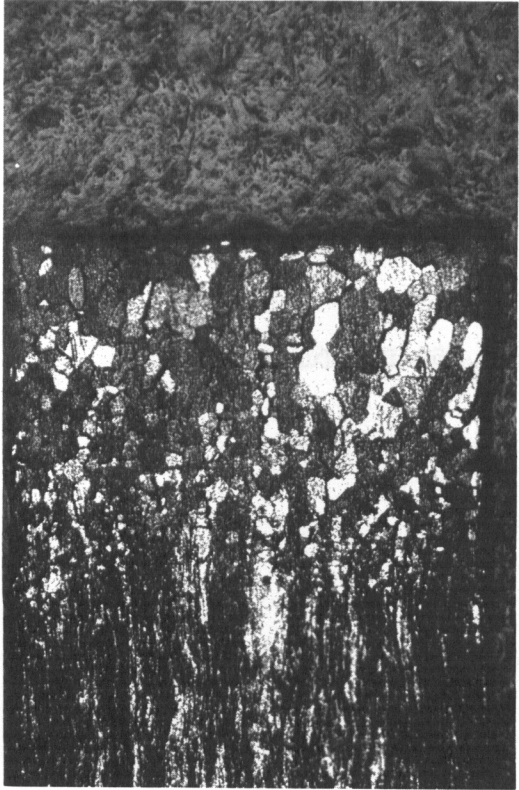


Fig. 130 Room-temperature Weld-zone Failure; X50; 0.050-in. Tungsten Weld



Fig. 131 2500 F Weld-zone Failure; X50; 0.050-in. Tungsten Weld

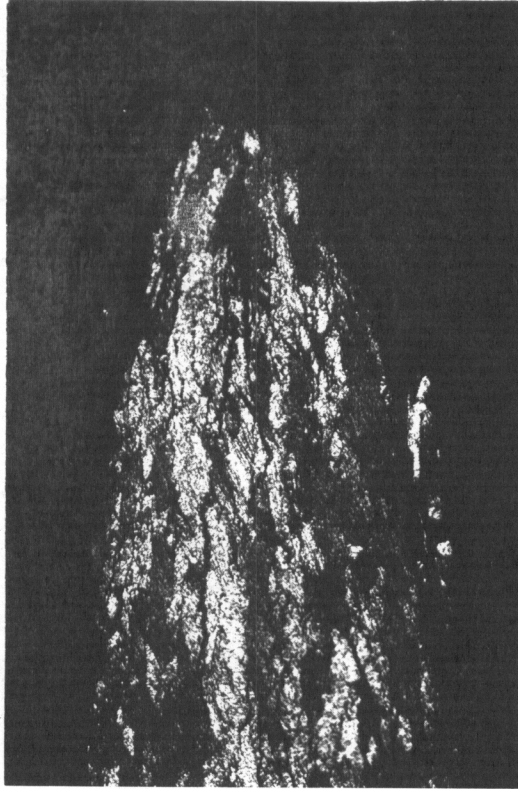


Fig. 132 2800 F Base-metal Failure; X50; 0.050-in. Tungsten Weld

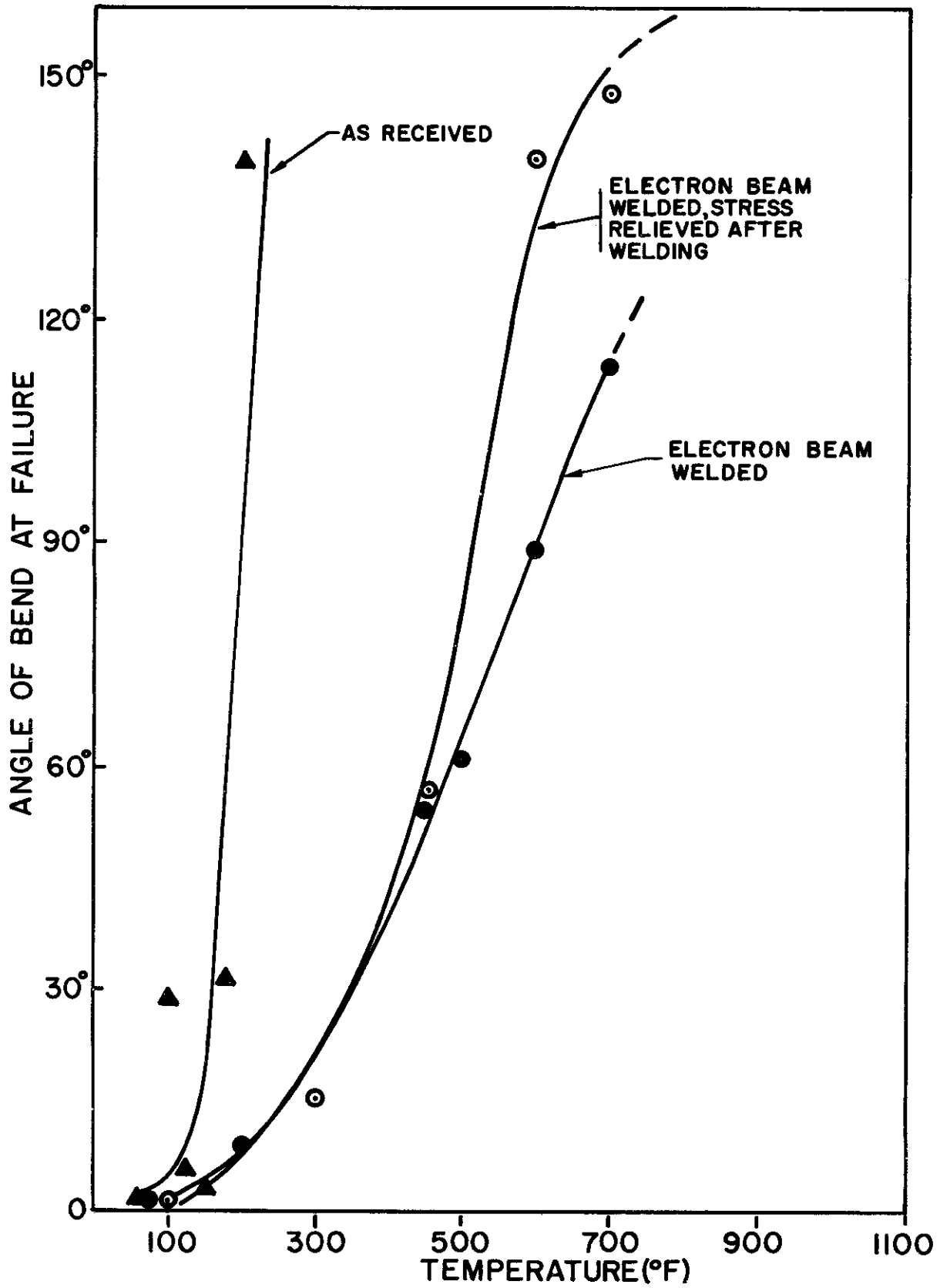


Fig. 133 Bend Angle vs Temperature; 0.055-in. Mo-0.5% Ti Welds

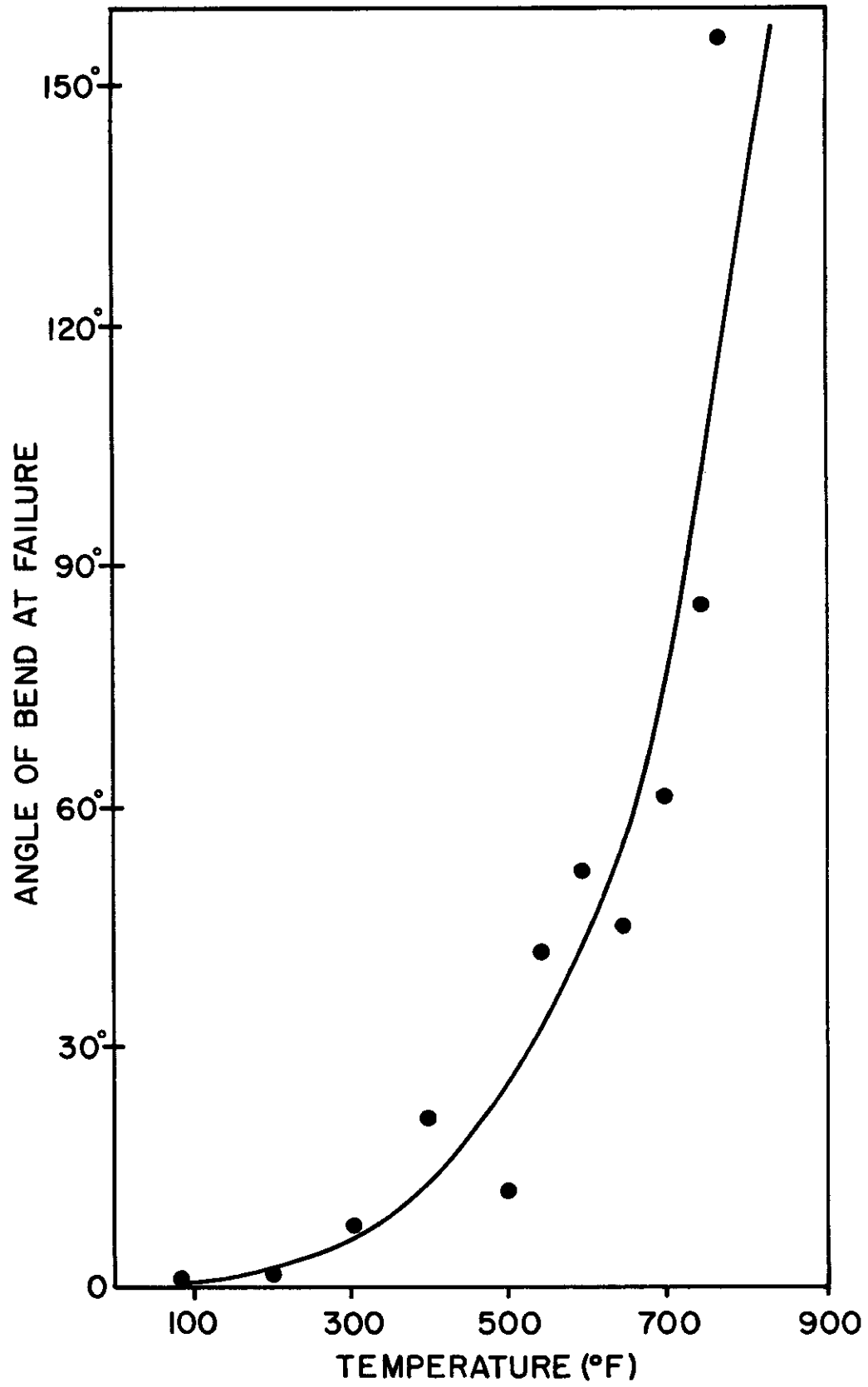


Fig. 134 Bend Angle vs Temperature; 0.100-in. Mo-0.5% Ti Welds

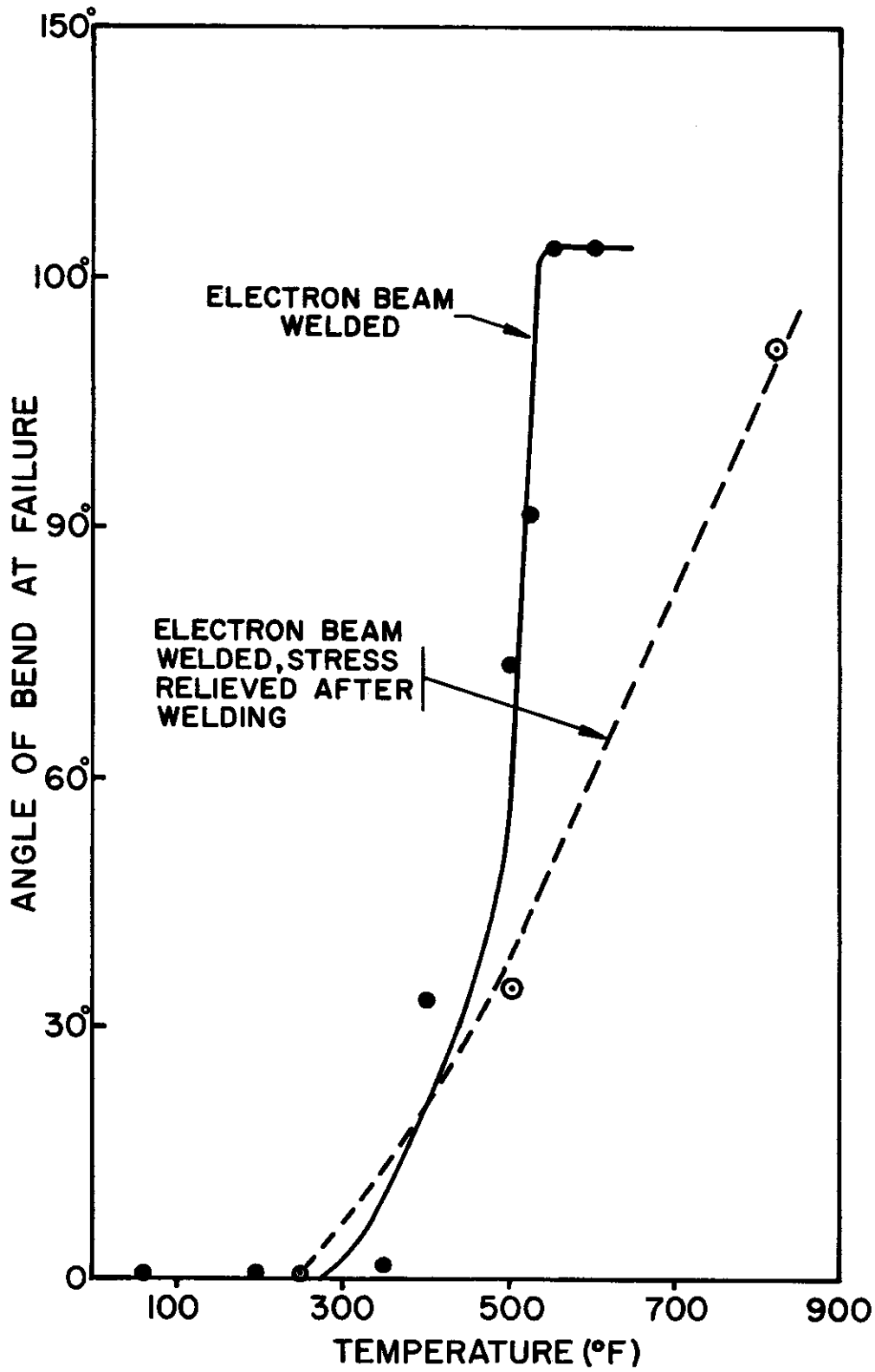


Fig. 135 Bend Angle vs Temperature; 0.005-in. Tungsten Welds

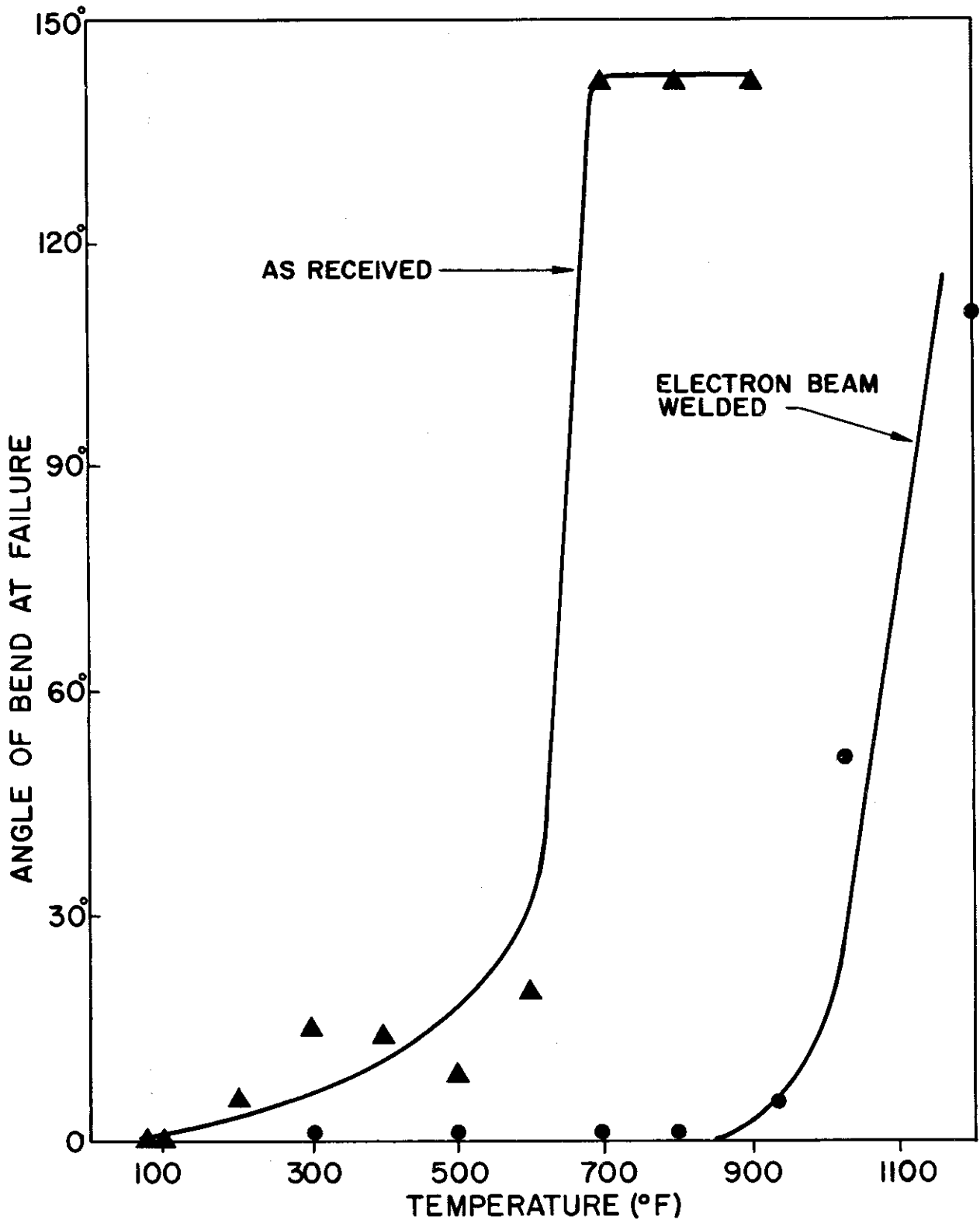


Fig. 136 Bend Angle vs Temperature; 0.050-in. Tungsten Welds